AD-A160 165 ADHERENCE AND BONDING OF THE ION PLATED FILMS(U) CAIRO UNIV (EGYPT) DEPT OF MECHANICAL DESIGN AND PRODUCTION M EL-SHERBINY ET AL. JUL 83 R/D-2723-MS-01 1/2

UNCLASSIFIED DAJA37-80-C-0034 F/G 7/4 NL

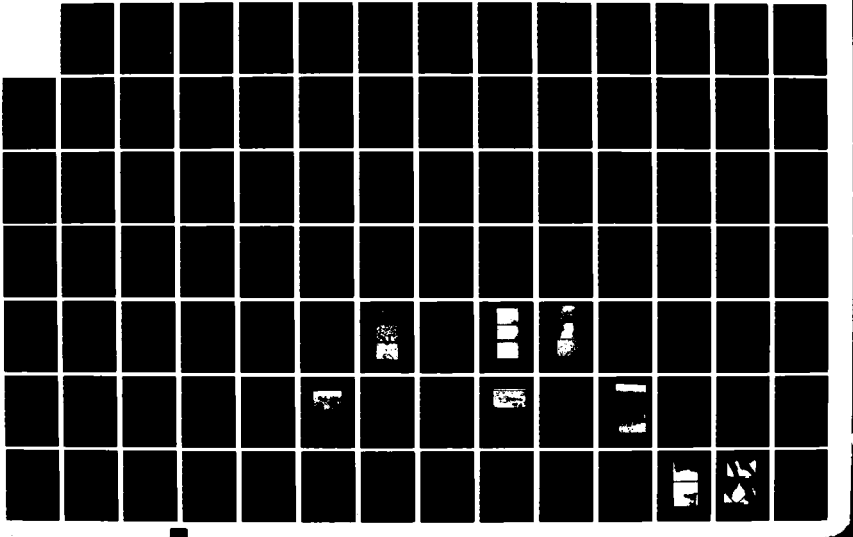

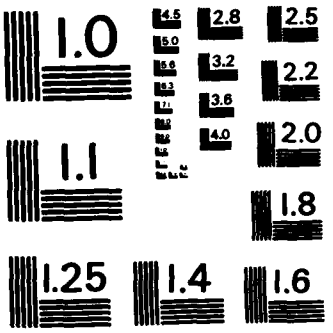

R&D 2723-MS-01 (1)

ADHERENCE AND BONDING OF THE ION PLATED FILMS

FINAL REPORT

Sept. 1979 – Sept. 1982

M. EL-SHERBINY ; F. SALEM

& G. SHAWKI

Research Contract : DAJA 37-80-C-0034

CAIRO UNIVERSITY

EGYPT

DAJA 37 - 79 - C - 34

ADHERENCE AND BONDING OF THE ION PLATED FILMS

Department of Mechanical Deaign and Production
Faculty of Engineering, Cairo University,
Cairo , Egypt.

July , 1983

FORWARD

This Project Was Carried out at the department of Mechanical Design and production, Cairo University, Giza , Cairo, Egypt, Under contract no. DAJA37-79-C-34, Partially Sponsered by the United States Army Research and standardization group and the European office of U.S.A. Air force, London, U.K.

The contract was initiated and finalized with Dr. R.Quattrone, chief materials branch, ERO and finally the project was concluded with Dr. Rothwarf the Successor chief of the materials branch.

Prof. G. Shawki was the principal investigator during the period sept. 79- sept. 80, while Dr. M. El-Sherbiny took over as a principal inverstigator during the period sept.80-sept. 81, and finally Dr. F.Salem was the principal investigator during the period sept. 81 -sept. 1982.

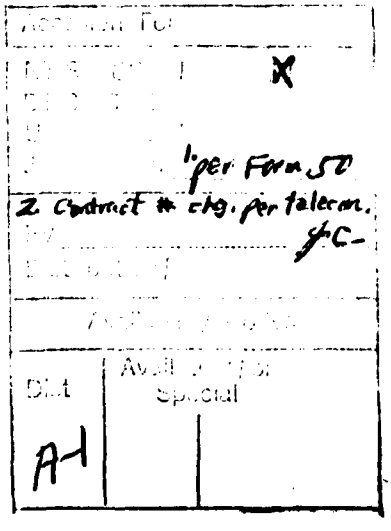

ACKNOWLEDGEMENT

The authors would like to express their thanks to Prof. Dr. Y. K. Hassan the former Dean of the faculty of Engineering. Cairo Univ., and Prof. Dr. A. Kamal the present dean of the faculty for their Unlimited encouragement and support.

Thanks are also due to Prof. Dr. S. Farag, the director of the UNESCO - UNDP project at Cairo University for providing the ion plating facilities.
Appreciations are also evpressed to Prof. Dr. M. El-Salamoni the present chairman of the department for his sincere help and responce.

ABSTRACT

This report presents a comprehensive study of the ion plating process. The dominant physical mechanism are discussed in details. The fundamentals of the technique as well as the ion - solid interactions are studied.

Factors affecting bonding and adhesion are reviewed. Experimental study of nucleation, growth, atomistic mixing and interface formation is presented.
Both qualitative and quantitative test results on adhesion are reported; and optimum processing conditions are concluded.

Experimental investigations of other characteristics including tribological properties are also summarized.

TABLE OF CONTENTS

Forward	i
Acknowledgement	ii
Abstract	iii
Table of contents	iv
List of figures	vii
List of tables	xi
List of published papers from the project	xii
Nomenclature	xiii
I. INTRODUCTION	1
II.ION PLATING	3
1. Ton plating focility and procedure	4
1.1. Introduction	4
1.2. Apparatus	5
1.3. Procedure	7
1.4. Sample precleaning	9
1.5. Thickness measurement	9
1.6. Processing conditions	9
2. Fundamentals of Ion Plating	11
2.1. Introduction	11
2.2. Collision Process	11
2.3. Ionization efficiency	14
2.4. Average energy	16
2.5. Energy distribution	19

2.6 Ion-Solid Interactions 24

2.6.1. Sputtering yield 24

2.6.2. Gas desorption 26

2.6.3. Particle entrapment 29

2.6.4. Atom sputtering 31

2.6.5. Atomistic mixing 32

2.7. Gas Scattering 33

III. ADHESION AND BONDING

3. Factors Affecting Adhesion 35

4. Nucleation 39

4.1. Introduction 39

4.2. Technique 39

4.3. Experimental 40

4.4. Results 42

5. Atomistic Mixing 50

5.1. Introduction 50

5.2. Experimental 52

5.3. Results 55

5.4. Optimum processing conditions 68

6. Adhesion Testing 70

6.1. Introduction 70

6.2. Adhesion test results 72

6.2.1. Preliminary tests 72

6.2.2. Tensile tests 75

6.2.3. Pull tests 78

6.2.4. Scratch tests 79

6.2.5. Shear tests 80

6.2.6. X-ray diffraction tests 84

IV. CHARACTERISTICS 89

7. Structural Details 90

7.1. Introduction 90

7.2. Experimental 91

7.3. Results 92

7.3.1. Microstructure 92

7.3.2. Surface structure 95

7.4. Nodule density 98

7.5. Porosity density 100

7.6. Optimum conditions 102

8. Mechanical Propesties 106

8.1. Microhardness 106

8.2. Yield strength 106

8.3. Fatigue strength 106

V. TRIBOLOGICAL PROPERTIES 112

9. Friction AND WEAR 113

9.1. Intsoduction 113

9.2. Friction-time relationship 113

9.3. Effect of stliding speed 113

9.4. Effect of film thickness 119

9.5. Wear mechanisms 124

VI. CONCLUSIONS 129

REFERENCES 131

LIST OF FIGURES

Fig.	1.1	Schematic layout of the ion plating apparatus	6
	2.1	Physical processes which may take place during ion plating	13
	2.2	Ion plating field and boundary conditions	17
	2.3	Energy distribution set-up	21
	2.4	Energy distribution before and during coating	23
	2.5	The effect of supporting gas pressure on energy distribution	23
	2.6	Sputtering yield-Energy relationship	27
	2.7	Effect of gas pressure on throwing power	27
	4.1	Nucleation of vacuum deposited films	43
	4.2	Nucleation of gas deposited films	45
	4.3	Nucleation of Ion plated films	46
	5.1	In-Cu interface	56
	5.2	Microprobe analysis of ion plated In-Cu interface	57
	5.3	Microprobe analysis of vacuum deposited In-Cu interface	58
	5.4	Microprobe analysis of gas deposited In-Cu interface	58
	5.5	Al-Ti Ion plated interface and the corresponding microprobe results	59
	5.6	Microprobe analysis of specimens no. 16 and 19 (AL-Ti)	60
	5.7	Sn-Ti interface specimen 8	61
	5.8	Sn-Ti interface specimen 10	61

5.9	Auger analysis of Zn-Fe interface	63
5.10	" " " Ag.Fe interface	63
5.11	" " " Ag-Ni "	64
5.12	" " " Cu-Ni "	64
5.13	Percentage contamination due to sputtering of Ni substrates	65
5.14	Effect of gas pressure on contamination	65
5.15	Percentage interface depth	66
5.16	Effect of bias voltage	66
5.17	Effect of evaporation rate	69
5.18	Optimum processing conditions	69
6.1	Tensile test micrographs (Ag/Brass)	76
6.2	Tensile test photographs (Al/Steel)	77
6.3	Pull test arrangement	81
6.4	Scratch tests (vacuum & Electro.)	82
6.5	Scratch tests (Sputtered & Ion plated)	83
6.6	X- ray set up.	85
7.1	Effect of substrate bias voltage on film structure (Cu-Cu)	93
7.2	Effect of substrate bias on film structure (Al-Ti)	94
7.3	TEM micrographs of shadowed carbon replica showing coarse grain structure	96

7.4 Microstructure of Al-Ti system demonstrating the effect of gas pressure 97

7.5 TEM micrographs for chemically etched cu film 99

7.6 Pitting pattern due to chemical etching 101

7.7 Effect of gas pressure and bias on the figure of merit of ion plated films deposited at low deposition rates 104

7.8 Effect of gas pressure and bias on the figure of merit of ion plated films deposited at high deposition rates 105

8.1 Microhardness measurements across Silver films deposited on copper substtate 107

8.2 Variation in hardness with film thickness for Al film on Ti substrate 107

8.3 Surface hardness of Al-Ti composite 108

8.4 Variations in yield stress and grain size with film thickness 109

8.5 S-N fatigue curve of coated and uncoated steel specimens 110

9.1 The effect of the deposition technique on frictional behaviour of silver films 114

9.2 The effectiveness of pb,In,Ag & sn Ion plated coatings as solid labricants 115

9.3	The effect of sliding speed on friction	116
9.4	The effect of sliding speed on film life	116
9.5	Measured sliding distance for film life	118
9.6	The effect of film thickness on friction	120
9.7	The effect of surface finish on the friction of coated surfaces	122
9.8	Measured life per unit film thickness for different films	123
9.9	Wear mechanisms of vacuum deposited Sputtered and ion plated films	125
9.10	Wear process in Ion plated films	126

LIST OF TABLES

2.1	The Q values for different target materials	25
3.1	Factors offecting interfacial layer	38
4.1	Experimental conditions for nucleation tests	42
5.1	Metal pairs for interface tests	53
5.2	Processing parameters for interface tests	54
6.1	Ultrasonic test	73
6.2	Tape test	74
6.3	X-ray diffraction results for Ag/cu	88
7.1	Processing conditions of Ion plated films	92
7.2	Nodule density in Ion plated and vacuum deposited films	98
7.3	Surface porosity of Ion plated films	102
7.4	Relative scale for the figure of merit	102

LIST OF PAPERS PUBLISHED FROM THE PRESENT WORK

1. "Thin Film Adhesion : A Critical Review" 1st Int. conf. on Mech. Design and production, Cairo Univ. Egypt. Dec. 1979 , paper MDP-79-MAT-19 , Also in the book "Current Advances In Mechanical Design and production" Edited by G. Shawki , Pergamon press, London, (1981)

2. "Nucleation And Interface Formation of Thin Films" Thin Solid Films, Vol. 75, P.29 (1981)

3. "Characterization Of The Ion Plated Coatings" Paper presented in the Inter. conf. on Ion and plasma assisted techniques, Amsterdam, June (1981)

4. "Tribological Applications of Ion Plating" Inter. Terotechnology conf. , New Delhi, India, Nov. (1981)

5. "The Strength of Ion Plated Films" 2nd Inter. conf. on Mech. Design and production, Cairo Univ., Dec. (1982), Paper MDP-1982-MAT-9 . Procedings of, Vol. I , P. 645 (1982)

6. "Tribological Properties of PVD Silver Films" Silver Inst.- ASLE Joint conf. on Lubricity of silver. To be held May 1985, New York, U.S.A. (1985).

NOMENCLATURE

a	Thomas - Fermi Screening radius of the interatomic potential
d	Grain Zize
d_{hkl}	Structure Planar Spacings
E	Energy , incident energy, And Young's modulus of elasticity
E_L	$=(M_1 + M_2)\ (Z_1Z_2e^2)\ /\ (M_2a)$
e	Electron Charge
G	Gas atom, G^+ gas ion
h	= 0.834 for $M_2 > M_1$ and Q.18 for $M_2 < M_1$
J	Flux density of ion beam or energetic particle flux
K	Constant defined in equn . 2.1
K_p	Molecular impingement rate per unit area at a given pressure (p)
k	$= \frac{S_e(\varepsilon)}{\sqrt{\varepsilon}} = 0.0793\ (Z^{1/6} / M_1)(Z_1Z_2/M_1M_2)^{\frac{1}{2}}\ (M_1+M_2)^{3/2}$ $(Z_1^{2/3} + M_2^{2/3})^{-3/4}$
L	Axial distauce between the negative glow edge and the Cathode
l	Charge exchange mean free path at working pressure
M_1	Mass of the incident ion
M_2	Mass of the target atom
N	Number of ions
n	Adsorbed atom areal density
n_s	Monoloyer density
n_e	Surface impurity concentration at equilibrium

P	Probability
P	Gas pressure , and also contact pressure
Q	Deviation of α_2 from sigmund α (table 2.1)
S	Substrate atom (S^+ substrate ion)
$s_e(E)$	Reduced electronic stopping cross section = $K E^{1/2}$
$s_n(E)$	Nuclear stopping cross section (ref. 27)
t	Time
U_s	Surface binding energy (≈ Sublimiation energy)
V	Field Strength
v_c	Cathode voltage
X	Axial coordinate within the chamber
Y(E)	Sputtering yield
Y_d	Sputtering yield of desorption
Z_1	Atomic number of incideut ion
Z_2	Atomic number of target atom
α_2	$= 0.1 + 0.155\ (M_2/M_1)^{0.73}$ for $M_2/M_1 < 50$
	$= 0.321 + 0.0332\ (M_2/M_1)^{1.1}$ for $M_2/M_1 > 50$
ξ_2	$= 1.5\ [1 + 1.38\ (M_2/M_1)^h\ ]^2/\gamma$
γ	$= 4\ M_1\ M_2\ /(M_1 + M_2)^2$, sticking coefficient of a given impurity
E	$= E/E_L$ and also the lattice strain
σ	Yield stress of the film
σ_d	Ion bombardment - induced desorption cross section

σ_c	Ion bombordment - induced desorption coefficient for coating species particles striking adsorbed atoms
σ_{ds}	Ion bombardment - induced desorption coefficient for support gas particles
ν	Poisson's ratio
$\eta(E)$	Entrapment propability
τ	Shear stress
θ_{hkl}	Refectance angle of x-ray beam
λ	Radiation wave length

I. INTRODUCTION

I- INTRODUCTION

The material of every engineering component must fullfil two basic functions. These are: the structural function such as strength, flexibility and rididity and the surface function such as low wear, corrosion and friction or any other optical, thermal and electrical functions. Surface coatings, therefore, provide the designer with a good apportunity to decouple these functions, and select a base metal for cost and structural reasons without much concern for the required surface properties. The surface function may then be subsequently fullfiled at a later stage in the design process by proper selection of coating materials and techniques.

When a coating is applied to a surface, the application method determines the bonding strength and adherence. These are generally reflected on the effectiveness, usefulness, durability and life of the coating itself.

Ion plating (1-10) is a recently explored technique which surpass the conventional methods of sputtering, gas and vacuum depositions. Outstanding adhesion through graded interface, unique film thickness uniformity and good control of film structure are frequently claimed for the ion plated coatings. However, at the begining of this project, the ion plating technology was still at different stages of development. For example research efforts were directed towards increasing the ionization efficiency and

deposition rates. The values quoted for both ionization efficiency and ion energy were rather speculative. The process was not optimized or fully characterized. The mechanism of adhesion was not well identified, and the role played by various process parameters was ill defined.

Therefore, the project was designed to look into the adherence and bonding mechanisms of ion plating with particular reference to the role played by different phases of the process and processing parameters. Furthermore, a study of the characteristics of the ion plated films such as uniformity, grain size, and mechanical properties was included. Before signing the contract however, applications on friction and weat were included upon a request from ERO.

The project was therefore performed in five major phases, with each phase devided into a number of minor tasks. This report is therefore, devided into the following four major sections :

1- Fundamentals of ion plating

2- Adhesion and bonding of ion plated coatings

3- Characteristics of ion plated coatings

4- Friction and wear of ion plated coatings.

II. ION PLATING

CHAPTER 1

ION PLATING FACILITY AND PROCEDURE

1-1 Introduction

In 1963 Mattox introduced a technique of physical vapour deposition which he called "ion plating" (1). Mattox compared the energy of deposition for both the sputtered and vacuum deposited coatings and related these energies to the experimental findings that sputtered coatings are usually more adherent than the vacuum deposited coatings. He then attempted to increase the kinetic energy of the depositing particles further by a glow discharge process inorder to further improve the addesion. He demonstrated that the ion plated coatings had excellent adhesion and this was attributed to the high energy of deposition.

The view implicit in most of the early papers (1, 11,12) was that substantial proportion of the evaporated atoms were ionised in the glow discharge and arrived at the substrate with the maximum energy (i.e. 5 Kev for a -5KV bias). A number of estimates of the efficiency of ionization in the process have been made (1,11,12). These vary from a low value of 0.1% (11,12) to a high value of 90% (1). Most of the high values (> 30%) were based on the ratio of film thickness at the back surface to that on the front surface. They assumed that the back surface coating resulted only from ions following the field lines,

whereas that on the front surface resulted from deposition of both ions and neutrals.

A tremendous amound of work was soon published on the structure and morphology of the ion plated coatings as prepared for specific engineering applications. These will be reviewed in the relevant sections of the report.

1-2 Ion Plating Apparatus

Fig.1.1 shows a schematic layout of a conventional ion plating apparatus which was used in the present work. The main part of the equipment comprises a conventional vacuum system. A 10 m^3/hr rotary pump is used to rough out the vacuum chamber from atmospheric pressure and down to 100 μm Hg, before the diffusion pump is operated. The same pump is then used to back a 1100 L/sec oil diffusion pump during the subsequent pumping of the chamber. A self protection magnetic valve is used on the backing line with automatically controlled thermal protection system and mimic display of operation and warm up sequence. A baffle valve including electrically operated throttling device used in conjunction with two controlled gas inlet systems is used to control the rate of pumping during deposition. A liquid nitrogen cold trap is also used to condense the oil vapour resulting from back streaming from the diffusion pump. Two more traps, (a sorption and discant), are used in connection with the rotary pump to absorb water vapour and volatiles from the system. Two

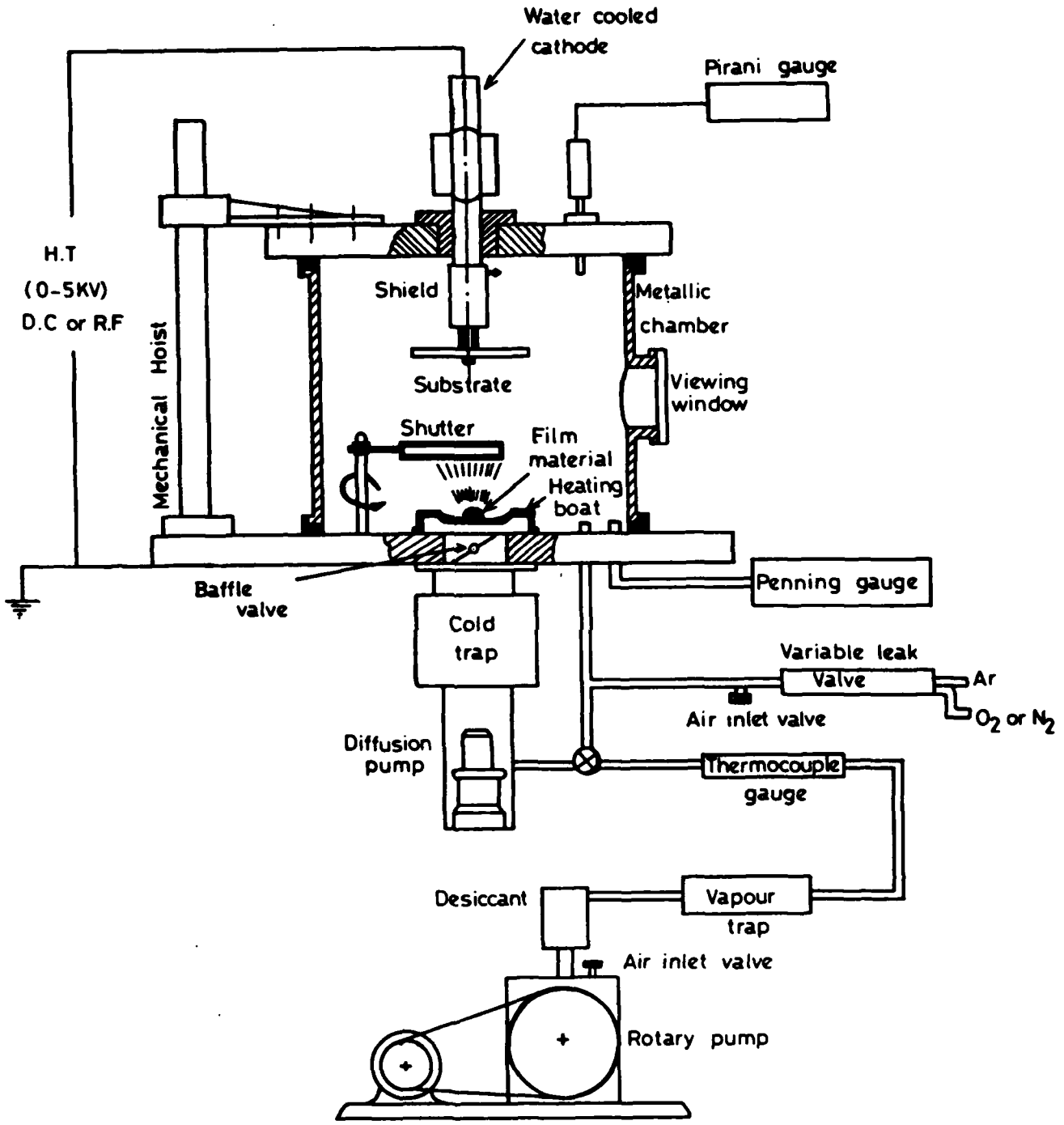

Fig. 1.1

SCHEMATIC LAYOUT OF IPAC-35 CONVENTIONAL ION PLATING UNIT

variable leak valves of needle type with flow meters are provided for admission of the discharge gas mixture.

Complete vacuum measurement system with 3 pirani gauges and one penning gauge are used to monitor the vacuum system. The vacuum chamber is a stainless steel cylinder 40 cm diameter and 30 cm high, with a viewing glass window. A stainless steel top plate is bolted to the cylinder and hooked to an electrically operated mechanical hoist. The base-plate however is 16 cm diameter stainless steel plate with 12 leadthrough positions. The chamber houses two electrodes one of which is a watercooled negatively biased substrate support connected to a 6KV DC HT Supply of 1 KW. The other being the anode is connected to the evaporation filament. Two independent 2 KVA Low tension supplies were routed to two pairs of watercooled electrodes which support two evaporation sources, with associated source shutters. A 150 W RF ion plating supply and matching network is also included for coating non-metallic substrates. A quartz crystal film thickness monitor is also housed in the chamber.

1-3 Ion Plating Procedure

The usual plating procedure is as follows. The pre-cleaned sample is connected to the H.T. electrode and a measured amount of coating material is placed in the filament boat. The chamber is then evacuated to a pressure of 10^{-5} torr or better. A constant pressure (typically

between 10-50 m torr) of argon may then be maintained by partially closing the baffle valve and opening the argon needle valve. The bias supply is then adjusted to the required level, usually between 2 to 5 KV.

Under these conditions an abnormal glow discharge is struck between the earthed parts of the apparatus and the sample (cathode). The sample is bombarded by the positive ions formed in the discharge, resulting in the removal of oxides and other contominants from the substrate surface, (Sputter etching phase).

When the sample is sufficiently clean the vapour source is energised and the metal vapour enters the discharge Electron-atom collisions ionize some of the vapour atoms, and may also result in some metastables and negatively charged atoms, (negative ions). When the metal ions reach the cathode dark space they are accelerated by the high field towards the substrate surface. Due to gas scattering, subsequent collisions take place and the scattered vapour atoms share the energy of the ions by atom-ion collisions. The final deposit is therefore the result of deposited high energy atoms and accelerated ions.

When the film material is fully evaporated, the high tension field is switched off and the sample is left to cool down in vacuum.

1-4 Sample Precleaning

Unless otherwise stated the specimens used in the present study were copper specimens 5 cm, square and 5 mm thick.

The specimens were first polished by silicon carbide paper of 220, 320, 400 and 600 grit. Final polishing was then done by diamond wheels using 6 and 1 microne diamond paste. Water rinse, alcohol cleaning and air drying were subsequently made before sputter cleaning the surface in the ion plating apparatus.

1-5 Film Thickness Measurement

Quartz crystal film thickness monitor was used to predict the average coating thickness on flat specimens during deposition. For curved surfaces, however, a small cube (1 cm each side) was mounted with the component to be coated and subsequently used for sectioning and thickness measurments on optical microscope. Thin films on the real substrates were also used for measuring film thickness by x-ray diffraction (5).

1-6 Ion Plating Conditions

Unless otherwise stated in the following sections, the ion plating conditions are as follows :

a) Sputtering

Substrate sputter cleaning is made at 15 μm Hg and 5 KV for about 20 minutes.

b) Ion plating

The gas discharge during deposition is maintained at 3 KV with an average gas pressure of 10 μm.

c) Evaporation rate

The average evaporation rate under normal conditions is maintained at 30 mg/s.

CHAPTER 2

FUNDAMENTALS OF ION PLATING

2-1 Introduction

The term ion plating is now established in refering to atomistic deposition process in which the substrate is subjected to a flux of high energy species in a gas discharge, which is sufficient to cause appreciable sputtering before and during film deposition. The gas discharge also provides some means to maintain reasonably high energy for the depositing particles.

A number of physical mechanisms need, therefore, to be discussed before considering the adhesion mechanism of the ion plated coatings.

2-2 Collision Process

During the sputter cleaning phase of the process, some of the inert gas atoms (G) are ionized (G^+) by electron-atom collision and accelerated across the dark space to the substrate surface. Many of these ions (G^+) become high energy neutrals by charge exchange process (9). The non-ionized gas atoms may suffer elastic collisions and be scattered to all exposed surfaces in the chamber. The high energy species hitting the substrate may become incorporated into the surface, or be neutralized and reflected back in the form of energetic neutrals or metaslables (G^+),

causing secondary electron emission (e^-) and sputtering of the substrate atoms (S). The sputtered atoms (S) may deposit in other portions of the chamber, scatter back to the substrate, or ionize by electron or metastable collisions and accelerate back as a positve ion (S^+) to the substrate.

When film atoms are liberated from the heated filament, a number of possibilities may happen to them. They may be 1) scattered back to the source or any other portions of the system, 2) ionized by a simple collision process or by cumulative ionization, or 3) collide with each other in the gas state and nucleate into fine particles (molecules) of the order of 100 A^0 and apparantly assume a negative charge in the plasma (9,13). As the film atoms and ions begin to deposit, some of the energetic species penetrate into the substrate surface, some are scattered back after sputtering some of the substrate atoms (S) and some may become neutralized on the substrate surface and remain there to begin film formation. The scattered back species of the film and substrate materials may be rescattered back to the substrate, lost in other parts of the system, or ionized and accelerated back to the substrate. Fig.2.1 shows the physical processes which may take place during ion plating.

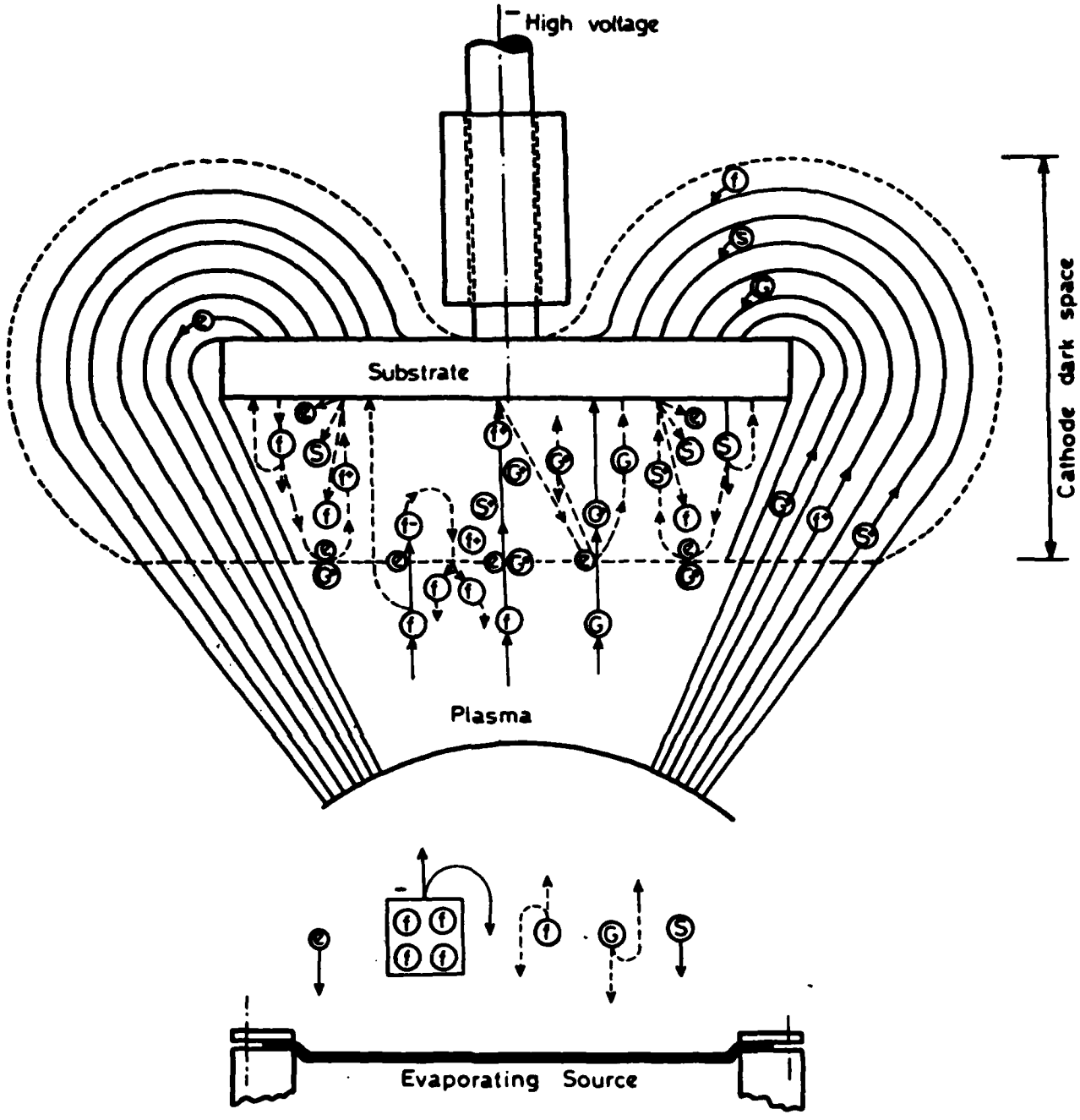

f Atom of film metal

G Gas atom

\+ Positive ion

e Electron

S Atom of substrate metal

G* Gas metastable

\- Negative ion

f-f / f-f Film agglomerate

Fig. 2.1

PHYSICAL PROCESSES WHICH MAY TAKE PLACE IN AN ION PLATING CHAMBER

At this point some quite interesting questions regarding the physics of the process may arise. They include :

(i) What is the percentage ionization ?

(ii) What is the average energy of energetic species ?

(iii) What are the associated rates of sputtering and the criteria for film formation ?

(iv) What is the mean and surface substrate temperatures ?

(v) What is the role of gas scattering ?

2-3 Ionization Efficiency

A number of estimates of the efficiency of ionisation in the ion plating process are published in the literature. These range from low values of 0.1-5% (11,12) to high values of 90% (1). Mattox (1) claimed an ionisation efficiency of 90% for copper-Argon plasma and 30% for gold-argon plasma, when using high current densities of the order of several milliamperes per square centimetere. Buckely et.al. (11) reported a low value of ionisation (1-5%) as a result of theoretical considerations of plasma physics and langmuir probe measurement of conventional plasma (single component argon plasma). In a discussion secion following a conference on ion plating (14), estimates varying from 1 to 30% were made. The high figures are generally based on the fact that the thickness of coating on the back surface of ion plated flat substrates was 30% of the thickness on

the front surface, and the assumption was made that the back surface coating resulted only from ions following the field lines, whereas that on the front surface was the result of both ions and neut als.

In the present work we measured the total substrate current under a wide range of plasma pressures and evaporation rates. A simple calculation based on the measured current and gas pressure during the sputter etching phase of the process (single component plasma), assuming that the measured current is due to gas ions only, showed ionisation efficiency values less than 0.1%. For example at 10 μm Hg argon the ion current density was 0.5 mA/cm^2. Assuming ion current only estimate of $3x10^{15}$ ion/cm^2/sec is calculated, while the number of atoms corresponding to the given pressure is $4x10^{18}$ atoms/cm^2/Sec. It is therefore apparant that the ionisation efficiency is 0.075% (<0.1%).

During the deposition phase, we assumed that the discharge current is due to metal ions only. Obviously such assumption results in overestimating the ionisation efficiency, and hence an upper bound estimate may be obtained. We summed up the total number of ions during the deposition period of 60 seconds and compared the figure with the total number of atoms deposited as calculated from film thickness measurements. The resulting efficiency fall within a range of 1-3% for P_b, S_n, In, and Ag deposits.

If is therefore shown that the ionization efficiency is rather low (<3%), and hence the majority of the metal species in the chamber are neutrals. This , however, leads to the importance of emphasizing both the role of gas scattering and the average energy of the depositing particle.

2-4 Average Energy

Following the approach of Davies et.al.(15) for which the following assumptions are made :

a) All ions originate in the negative glow discharge.

b) The electric field is linear within the region bounded by the cathode and the negative glow edge as shown in Fig.(2.2).

c) Symmetrical charge transfer collisions are only responsible to the energy spectrum.

d) The collision cross section does not change with energy and considering the boundary conditions of the ion plating process (16) as illustrated in Fig.2.2, the linear field strength gives ;

$$\frac{dv}{dx} = k \frac{x}{L} \qquad (1)$$

Integrating equ.1 yields ;

$$V = K \frac{x^2}{2L} + C \qquad (2)$$

Applying the boundary conditions V=O at $x = 0$ and $V = V_c$ at $x = L$ gives $K = \frac{2V_c}{L}$ and $c = o$.

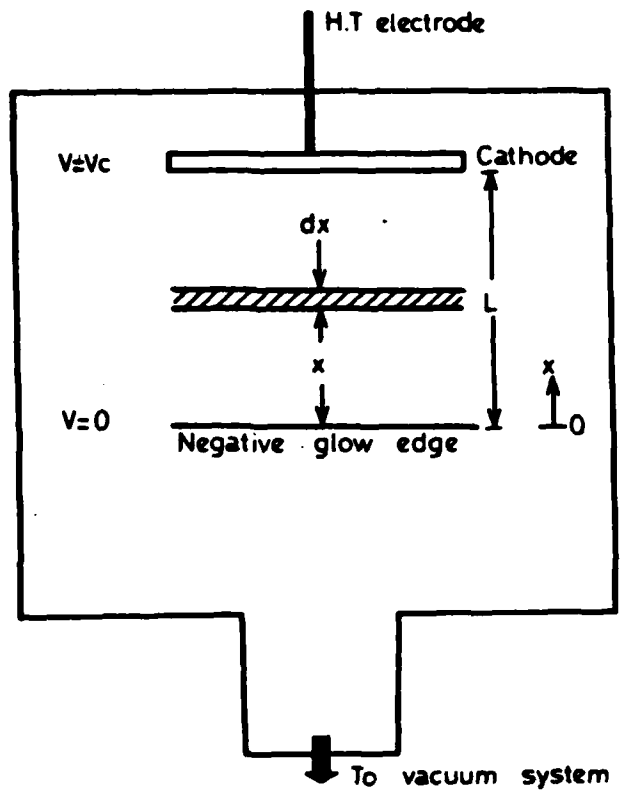

Fig. 2.2

ION PLATING FIELD AND BOUNDARY CONDITIONS

Therefore, equn.2 reduces to ;

$$V = \frac{V_c}{L^2} x^2 \qquad (3)$$

Assuming a number of ions N leaving the negative glow, the number of collisions within an infinitizmal slice Δx is given by $N \frac{dx}{l}$. The probability of these ions, resulting from collisions with the slice Δx, reaching the cathode without further collisions is given by ;

$$p = e^{-(L-x)/l} \qquad (4)$$

Therefore, the number of ions arriving at the cathode with energy $V_c - V$ is

$$dn = \frac{N}{L} e^{-(L-x)/l} dx \qquad (5)$$

Substituting for x from equn.3 gives ;

$$dn = \frac{NL}{2l\sqrt{VV_c}} e^{-L(1-\sqrt{\frac{V}{V_c}})/l} dv \qquad (6)$$

The total ion energy arriving at the cathode is therefore given by ;

$$E = \int_0^{V_c} (V_c - V) \, dn \qquad (7)$$

Substituting for dn from equn.6 and integrating gives ;

$$E = NV_c \frac{2l}{L} - \frac{2l^2}{L^2} + \frac{2l^2}{L^2} e^{-l/L} \qquad (8)$$

In absence of collisions the total energy received by the

substrate is NV_c. However for small values l/L the ion energy loss is quite high. It can simply be approximated by $(2l/L)N V_c$. Under typical ion plating conditions l/L is 0.05 or slightly higher. This means that 10% of the maximum energy is carried by ions, while the other 90% is transfered to energetic neutrals resulting from the collision process. Measurements (17) showed that 70% of the energy transfered to the neutrals reaches the cathods. In order to calculate the average neutral energy, the same distance L is divided into (L/l) regions, and we assume collisions to take place at the boundary of each region. The energy gain for ions within the n region is therefore given by $(V_c l^2/L^2)(2n+1)$. For the last region in the vicinity of the cathode the maximum neutral energy is $(V_c l^2/L^2)(2(\frac{L}{l})+1)$ while for the 1st region in the vicinity of the negative glow edge, the minimum neutral energy is $V_c l^2/L^2(1)$. Assuming equal number of collision in each zone the average energy of the neutrals is therefore given by ;

$$E_{ar} = \frac{V_c\, l^2}{L^2}\left(\frac{L}{l} + 1\right)$$

A typical L/l value for ion plating is 20, therefore for a typical ion plating run at 5 KV the average energy of the neutrals can be estimated by 262.6 ev.

2-5 Ion Energy Distribution

In ion plating a self sustained abnormal glow discharge at a working pressure of 10^{-2} torr is used as a

working medium. This type of discharge has been subjected to a century of study by an impressive list of scientists (18-20). The present work, however, aims at comparing the energy distributions of the glow discharge before and during film deposition.

The experimental setup is a simplified version of the one used by Houston (20), and comparable to the one used by Ahmed (19). Basically the arrangement consisted of two cascade chambers as shown in figure 2.3. This was necessary to avoid using differential pumping systems and to maintain the energy analyser at a good vacuum of 10^{-5} torr while injecting the argon gas in the plating chamber. A glass discharge tube 150 mm high, 120 mm in diameter was mounted inside the ion plating chamber. The discharge gas was fed directly to the glass tube by means of a flexible tube connecting the gas inlet of the ion plating chamber to the gas inlet of the discharge glass tube. The glass tube was also provided with seated feedthrough ports for the high current connections of the evaporation boat (A). This evaporation boat was mounted 100 mm away from the cathode (C), and also served as the discharge anode. The cathode (C) was made of stainless steel disc 130 mm diameter and 5 mm thick. A 1 mm diameter hole was provided at the center of the cathode as an aperture for extracting the gas ions.

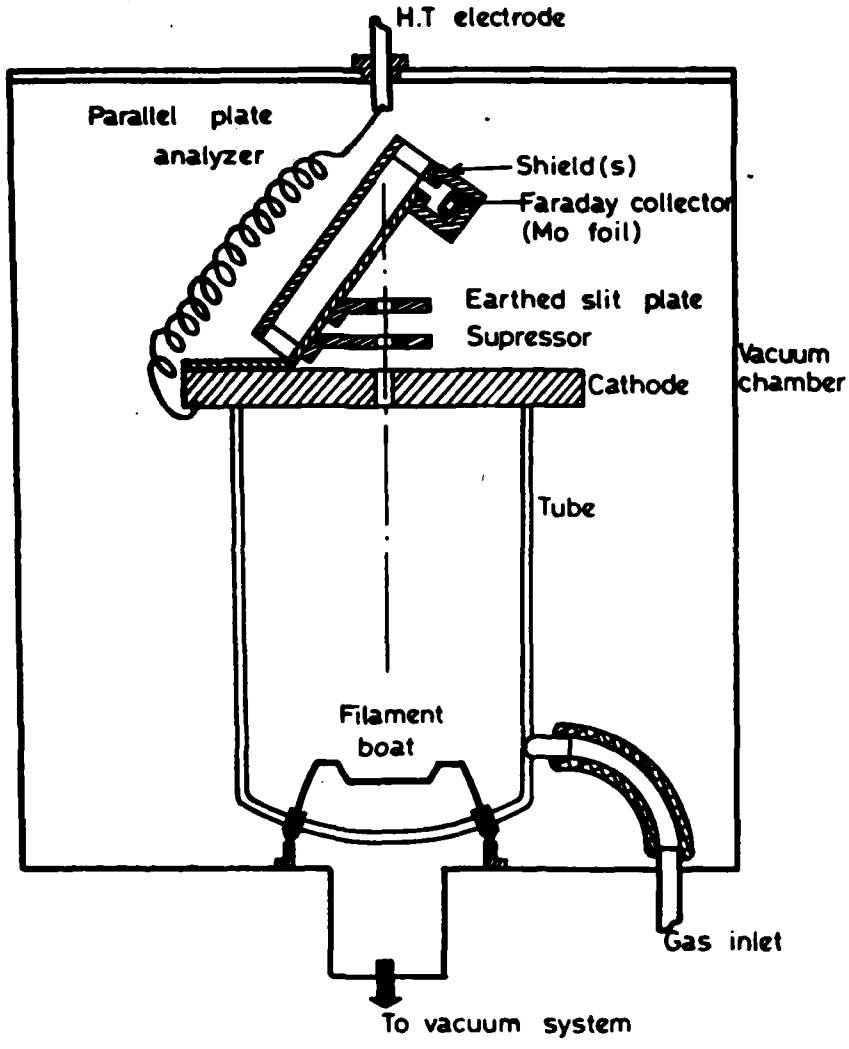

Fig. 2.3

ENERGY DISTRIBUTION SET UP

The analyzer consisted of two parallel stainless steel sheets of 60x40x1.0 mms. These were separated by a gap of 20 mm. The lower sheet had two slits (8x1 mms each) as an inlet and outlet ports for the ions. Two collimating operatures were used to focus the ions into the analyzer. A screening can (s), containing the faraday cup collector was mounted at the free end of the analyzer, while the analyzer was rigidly fixed to the cathode at the other end with a tilt of 45^{o}. The measurements of the energy spectrum of the extracted ions were made by using a linear positive voltage sweep on the upper sheet of the analyzer. The lower collimating aperture was negatively biased by 150 v to supress the negative current readings.

Fig.2.4 shows a repesentative sample of the results obtained at 10 μm Hg (0.02 torr) and a negative bias of 1.5 KV. In this figure the solid lines is obtained for the gas discharge before metal evaporation, while the dashed line is obtained during film deposition. The high pressure deposition is generally characterized with a double peak with notable shift of the peaks towards lower energy values. At lower perssures however the double peak gradually disappears and the peak generally moves to higher energy values as illustrated in Fig.2.5.

Houston et.al (20) showed that the higher energy peak may be due to doubly ionized argon A_r^{++} for which the charge transfer cross section is generally lower than that for the singly ionized atom A_r^{+}. It is therefore

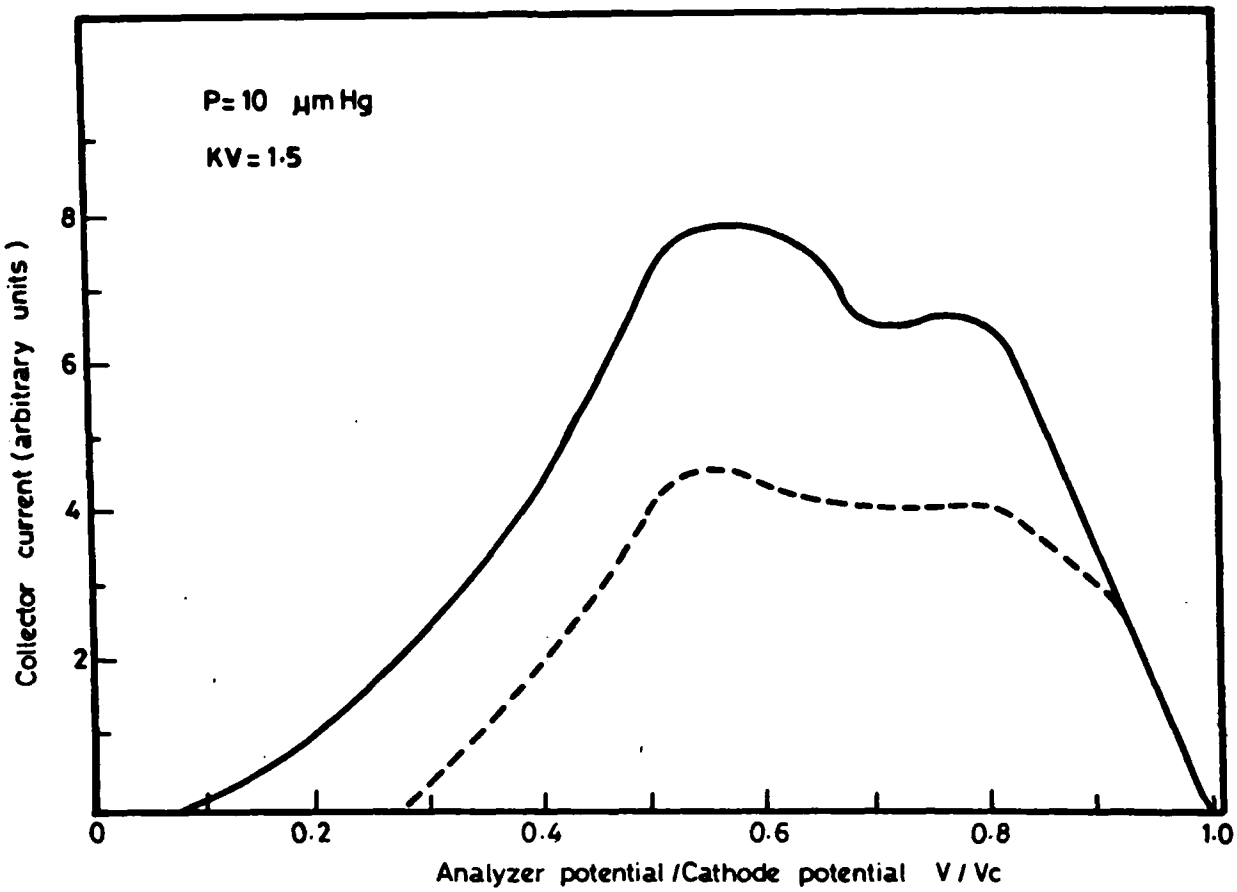

Fig. 2·4

ENERGY DISTRIBUTION BEFORE AND DURING DEPOSITION

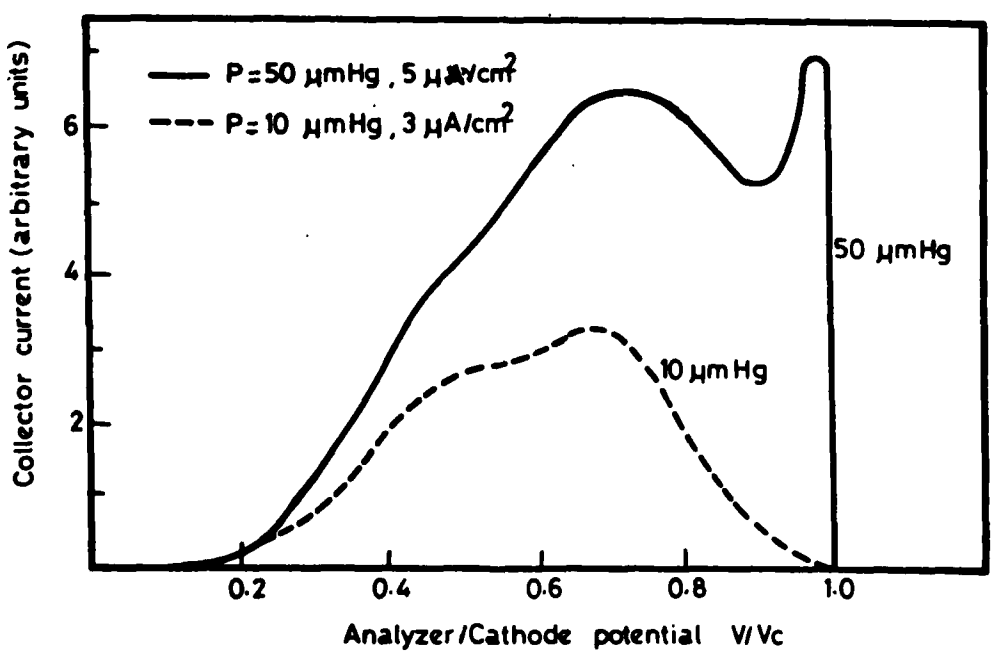

Fig. 2·5

THE EFFECT OF GAS PRESSURE ON ENERGY DISTRIBUTION

expected that A_r^{++} ions would have a higher average energy as compared with the A_r^{+}.

2-6 Ion-Solid Interactions

One of the most important mechanisms of ion-solid interactions which occurs before and during ion plating is the sputtering of target-surface atoms by ion bombardment. This mechanism provides atomically clean surfaces prior to and during film deposition. It reduces the growth rate of the coating but eventually leads to atomistic mixing via recondensations after gas phase collisions. Displaced substrate-surface atoms and lattice deffects are generated by sputtering and contribute to the intermixing of the substrate and film atoms. Enhanced defect density also promotes rapid interdiffusion. Finally the high energy coating species penetrate into the surface, resulting in extensive graded interfaces, while the low energy ones remain closer to the surface and therefore are subject to preferential sputtering.

2-6-1 The sputtering yield

The sputtering yield at normal incidence has been estimated from analytical expressions (21,22), empirical relations (23,24), and computer simulation (25) of sputtering processes. The analytical predictions (21) were found to deviate from experimental values for some cases such as light ion sputtering and low energy sputtering. In order

to obtain the universal formula which is valid for both heavy ion sputtering and light ion sputtering, Yamamura (26) propose the following equation ;

$$Y(E) = 0.042\, Q(Z_2)\, \frac{\alpha_2 (M_2/M_1)}{U_s}\, \frac{S_n(E)}{1+0.35\, U_s S_e(E)} \left| 1-\left(\frac{U_s\, \xi_2}{E}\right)^{\frac{1}{2}} \right|^2$$

where $Q(Z_2)$ values are given in table 2.1 for different target materials and all tother variables are defined in the nomenclature.

Table 2.1 The Q values for different target materials (ref.26)

Target Material	Q	Target Material	Q
Be	1.78	Nb	0.94
C	2.74	Mo	0.84
Al	1.00	Ru	01.32
Si	0.73	Rh	1.14
Ti	0.55	Pd	1.00
V	0.85	Ag	1.09
Cr	1.17	Hf	0.63
Mn	1.09	Ta	0.72
Fe	1.03	W	0.93
Co	1.05	Re	1.07
Ni	1.05	Os	1.21
Cu	1.26	Ir	1.18
Ge	0.75	P_t	0.94
Z_r	0.61	Au	0.93

The theoretical predictions based on this empirical formula was found to agree well with the experimental findings for a number of target materials bombarded with various ions over a wide range of energy spectrum. Fig.(2.6) shows the sputtering yield for Fe target bombarded with Ar and Ag ions within the energy range $10\text{-}10^6$ e.v.

2-6-2 Induced gas desorption

The ion bombardment-induced desorption cross section σ_d is defined (28) in terms of the equation describing the rate of depletion of adsorbed atom areal density n due to bombardment with an ion beam of flux density, J i.e.

$$J\, n\, \sigma_d = -\frac{dn}{dt}$$

The equivilant sputtering yield for desorption is then conveniently defined as ;

$$Y_d = n_s\, \sigma_d$$

where n_s is the monolayer density

For low energy bombardments, experimental results (29,30) have typically yielded values for σ_d of about $10^{-15}cm^2$ corresponding to sputtering yields within the range 0.1-1.0. Winters and sigmund (31) explained the experimental results within the assumption of specific series of binary elastic collisions involving the bombarding ion, the adsorbate and substrate ions. In terms of this explanation , the ion impact desorption process for low energy ions is associated

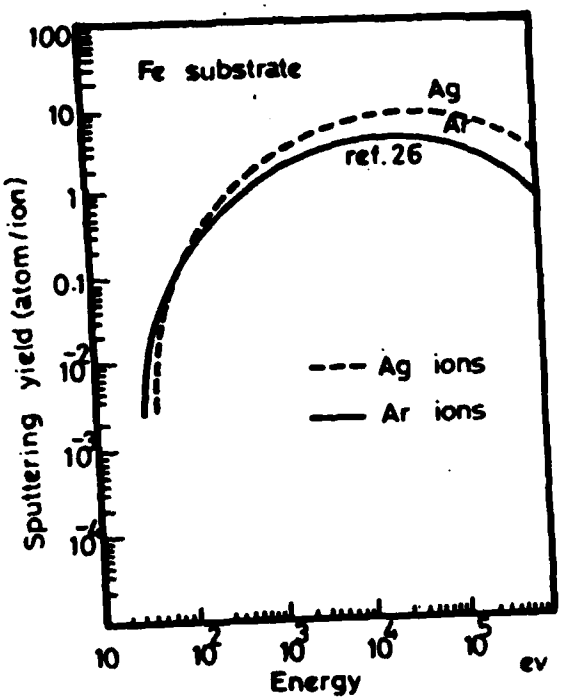

Fig. 2.6 SPUTTERING YIELD-ENERGY RELATIONSHIP FOR PLASMA IONS.

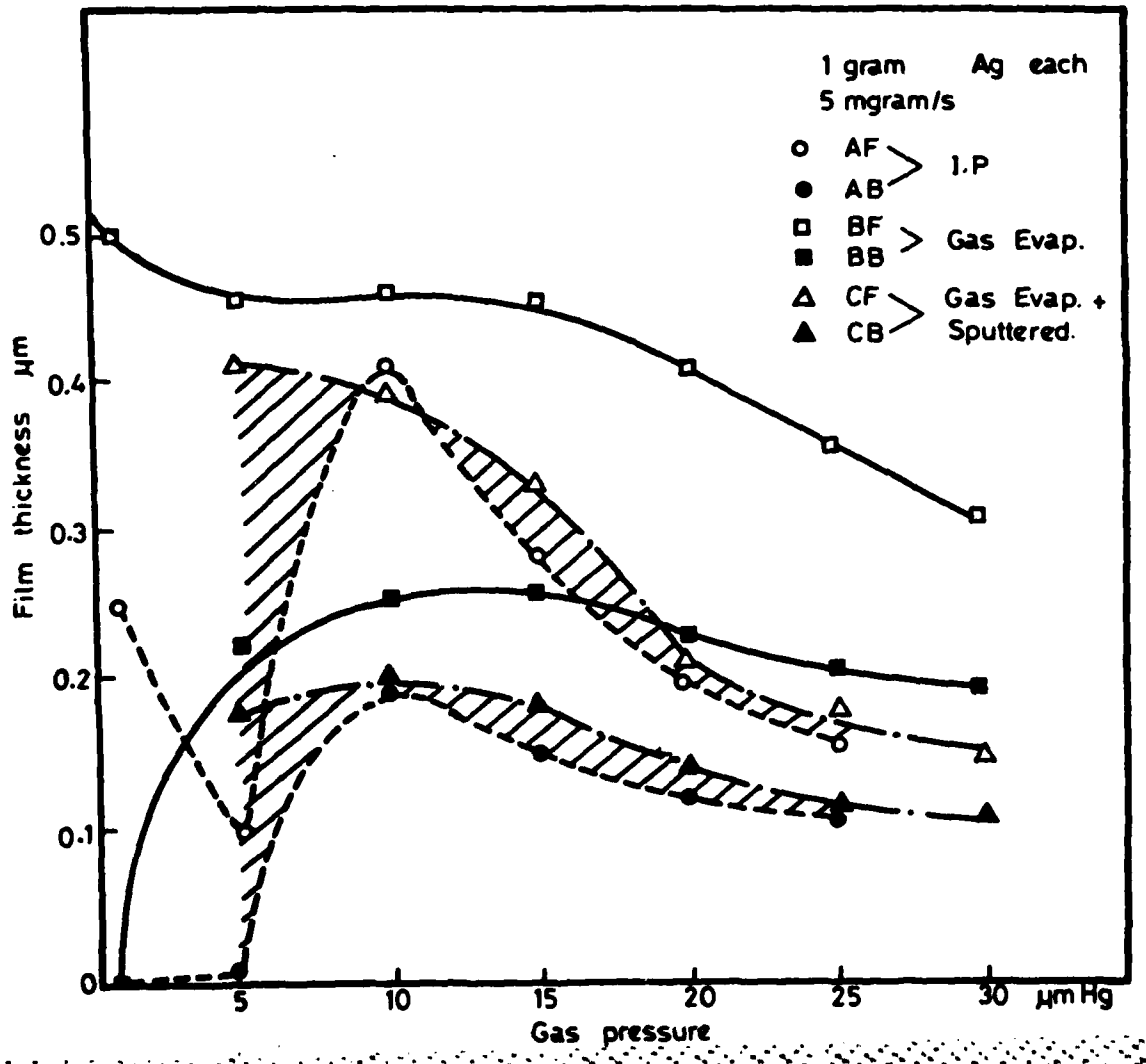

with direct recoils and reflected recoils of substrate atoms and ejection of adsorbate atoms by reflected primary particles. In typical ion plating systems of few hundred electron volts, the adsorbate atoms are sputtered as part of the general flux of sputtered substrate atoms, and their sputtering yield is expected to be similar to or smaller than the matrix sputtering yield. It is therefore important that residual gas levels be minimized to avoid the militation of the adsorbed gas against film growth or structure.

The equicibrium surface impurity concentration n_e can be obtained by considering the gas adsorption kinetics (28) and is expressed as ;

$$n_e = \frac{\gamma K_p}{J \bar{\sigma}_d} \quad \text{for} \quad n < n_s$$

where J is the total energetic particle flux

n_e surface impurity concentration at equilibrium

γ sticking coefficient of given impurity

K_p Molecular impingement rate per unit surface area at a pressure (P)

For an active gas partial pressure of 10^{-6} torr, $K_p = 10^{15}$ $cm^{-2}S^{-1}$. Assuming an average bombardment induced gas desorption cross section of 10^{-15} $cm^2 ion^{-1}$, then for a discharge current to substrate of 10 mA cm^{-2} (10^{17} particles $cm^{-2}S^{-1}$) $n_e = 10^{13}$ atoms $cm^{-2} = 10^{-2}$ monolayer. It is apparent that there will be 1% impurity in every coating monolayer formed. This leads to the conclusion that in

order to reduce the fractional impurity incorporation rate, the flux density of energetic impurities must be reduced relative to that of the coating flux. This can be achieved by thorough degassing of the whole system and by using high speed vacuum pumps.

2-6-3 Energetic particle entrapment

When an energetic atom approaches a surface both attractive and repulsive forces operates depending on the separation, but these must be integrated over all atoms of the solid and particularly those of the surface. In this context an energetic ion may be treated as an atom since charge neutralizatiot is generally a very effective process near a surface . It follows that the energetic atom moves from infinity towards the surface, it accelerates and passes through the potential well and is then treated as it approaches more closely the atomic surface plane. If the initial energy of the atom is insufficient to enable it to pass through the surface plane the atom sill reflect back outwards towards the potential minimum. During such repulsive phase, the surface atoms will recoil and dissipate lattice wave energy into the solid, and therefore the impinging atom recoils with reduced energy. If this recoil energy is low and the potential well outside the surface is deep there can be high propability of atom condensation or accommodation on the surface. This process is

expected to be efficient for chemically active incident atoms and inefficient for incident inert gas atoms.

If the incident particle kinetic energq is sufficient to allow penetration of the atom beyond the surface plane, then entrapment may occur within the solid for light inert gases this entrapment will generally occur at lattice vacancies, whilst for heavy ions non-substitutional dissolution may occur. Having passed from the surface plane, the incident particles will suffer further collisions with atoms of the solid, thereby losing energy and suffering directianal changes. Particles much lighter than the solid may therefore suffer sufficient collisions and gain reversal momentum to exit back across the surface, while heavier particles (coating) will generally come to rest within the solid, at depth of the order of 50 A^0.

Substantial experimental evidence (32-36) exists for trapping probability density close to one for incident particles having low energq within the range 1-200 ev. Thus the self-trapping coefficient of plating atoms may be safely assumed to be close to unity. On the contrary Carter (28) derives an approximate value for trapping probability density of supporting gases $\eta(E)$ less than 0.1 for particle energy E <100 ev. He states that this trapping mode can be more effective for gases lighter than argon and less effective for heavier gases. It can therefore be concluded that for many plating species $\eta(E) = 1.0$

whilst for the energetic support gas species $\eta(E)$ is much less than unity.

2-6-4 Energetic atom sputtering

The Energetic plating species, depending on their energy, would have either to penetrate and be trapped into the solid torget, or (if they have insufficient energy) lose energy, reflect back and condensate on the surface af the target, with a low binding energq U_o.

Subsequent bombarding particles enter into the solid, suffer a series of collisions, lose energy and transfer recoil energy to the target atoms. If this energy is sufficiently large and grater than the displacement energy for dynamic recoil target atoms may be temporarily or permenantly displaced from their lattice positions, creating target defects. The first generatian or primary recoils may go on to form further generation of recoil or a cascade. If some recoils in this cascade are near-surface atoms and receive energy greater than the surface binding energy U_o, the low energy deposites can be sputtered back and therefore the coating thickness is built up of moderately high energy species . One however may decide for a reasonable sputtering yield which is less than the deposition rate or otherwise the film will never form or grow.

2-6-5 Atomistic mixing

Apart from direct penetration and implantation of a fraction of the plating atom flux initially into the substrate and subsequently into the growing film, one can expect interfacial mixing due to a number of other possible mechanisms. These are :

1- Thermal interdiffusion of coating and substrate atoms as a result of the energy dissipated into the target and the subsequent rise in target temperature.

2- The increased population of lattice defects due to recoil events between incident particles and target. If these vacancies generated by lattice-atoms displacement are highly mobile then radiation-enhanced diffusion occurs.

3- The generated target-atom recoils can move such atoms for short distances at high frequency thereby allowing both film and substrate atoms initially and film atoms alone at a later stage to mix effectively by what is known as casced mixing (37) .

2.7 Gas scattering

Unlike vacuum evaporation, ion plating is claimed to give good coverage on surfaces out of line of sight of the vapour source. Mattox (38) gives details of the thickness distribution of material ion plated over the outer and inner surfaces of 12 mm diameter tube held with its axis normal to the main direction of the vapour stream. Champers and carmichael among others(39-41) studied the throwing power and reported the dependence of coating deposition rate on gas pressuse.

Earlier papers on ion plating (1,14,41) attributed the good throwing power to ionised vapour atoms following the field lines to all parts of the surface. However as indicated earlier, the ionization efficiency is low and can not account for coating of internal surfaces as claimed.

The authors therefore searcred for other possible reasons such as gas scattering (9,12and 40). A study of the variation of thickness with gas pressure on the front and back surfaces of flat test specimens (5x5 cms) was then made. In there tests two sets of specimens were coated by ion plating and gas evaporation in argon atmosphere. The mean film

thickness on front and back surfaces of each specimen was measured, and the results were plotted in figure 5.7, where Curves A_f and A_B are made for the ion plated films front and back thicknesses respectively while Curves B_F and B_B are the corresponding curves for the gas evaporated films . The gas evaporated films were then sputter etched under typical ion ploting conditions for the same deposition time, and the mean film thickness was again measured for both the front and back surfaces. These results are shown on the same figure by Curves C_F and C_B .It is shown that at high gas pressures ($\geq$10 μm Hg) curves A_F and A_B are very close to Curves C_F and C_B respectively. This indicates that the major effect in defining the film thickness at the back surfaces is gas scattering and not the ionization phenomena as previously claimed. Furthermore the present effect of ionization is to reduce the thickness of the coating by ion bombardment.

The preceding results favour the use of high gas pressures to achieve a high throwing power during the coating of components having complex shapes, while the preceding discussions of section 2.3.2 suggests a reduced argon gas pressure during deposition for minimization of trapped gases and their consequences on thickness build up and film morphology.

A compromise is therefore to be made in each coating application as to whether the gas pressure should be increased or kept at a reasonably low value.

CHAPTER 3

FACTORS AFFECTING ADHESION

The word adhesion is frequently used in broad sense to describe sticking together of two materials with or without interfacial layer. Homohesion and Hetrohesion, however, are used to describe the two situations in which, the two metals are either indentical or dissimilar respectively (42). It generatly describe how a film and a substrate remain in contact, while the word bonding is used to refere to specific interactions across the interface.

In a recent review paper(43), the authors showed that the factors influencing adhesion can be summarized as follow:

a- The deposition technique as influencing the nature and type of the interfacial layer .

b- Substrate surface and gross contamination as affecting film nucleation

c- Nucleation as affecting stress concentration in the interfacial region.

d- Interface formation and type as determining the bonding mechanism.

The first two factors are obvious and therefore are discussed herein after, while the other two factors need further detailed studies and therefore are dealt with in chapters three and four.

There exists sufficient evidence in the literature (2,4-6,44) to show that the deposition technique plays an important role in determining the nature and type of the interfacial region. The initial state of the surface, and the energy of the depositing atom is particulary important for considerations regarding penetration, bonding and diffusion. In table 3.1 three well known and estableished techniques are compared with ion plating with particular reference to factors affecting interface formation and bonding.

Atomically clean surfaces are those surfaces free of all but a few percent of a single monoloyer of foreign atoms either adsorbed on or substitutionally replacing some surface atoms of the parent lattice. One monolayer of contaminants coverage is actually formed in two seconds at 10^{-6} torr and 25 $^{\circ}$C . Therefore both vacuum and sputtered coatings suffer from lack of intimate contact with the substrate due to surface contamination. In ion plating, however, the surface is maintained atomically clean by ion bombardment. Furthermore it has been shown in (2.6.2) that gas desorption is less than 1% in each monolayer and this can be further reduced by proper selection of supporting gas atoms.

The lack of intimate contact across the film-substrate interface can be partly attributed to the presence of gross contomination, physically adsorbed gases, chemisorbed gases and compound layers.

Gross contaminations with substances such as grease, oil and dirt are quite detectable, with normal cleaning procedures being liable to render such layers. Physically adsorbed gases are usually bound to the substrate with 0.1-0.5 ev (45) , while chemisorbed gases and compound layers are normally bound with 1-10 ev(46,47). Unlike sputtering and the sputter cleaning of the ion plated films, low thermal energy atoms deposited by converntional methods are incapable of affecting most of these contaminating layers . In sputtering, the kinetic energy of the depositing particles is comparable with the binding energy of adsorbed gases. It is therefore possible that the process affects the state of the surface, but not necessarily assured. In ion plating, however, the kinetic energy of the impinging particles is much higher than the binding energy of the substrate atoms. Fresh and atomically clean surfaces are thus generated prior to and during film deposition.

Property	Vacuum and gas deposition	Electroplating	Sputtering	Ion plating
Surface precleaning	Requires extensive precleaning	Requires extensive precleaning	Requires extensive precleaning	Regular precleaning only as the sputter etching process ensures atomically clean surfaces prior to film deposition
State of the surface during deposition	Can be maintained only in high vacuum of 10^{-9} torr	Contaminated with chemical compounds	Contaminated as the deposition pressure is high	Maintained atomically clean by continuous ion bombardment
Type of interface	Mechanical interlocking and Monolayers	compound	diffusive	Graded by atomistic mixing
Mismatch of physical parameters and residual stresses	Mismatched physical parameters across the interface	High residual stresses	Mismatch of physical parameters	intermetallic alloy with gradual change of properties
Deposition energy	1.0 ev	0.1 ev	10-100 ev Sufficient to cause bulk diffusion	100-500 ev Sufficient to cause penetration and entrapment
Surface defects and voids aiding interdiffusion	No.	No.	No.	Generated by ion bombardment
Thermal diffusion	Very limited and require external heating	No.	Limited and require supporting external heating	Self induced due to energy dissipation in substrate

Table 3.1 Comparison of factors affecting the interfacial layer

CHAPTER 4
NUCLEATION OF ION PLATED COATINGS

4.1 Introduction

Stress concentrations in the interfacial region result from imperfections such as voids, microcracks, and loss of intimate contact. These are determined by the mode of nucleation and nuclei density and are reflected on the structure of the interface, thereby affecting film-substrate adhesion.

This chapter is concerned with the role played by high energy particles in the nucleation of the ion plated films, which in turn influences the film-substrate adhesion, especially in situations involving mutually incompatible materials.

4.2 Selection of a proper technique

Because of the high resolution needed for the study of such phenomena, transmission electron microscopy is generally used (48). Unfortunately the ion plating process necessarily requires a gaseous plasma at a pressure of at least 10 μm Hg. Consequently the tradational advantage of being able to examine the film during deposition inside the vacuum column of the microscope has been lost. One limitation, however in using the transmission microscope is that the film substrate must be thin enough to allow direct transmission. On several occasions, it has been found impossible to detach the ion plated film from the substrate . An ultimate solution is therefore to find a suitable dissolvable substrate.

One way of overcoming such difficulties is to use a vacuum-cleaved NaCl (49) . Substrate, which can be easily dissolved in water. The main disadvantage of this technique however, is the problem associated with Ultrathin island deposits which can not support themselves after dissolution of the substrate. In the present work a thin carbon film (50 A thick) is used (50).

4.3 Experimental

The substrate was made of 0.1 x 0.02 m glass sheet onto which a carbon film, 50 Å thick, was deposited by arc evaporation of carbon in vacuum. Because of the smooth surface of the glass sheet and the poor adhesion of the vacuum deposited carbon film, the film can be easily detached from the substrate at any stage by wetting the glass sheet with distilled water. The high porosity of vacuum deposited carbon assists the action of water surface tension in separating the film.

Silver of purity 99.99% was deposited onto the substrate specimen (carbon coated glass) by three different techniques, in such a way that when the carbon film was detached from the glass it could still support the deposit. Since carbon is amorphous and the carbon film is thin, the presence of such a film is not expected to affect the transmission results in any way. The ion plating apparatus was used for depositing ion plated, conventional gas deposited

and vacuum deposited films. The high tension diode system was therefore used only when ion plated films were required . The carbon-coated glass substrates were mounted at a fixed distance of 0.16 m from the evaporation source. The deposition rate was kept constant throughout these investigations at 0.05 mg S^{-1}. The processing parameters are shown in table 3.1 for different test specimens .

Owing to the fact that the carbon film was so thin and ion bombardment of the coated substrate might have resulted in sputtering the bulk of the poorly adherent carbon film, the sputter cleaning part of the ion plating process was completely cancelled. Therefor the field was switched on only when the evaporation of silver was started.

The average size of the nuclei was estimated from the transmission micrographs and the average film thickness was estimated both from the amount of metal evaporated and from the volume of the deposit, assuming spherical nuclei. The average values for each micrograph are quoted in the relevant caption.

Sample no.	Deposition technique	weight evaporated (mg)	Bias voltage (KV)	Gas pressure (μm Hg)	Vac uum torr
1	Vacuum deposition	0.1	——	——	10^{-5}
2	Gas deposition	0.1	——	12	——
3	Ion plating	0.1	2	12	——
4	Vacuum deposition	0.2	——	——	10^{-5}
5	Gas deposition	0.2	——	12	——
6	Ion plating	0.2	2	12	——
7	Vacuum deposition	0.5	——	——	10^{-5}
8	Gas deposition	0.5	——	12	10^{-5}
9	Ion plated	0.5	2	12	——

Table 4.1 Experimental conditions for ion plated, gas, and vacuum deposited films.

4.4 Results

Figure (4.1) shows the electron micrographs obtained for vacuum deposited films. It is seen that vacuum-dposited films behave in the now well known liquid-like behaviour, namely the nuclei density first increases and then decreases during the nuclei growth.The early nuclei are usually rounded (Fig. 4.1 a) but they exhibit sudden changes in when two join together(Fig. 4.1 b). As the unclei growth continues, the average nuclei size increases from, 260 °A by either surface diffusion or by the coalescence of the near neighbouring nuclei. The final deposit (Fig. 4.1 b) appears to be a network of grown nuclei with some open areas. As the film continues to build up (homoepitaxial growth), twin bands and st stacking faults are rapidly initiated, they spread over the

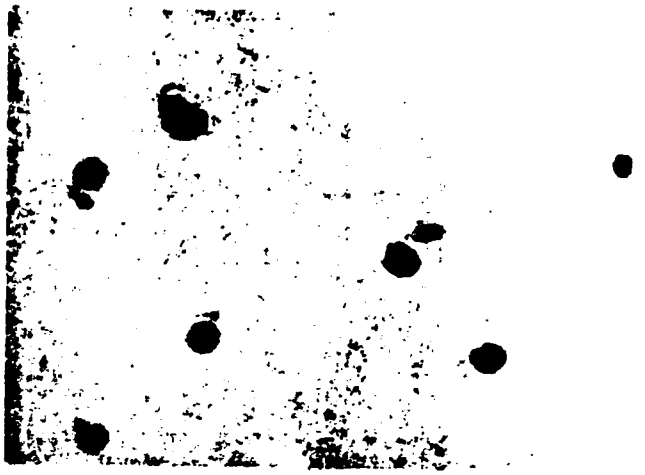

(a) 10 Å

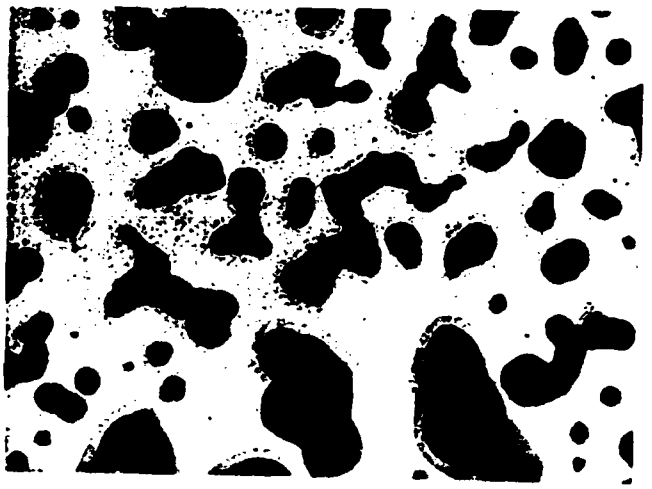

(b) 200 Å

(c) 400 Å

FIG. 4.I NUCLEATION, EPITAXIAL & HOMOEPITAXIAL GROWTH OF VACUUM DEPOSITED FILMS

entire surface crystals as shown in Figure 4.1.c.

Figure (4.2) shows the nucleation and growth of silver films as deposited in gas atomosphere (12 μm Hg argon). The presence of gas scattering appears to be strongly influencing the behaviour of the film. The most significant effect is the fine nuclei size (130 A°). The nuclei retained the same liquid-like behaviour. The deposit appears to be more uniform(compare figures 4.1 b and 4.2 b) resulting in less pronounced islander form and much less open areas. The increase in nuclei size during the epitaxial growth, however, is relatively low (15%) as compared with the increase in the nuclei size of vacuum deposited films (50%). During the homoepitaxial growth(Figure 4.2 c), the stacking faults and the twin bands disappeared, and the deposit is apparantly uniform with fine grain structure, but relatively discontinouns (compare figures 4.1 c and 4.2.c).

Figure (4.3) displays the nucleation of the ion-plated films, which unlike the conventional films, exhibit a very distinct behaviour. The nuclei size is considerably smaller (100 A°) and the nuclei density is the highest of the three different deposits(compare figures 4.1 a,4.2 a and 4.3 a). The nuclei enjoy a uniform distribution over the entire surface of the substrate without significant coleascence or 1 liquid-like behaviour. The nuclei remain rounded during the entire time of epitaxial growth without significant changes

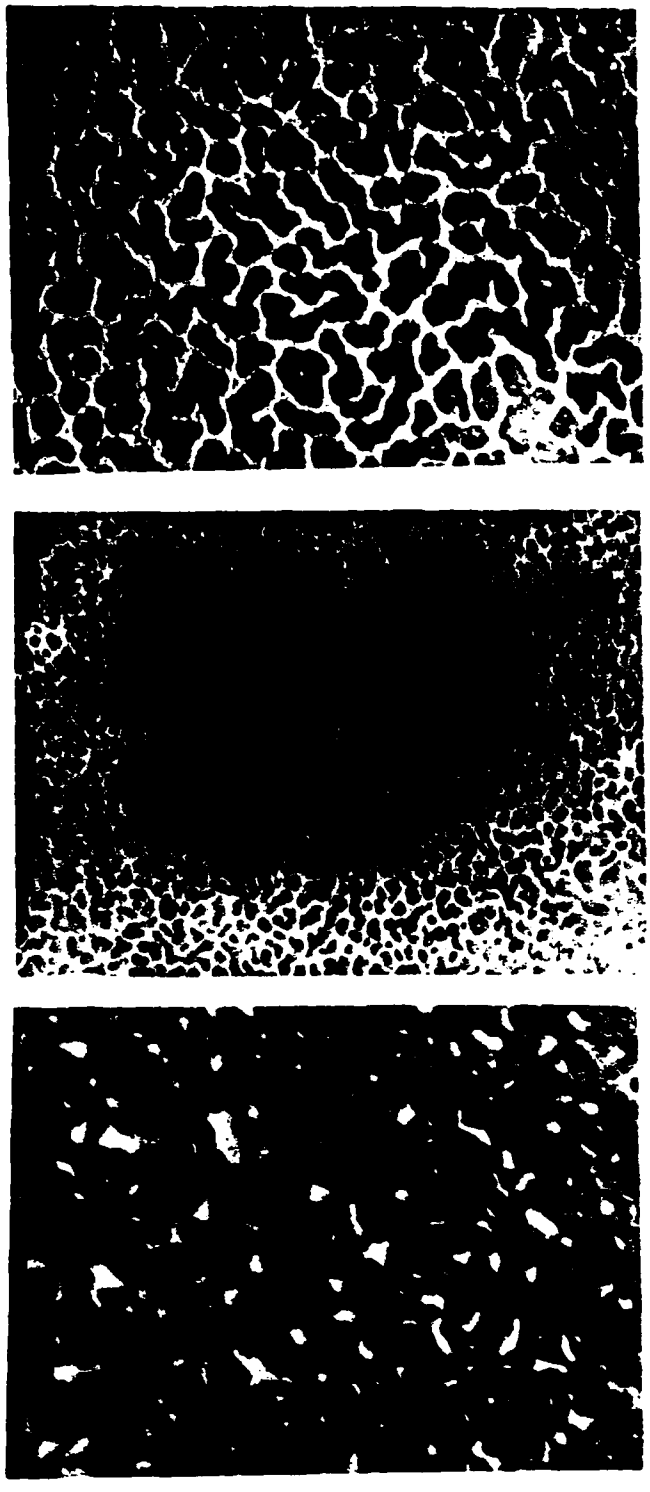

(a) 50 Å

(b) 100 Å

(c) 200 Å

FIG. 4.2 NUCLEATION, EPITAXIAL &HOMOEPITAXIAL GROWTH OF SILVER FILMS DEPOSITED IN 12 μm Hg ARGON ATMOSPHERE (X150 000)

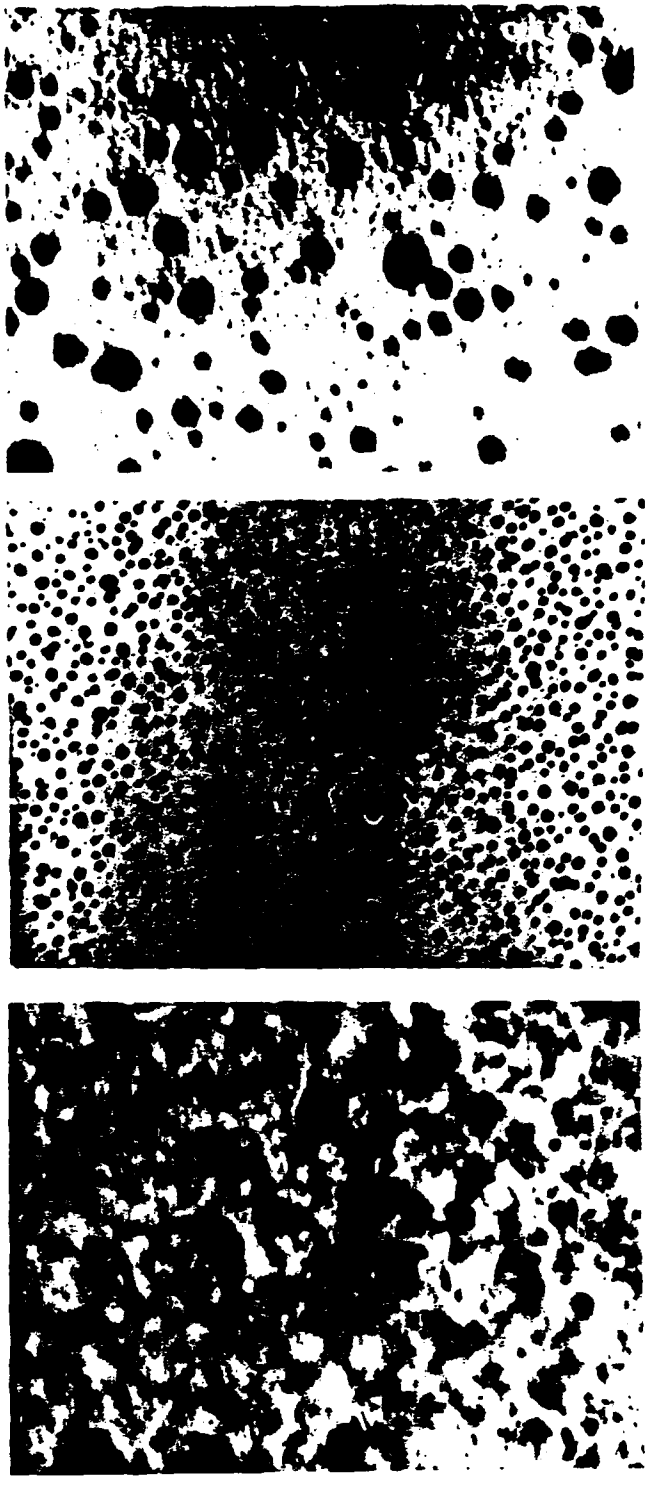

(a) 40 Å

(b) 80 Å

(c) 120 Å

FIG. 4.3 NUCLEATION, EPITAXIAL & HOMOEPITAXIAL GROWTH OF ION PLATED FILMS (X150 000)

in diameter(Figure 4.3 a and 4.3 b). This would imply that the basic deposition mechanism is forming new nuclei or depositing onto previous nuclei thus resulting in columnar growth. A continuous film is observed at about 130 °A thickness(Figure 4.3 c) which is considerably thinner than that of the discontinuous gas-depo-sited film(200 °A) shown in figure (4.2 c). The final grain size is about 16% higher than that of the initial nuclei size.

DISCUSSION

Basset et al (48) put forward an argument based on the classical theory of frankel, that in vapour deposits, atoms arrive on the substrate surface and move freely for some finite time, during which they can collide with other deposited atoms, form pairs of longer life amd act as nucleus for further collissions. The argument is shown to hold for vapour-dposited films either in vacuum or in gas atmosphere. Vapour deposited films made by ion plating, however, are different. The high energy particles(ions and atoms) arrive at the substrate with energy, high enough to cause particle implatation into the substrate at the localized points of bombardment. The high energy particles loose their energy in patticle implantation rather than in free motion on the substrate surface .

Because of the low ionization efficiency of the ion plating process, atoms are expected to arrive at the substrate

with a range of energies including some low energy atoms. These low energy particles are not expected to be implanted into the surface and may behave according to Basset's(48) argument. The continuous ion bombardment of the substrate during ion plating, however, may result in sputtering back such poorly adherent free atoms. Thus, the final deposit at any stage will be the implanted high energy particles. This is evident from the distinct nature of the results obtained on the nucleation of the ion plated films(compare figures 4.1, 4.2 and 4.3).

The old theory of preferable nucleation, namely that for vapour deposited films, the early nuclei take place at selected surface sites (2) lattice steps, point defects, and vacancies(49) is seen to hold true for the results presented in figures(3.1) and (3.2). In these particular cases, few nuclei took place at randum points which do not correspond to the uniform distribution of the arriving atoms through the uniform vapour stream. On the other hand, the uniform nucleation over the entire area of the substrate as shown in figure(3.3) for the ion-plated films suggest either a rather uniform ion-implantation independent of surface defects or otherwise preferential nucleation at newly generated surface defects produced by uniform ion-bombardment.

In the present work, water cooling of the substrate was of negligible effect owing to poor conductivity of glass.

Terefore, the influence of substrate temerature on the nucleation mechanism must be considered. It is generally accepted that the measurement of substrate (H.T. cathode) temperature in the ion plating apparatus is somewhat difficult. The problem is even more complicated, when the substrate su surface layer of maximum temperature is very thin (50 °A carbon film). However, because of the low ion energy (10 watt/sec) and the short time of deposition (2 sec), the substrate temperature is not expected to be considerably high, specially with the high surface to volume ratio the carbon film.

CHAPTER 5

ATOMISTIC MIXING AND INTERFACE FORMATION

5.1 Introduction

The strength of the interfacial region largely depends on the type of interface with particular reference to the bonding mechanism(e.g. Physical, chemical or mechanical). The film-substrate interfaces formed by coating techniques can be classified into the following categories:

a) Mechanical interlocking

When soft low melting point metals or materials of high surface mobility(Such as cadmium) are deposited onto porous substrates, the film material fills the pores and mechanical interlocking provides reasonable adhesion.

b) Monolayers

Monolayer to monolayer interfaces are reported in situations where there is no diffusion of the depositing atom into the substrate surface, while little chemical reactions are taking place between the two parent metals(2). In such cases an abrupt change from the film to the substrate material is observed in a distance of the order of the spacing between atoms(2-5 °A). The adhesion strength is, therefore, governed by the physical interactions and van der waals forces yield the lower bound estimates(42).

c) Compound interfaces

In electroplating, chemical interactions taking place at the film-substrate interface result in either intermetallic compounds or other chemical compounds, such as oxides.

These are known as compound interfaces and are characterized by constant composition over several lattice parameters in thickness. The compound itself is usually brittle and can well be unstable under different conditions.

d) Diffusion interfaces

Diffusion interfaces are formed in situations involving some degree of solid solubility between the two parent metals. Furthermore, the deposition technique must provide enough kinetic or thermal energy for film atoms to overcome the actiration energy for bulk diffusion(1-5 ev). The diffusion interface is characterized by a grodual change in lattice parameters, across the interfacial region, which is usually thousands of angstroms in thickness. The adhesion is therefore enhanced by the diffusion mechanism.

e) Extensive graded interfaces

When a high energy particle impings on a surface, if penetrates into the substrate lattice withoud need of a diffusion mechanism. Experiments involving ionization and acceleration of ions towards the substrate indicate penetrations of the order 0.1 50 °A per kiloelectron volt(51). The adhesion can thus be greatly improved by atom and ion implantations. On the basis that the particle impinging on the substrate may ponetrate into the lattice without need of a diffusion mechanism, this was called "pseudo-diffusion interface (2). Atomistic mixing of sputtered atoms and film atoms, however, provides a graded type interface (52). Combinations

of these mechanisms and the thermal diffusion mechanism may result in extensive graded interfaces with or without intermetallic compounds (2,52 & 53).

This chapter is devoted to the experimental study made on different metal pairs of different solid solibility to examine the conditions leading to the formation of such extensive interfaces.

5.2 Experimental

Thirteen groups of test specimens were prepared under different processing conditions on thirteen different metal pairs. Twenty processing conditions were selected for each matal pair. These included low energy deposition starting with 10 μm Hg argon and 2 kv bias voltage on water cooled substrates at bulk substrate temperature of 80 °C, as well as high energy deposition at 50 μm Hg argon, 5 kv bias voltage on uncooled substrates at 500 °C . The different metal pairs which were used in this mini-program are shown in table 4.1 while the processing conditions selected for any metal pair are shown in table 4.2. In all cases the coated test specimens were sectioned for optical microscopic examination, x-ray diffraction, microprobe analysis. In few cases Auger electron spectroscopy was made in other laboratories for our test specimens.

Metal pairs		Metal pairs	
Substrate	Film	Substrate	Film
Ti	Al	Ni	Ag
Ti	Sn	Ni	Cu
		Ni	Pb
Fe	Ag		
Fe	Al	Cu	Al
Fe	Pb	Cu	In
Fe	Sn	Cu	Ag
Fe	In	Fe	Zn

Table 5.1 Metal pairs used for testing the interface formation

In these Auger tests, the substrate was lapped to specularly smooth finish and the surface finish was measured by Taylor-Hobson talysurf-4. The sputter etched substrates were also checked for changes in surface texture parameters. The surface of the coated test specimen was also checked for changes in surface topography and then polished to be as smooth as possible, before final assesment of surface roughness.

In the sectioning tests, however, a hard retainging layer was usually electroplated on the top of the coating to facilitate proper plishing of the section.

Specimen no	technique	Sputtering phase				Deposition phase				evaporation rate mg/S	Remarks
		Argon pressure (μm Hg)	Bias voltage (KV)	Time (60s)		gas pressure (μm Hg)	KV	Subs. temp. (°C)	Time (S)		
1	ION PLATED	—	—	—	Just polished	10	2	50	30	.05	
2		—	—	—		10	2	80	60	.08	
3		—	—	—		50	5	150	30	.05	
4		—	—	—		50	5	180	60	.08	
5		—	—	—		50	5	150	20	.08	
6		30	3	20	Polished/etched	10	2	100	30	.05	
7		30	3	20		50	5	210	30	.05	
8		50	5	30		10	2	200	30	.05	
9		50	5	30		50	5	290	30	.05	
10		50	5	30		50	5	290	30	.1	
11		30	3	20		20	4	80	multi evaporations	.1	
12	Gas deposited	—	—	—		10	—	30	30	.05	cooled down before dep.
13		30	3	20		10	—	30	30	.05	"
14		50	5	30		10	—	30	30	.08	
15		50	5	30		50	—	80	30	.05	
16		50	5	30		50	—	120	30	.08	
17	Vacuum Deposited	—	—	—	10^{-6} torr	—	—	50	30	.05	10^{-6} torr
18		—	—	—		—	—	200	30	.05	
19		—	—	—		—	—	50	30	.08	
20								200	30	.1	

Table 5.2 Processing Parameters

5.3 Results

5.3.1 Optical examination and microprobe analysis

Fig. 5.1 shows the most extensive graded interface obtioned for indium film ion plated on copper substrate at 4 Kv and 20 μm Hg argon. It is shown that a thick region, 28 μm in thickness, of eutectoid In-Cu alloy is formed with α and γ phases, (of about 1μm thickness each) on sides. The total interface depth however is 30.2 μm, while the indium film itself is 12 μm thick. The composition of indium-copper interface is shown in figure 5.2 as obtained with microprobe onalysis using 5 μm probe diameter.

Figs. 5.3 and 5.4 shows the corresponding inderfaces of gas and vacuum deposited coatings as produced under the conditions no. 15 and 8 of table 4.1

Figure 5.5 shows a simmilar result for an extensive interface with an intermetallic compound for aluminium film ion plated on titanium substrate . In this case the intermetallic compound $TiAl_3$ extended over a depth of 25 μm , while the Al film itself was only 5 μm thick. The microprobe results shown in the same figure did not show any other stable phases but only gradual change in composition on both sides of the compound. Fig 5.6 shows the corresponding microprobe results obtained for specimens no. 16 and 19 of the same metal pair. Fig 5.7 shows the Sn-Ti interface (10 μm thick) obtained for specimen no. 8 . It was noted however that at very high energy

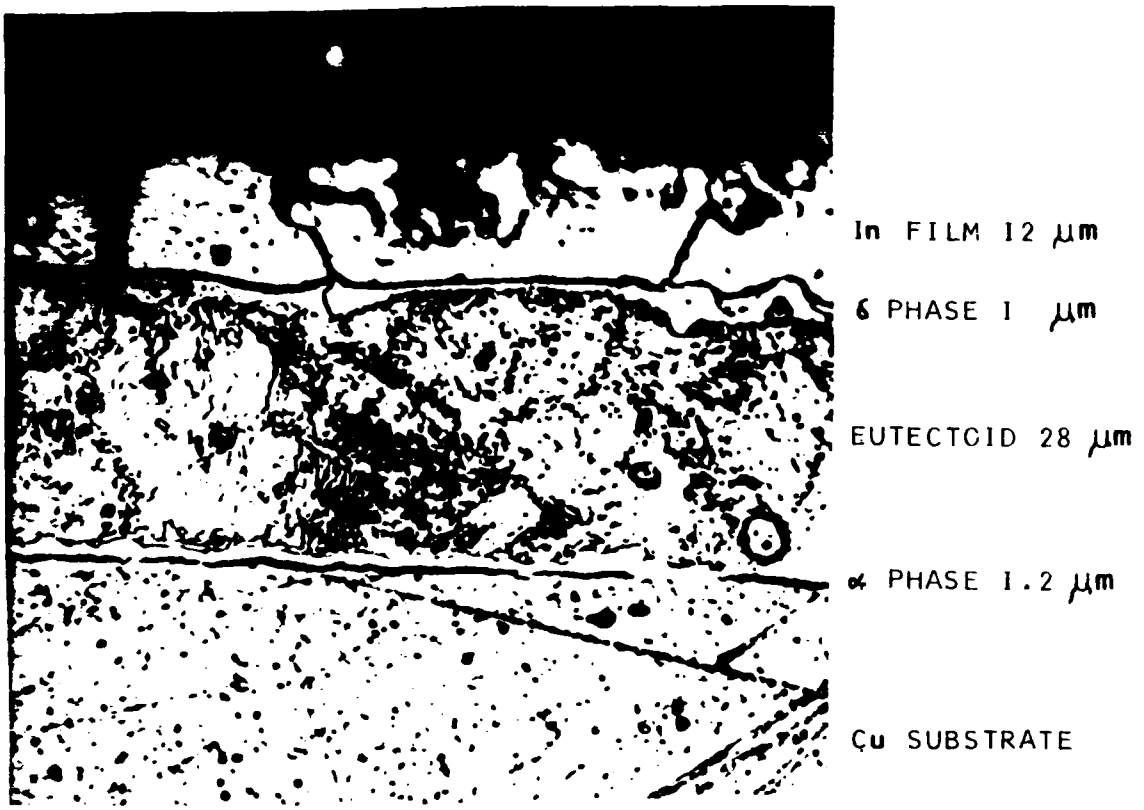

FIG. 5.1 ATOMISTIC MIXING AND INTERFACE FORMATION
In-Cu SYSTEM (4 KV, 20 μm Hg ARGON)

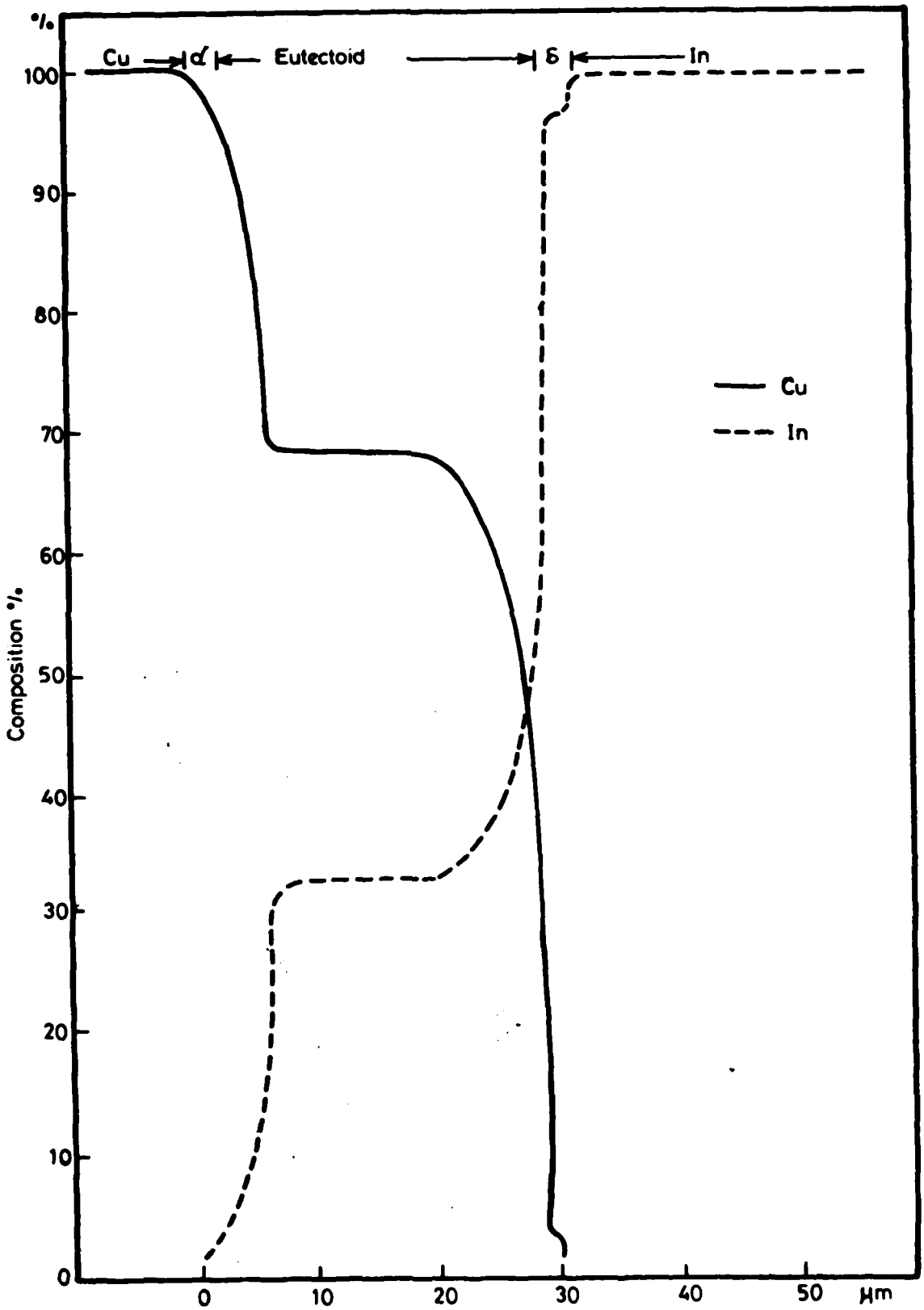

Fig. 5.2

MICROPROBE ANALYSIS SHOWING THE COMPOSITION ACROSS AN In-Cu INTERFACE (ION PLATED, FIG. 5.1)

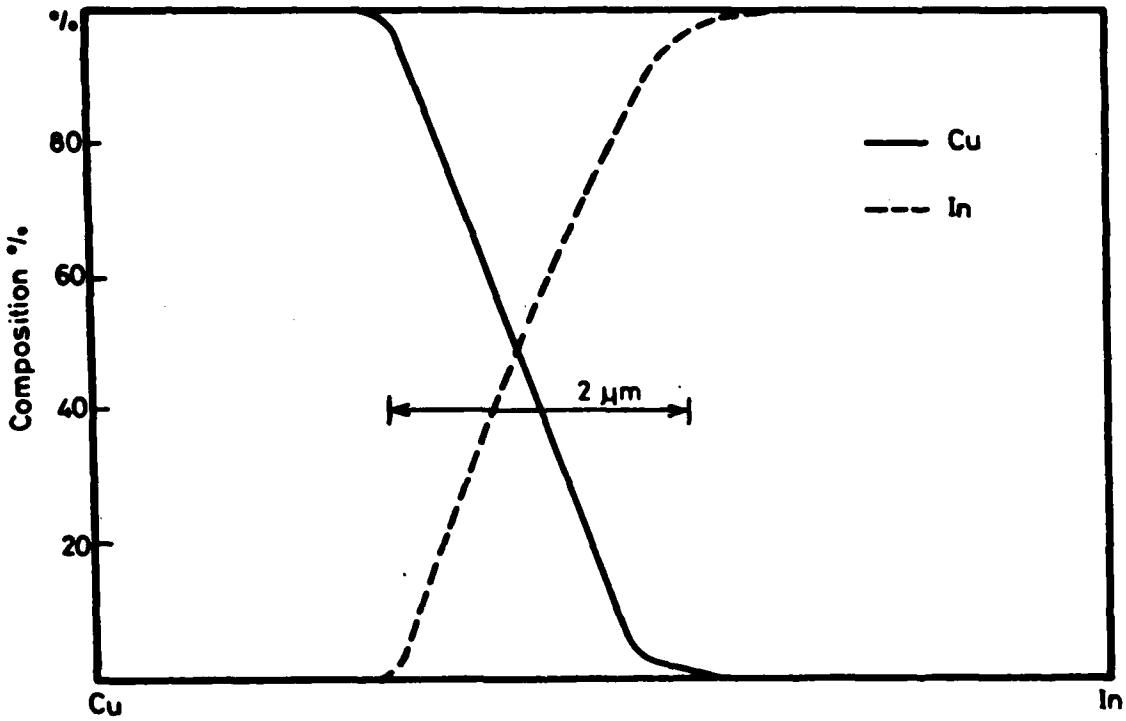

Fig. 5.3 MICROPROBE ANALYSIS OF VACUUM DEPOSITED INDIUM FILM ON COPPER (N.B. THIS RESULT IS ONLY QUALITATIVE BECAUSE OF PROBE SIZE)

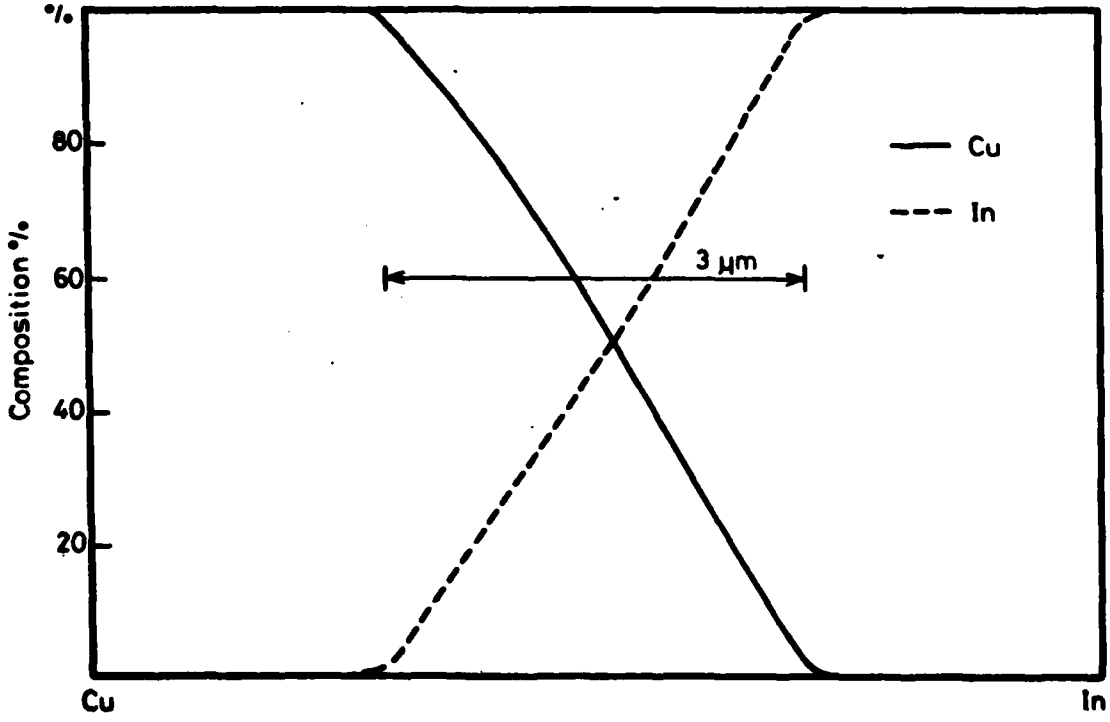

Fig. 5.4 MICROPROBE ANALYSIS OF INDIUM FILM DEPOSITED AT 40 MICRONE OF ARGON PRESSURE ON COPPER SUBSTRATE (QUALITATIVE)

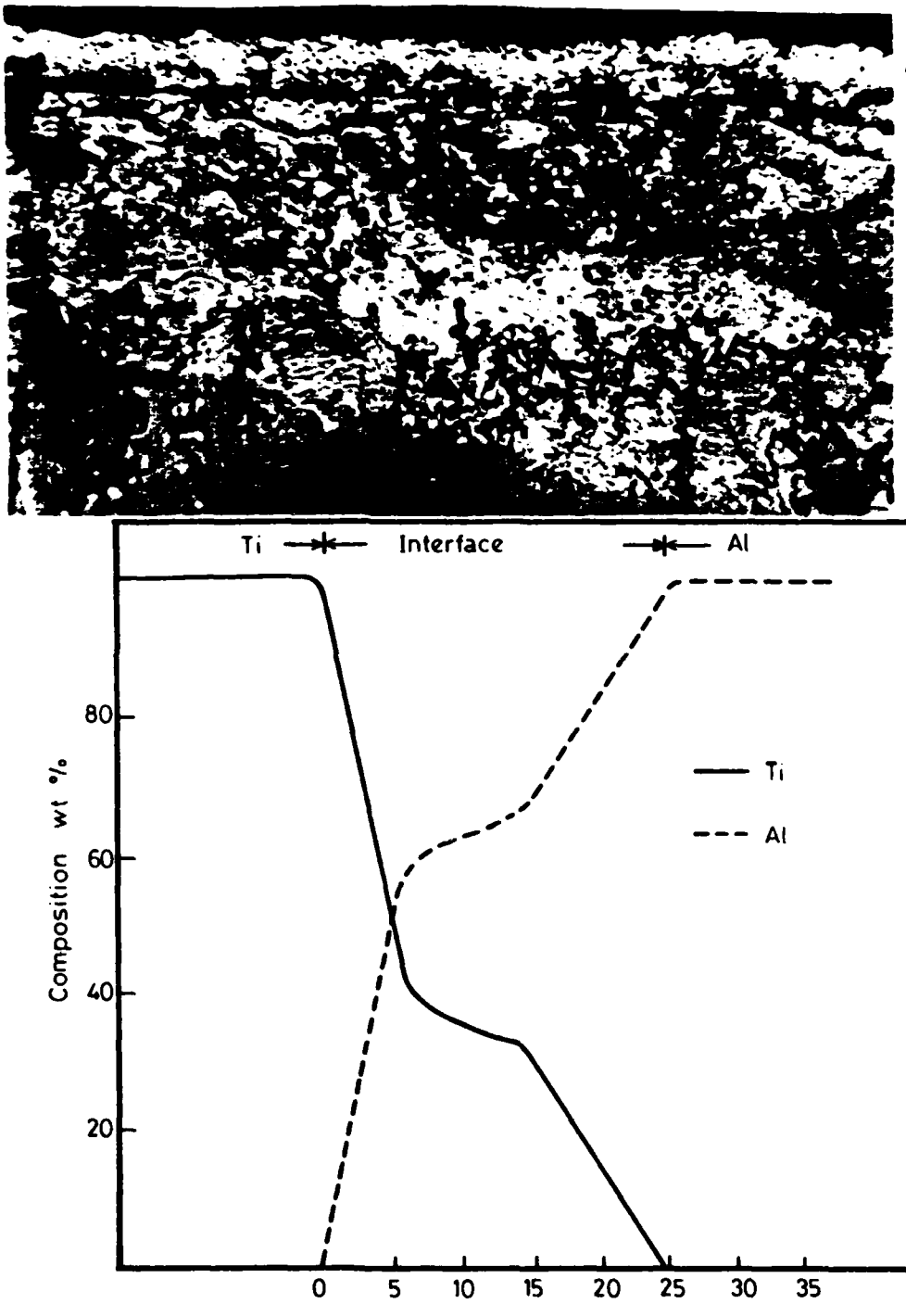

Fig. 5.5 MICROSTRUCTURE MICROGRAPH SHOWING AN ALUMINIUM- TITANIUM INTERFACE AND THE CORRESPONDING MICROPROBE COMPOSITION (ION PLATED)

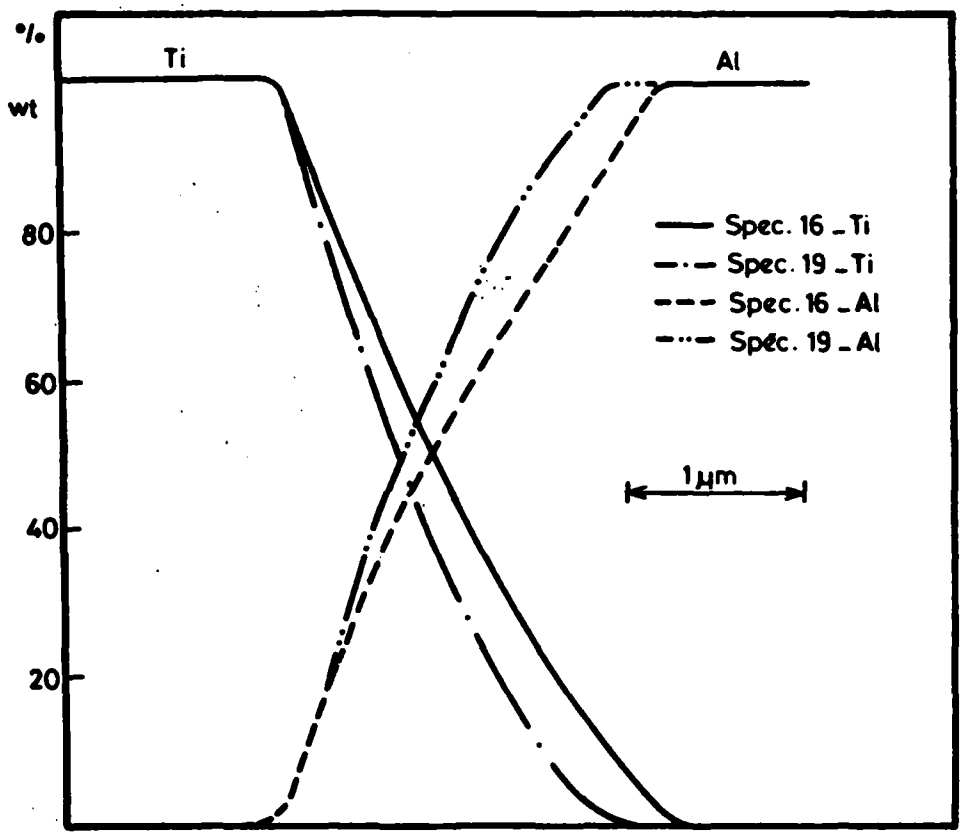

Fig. 5.6 MICROPROBE ANALYSIS OF SPECIMENS 16 & 19.

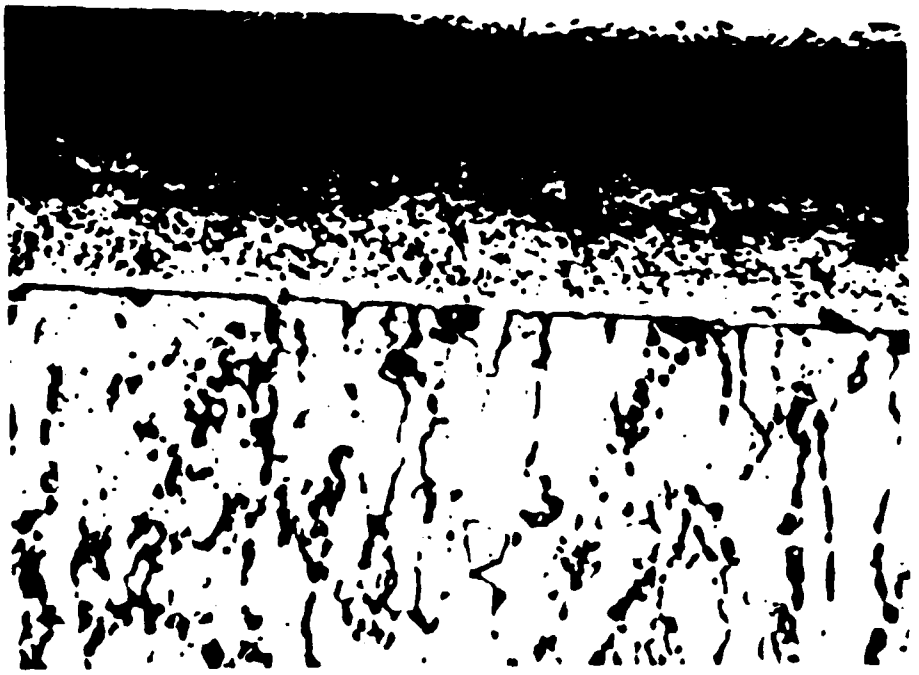

X1000

FIG. 5.7 MICROSTRUCTURE OF THE INTERMETALLIC COMPOUND OF ION PLATED TIN FILM ON TITANIUM SUBSTRATE.

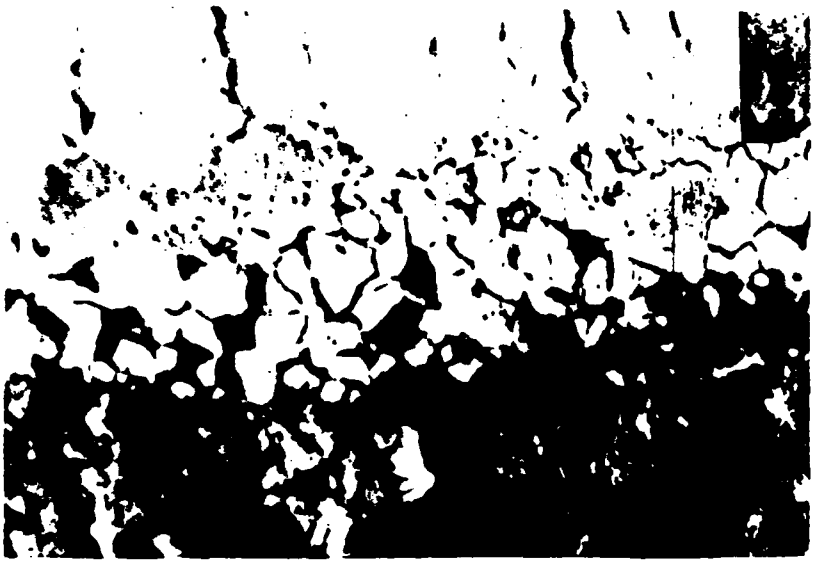

FIG. 5.8 BRITTLE INTERMETALLIC COMPOUND FOR ALUMINIUM-TITANIUM SYSTEM (CONDITION 10, TABLE 5.2)

particularly with titanium substrates, contaminations by Ti C_x and Ti O_x (carbides and oxides) was readily introduced within the interface. This usually results in a brittle intermetallic layer as demonstrated in fig 5.8 for an Al-Ti specimen prepared according to the conditions no. 10 of table 4.1

5.3.2 Scanning Auger analysis

Figures 5.9 and 5.10 show the Auger analysis of a Zn-Fe and Ag-Fe specimen as deposited by the two different techniques. While figures 5.11 and 5.12 show the results obtained for Ag-Ni and Cu-Ni systems respectively. Fig. 5.12 also shows the percentage contamination due to sputter etching of the Ni substrates.

5.3.3 Effect of plasma gas pressure

In the present investigation, it was generally noted that the depth of the graded interface can be increased by increasing the deposition energy. One way to achieve such high energy values is to increase the gas pressure. However increasing the gas pressure usually resulted in higher contamination levels of oxygen, carbon and nitrogen(up to 10%). Fig. 5.14 shows the effect of increasing the gas pressure from 10 to 50 μm Hg on the contamination atomic percent for both silver coated and uncoated copper substrate. Fig. 5.15 shows the corresponding gain in the interface depth as a percentage of the total thickness of both film and interface regions,.

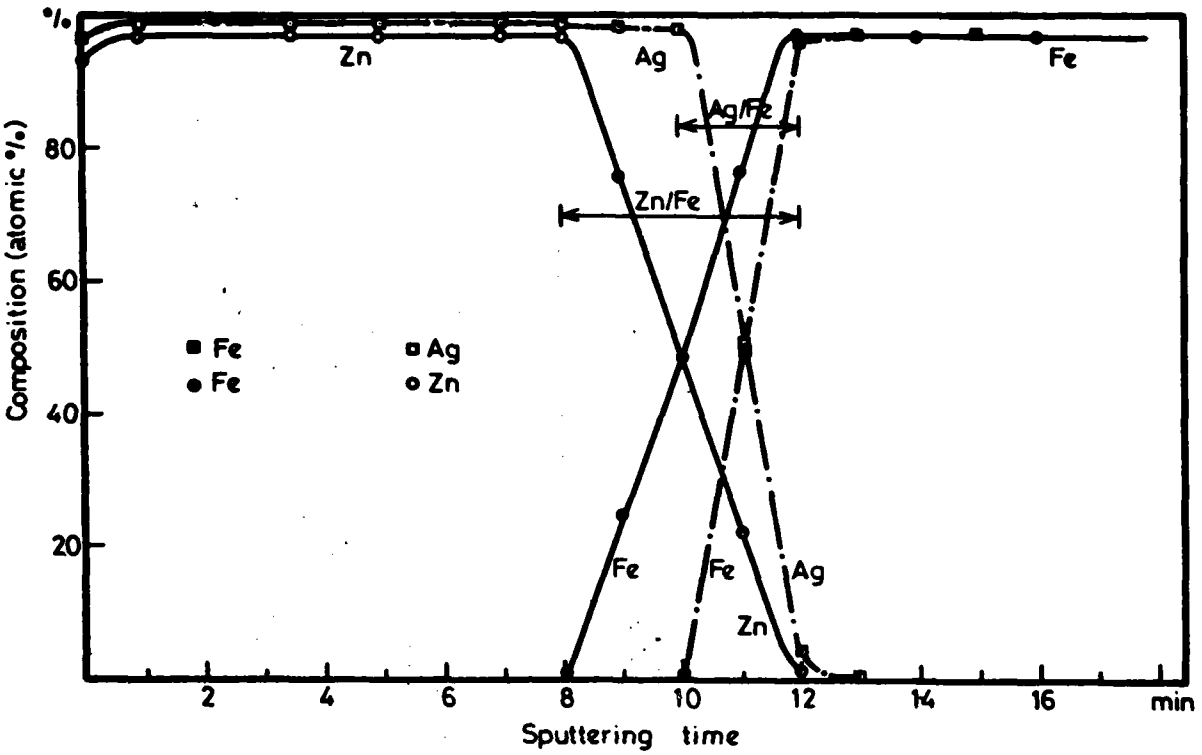

Fig. 5.9

COMPOSITION DEPTH PROFILE THROUGH GAS DEPOSITED SILVER AND ZINC COATINGS ON FERRITE SUBSTRATES

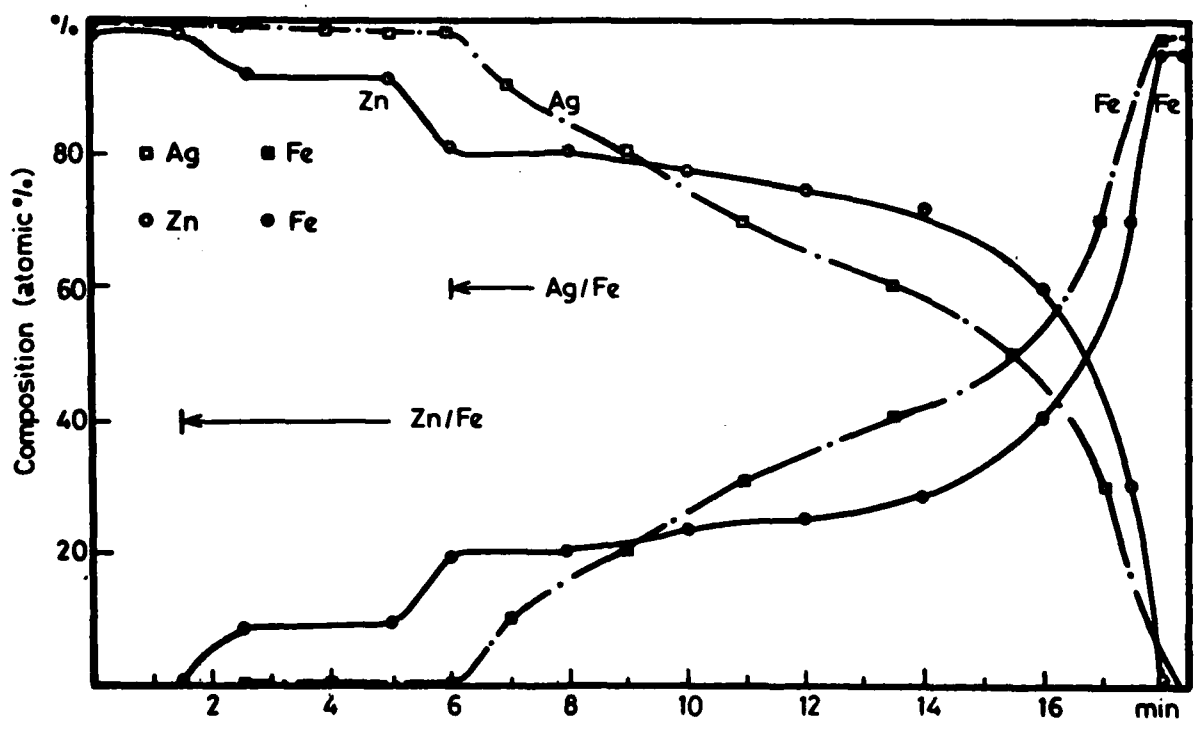

Fig. 5.10

COMPOSITION - DEPTH PROFILE THROUGH ION PLATED SILVER AND ZINC COATINGS ON FERRITE SUBSTRATES.

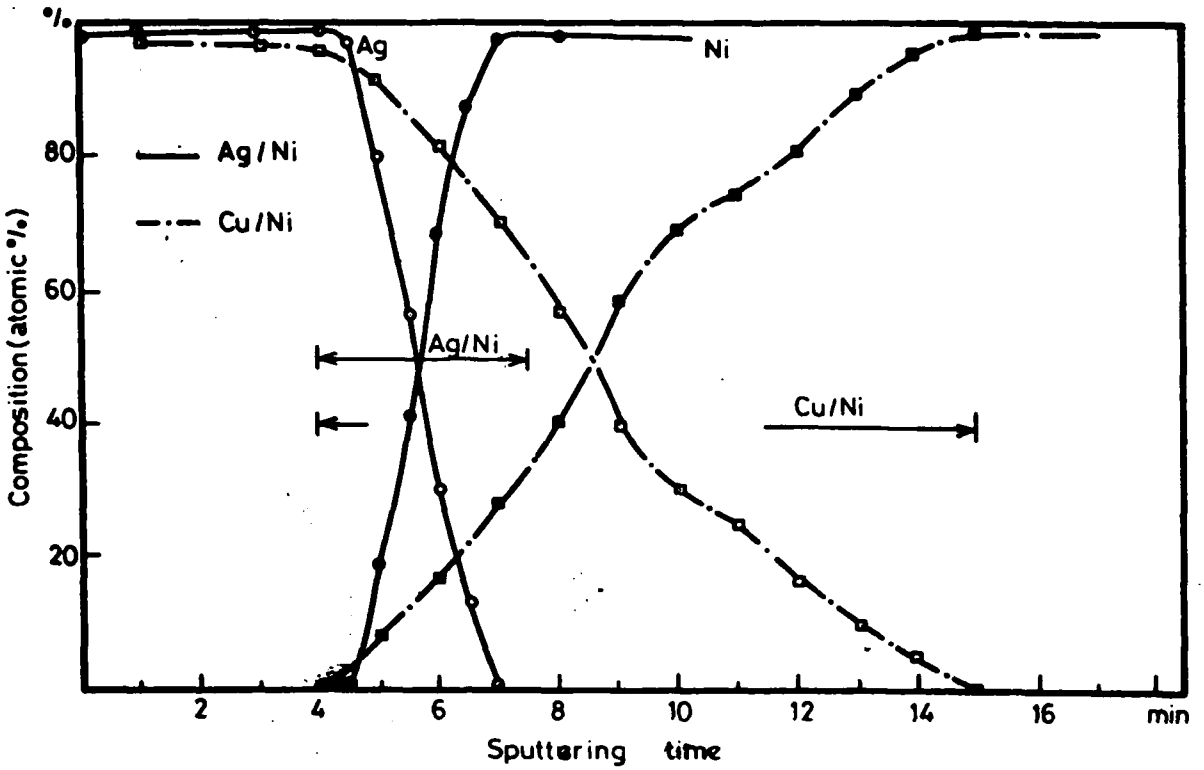

Fig. 5.11 COMPOSITION- DEPTH PROFILE FOR SILVER AND COPPER COATINGS WHICH WERE GAS DEPOSITED ON NICKEL SUBSTRATE

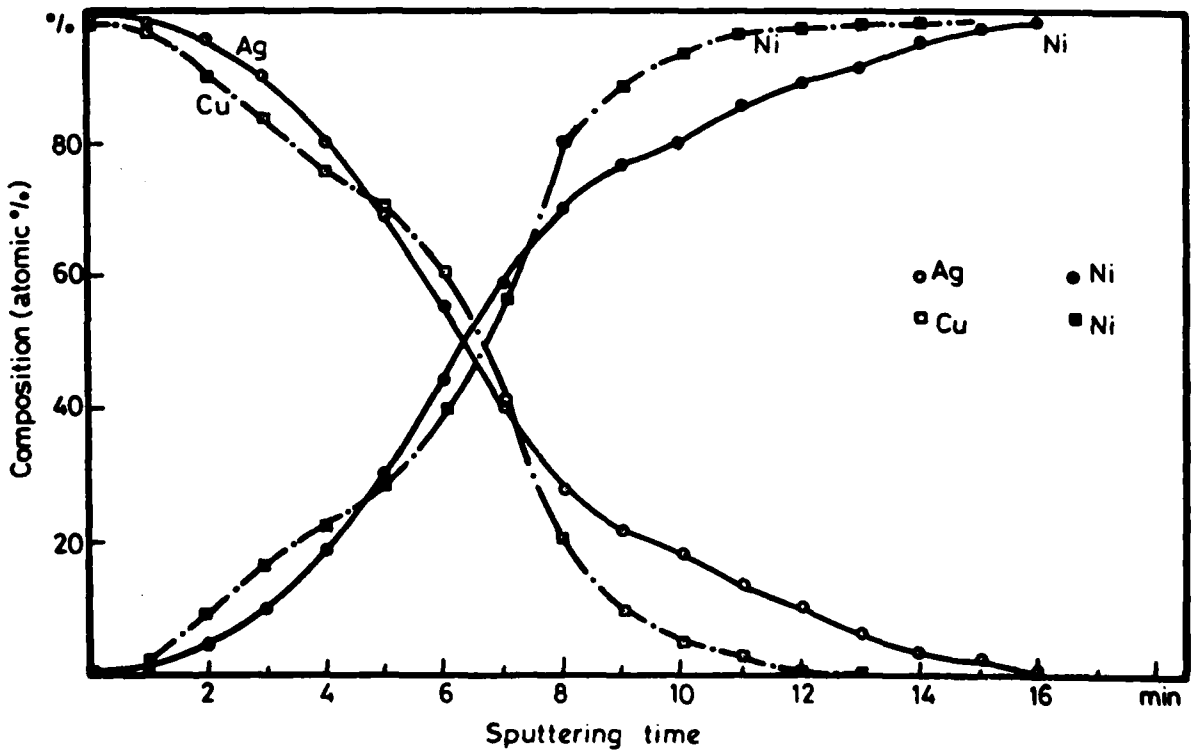

Fig. 5.12 COMPOSITION-DEPTH PROFILE FOR ION PLATED SILVER & COPPER FILMS ON NICKEL SUBSTRATES.

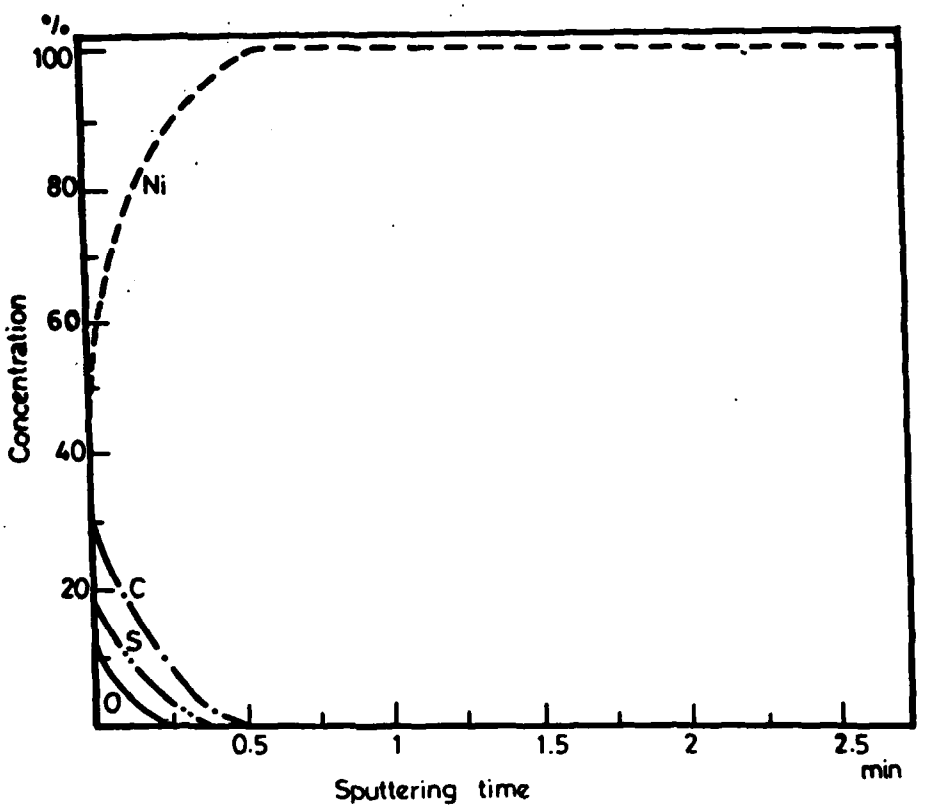

Fig. 5.13

CONTAMINATION OF SPUTTER ETCHED NICKEL

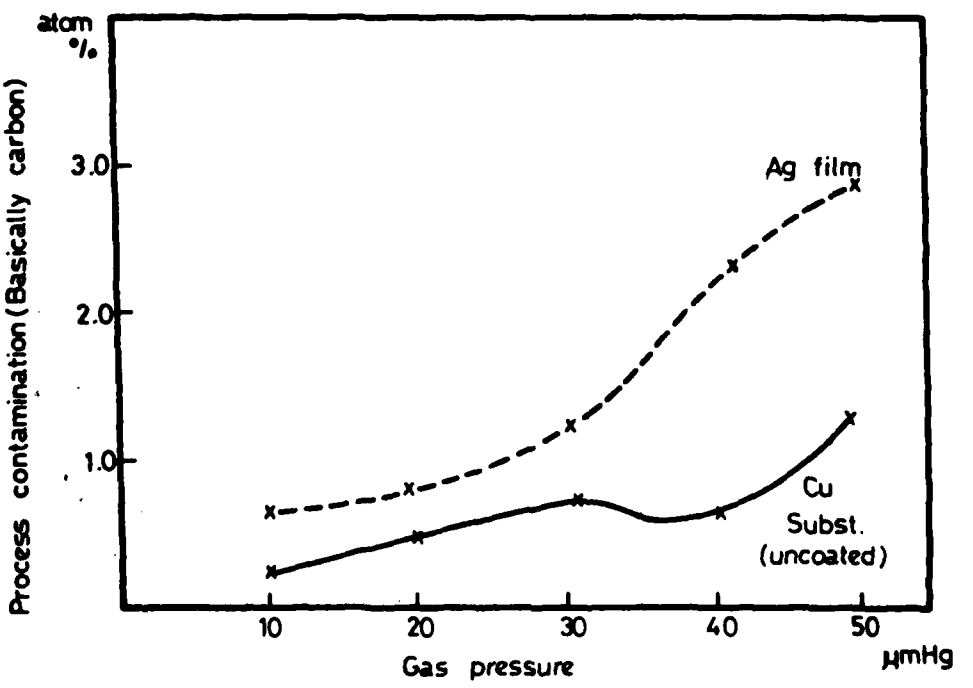

Fig. 5,14

CONTAMINATION - GAS PRESSURE RELATIONSHIP

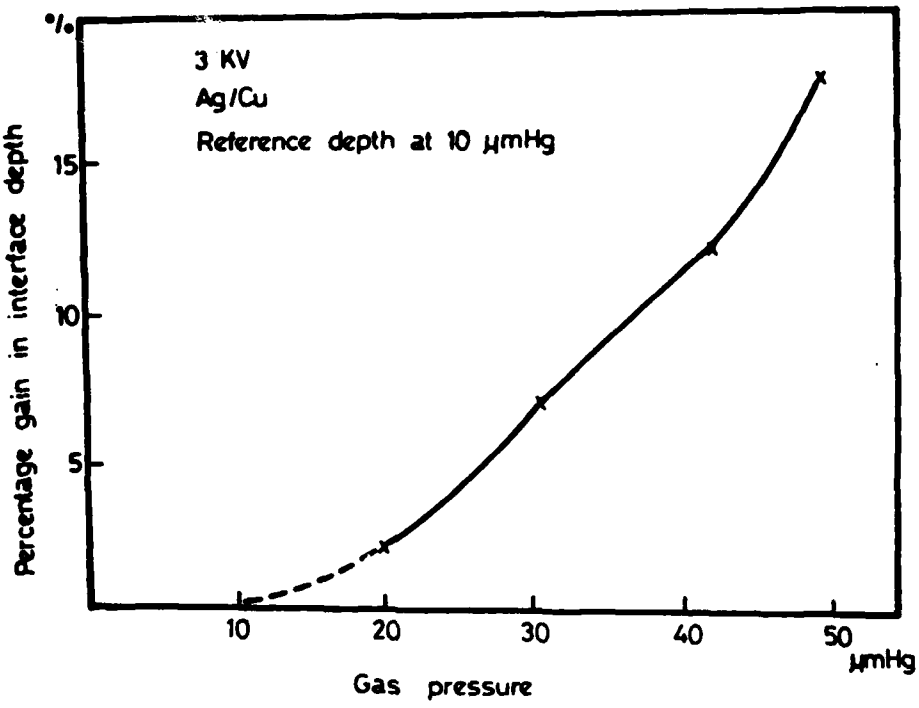

Fig. 5.15

GAIN IN INTERFACE DEPTH AT HIGH GAS PRESSURES

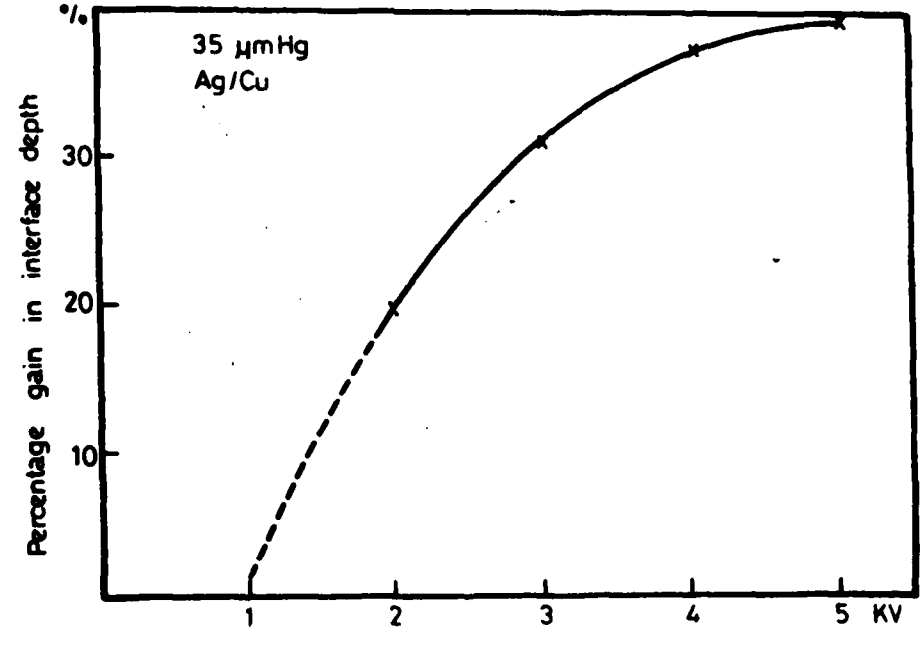

Fig. 5.16

VARIATIONS OF INTERFACE DEPTH WITH BIAS VOLTAGE

These results confirms the early mentioned speculations (see atomistic mixing 2.6.5 and particle entrapment 2.6.3) That apart from thermal diffusion and coating atom penetration, the atomistic mixing can be enhanced by radiation diffusion and cascade mixing due to the increasing population of lattice defects and target-atom recoil movements at high energy levels.

The increase in contamination levels at high argon pressure can also be reasoned on the basis that the initial vacuum was 10^{-5} torr and therefore the presence of oxygen during deposition was not completely eliminated. Hydrocarbons back streaming from the diffusion pump were also there. Therefore increasing the gas pressure and hence the average energy of the impinging particle and subsequently the lattice defects results in trapped argon atoms at lattice vacancies and non-substitutional dissolution for oxygen and carbon atoms.

5.3.4 Effect of bias voltage

Fig 5.16 shows the effect of bias voltage on the percentge depth of the interfacial region. Again the same arguments depicted in the preceeding section(5.3.3)for radiation diffusion and cascade mixing are applicable. An important advantage, however of using high ion plating at reasonably low gas pressure is that the contamination level is kept to minimum. For example the atomic percentage of trapped argon did not exceed 2% while the atomic percentages of contaminants of oxygen and carbon did not exceed 4.5%.

5.3.5 Effect of evaporation rate and substrate temperature

Fig. 5.17 shows the effect of evaperation rate on the interfacial-region depth. It is shown that increasing the evaporation rate results in decreasing the graded depth. The effect of substrate temperature is also shown on the same figure.

5.4 Optimum processing conditions for extensive graded interfaces

The optimum processing conditions leading to the formation of extensive graded interfaces are summarized in fig. 5.18. These results are all obtained for coated substrates at 180 °C or less Higher substrate temperatures would grenerally enhance the diffusion process. It is shown that such interfaces can be formed at moderately low gas pressure and high bias voltage. For light substrate atoms and reactive substrates it is recommended to use the low gas pressure zone. For heavy substrate atoms and less reactive substrates the high pressure zone would generally give more extensive interfaces. In all cases the operating mechanisms are the radiation-enhanced diffusion, cascade diffusion, atomistic mixing of substrate and film atoms, penetration and entrapment. At high substrate temperatures however, thermal diffusion may dominate the formation of diffused interfaces.

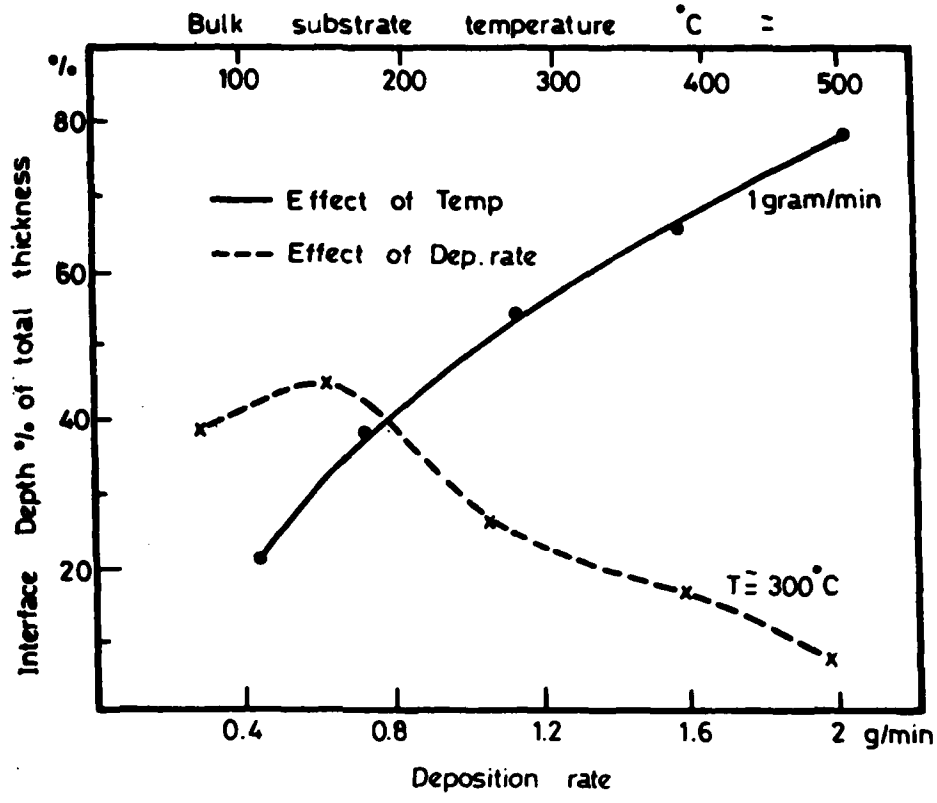

Fig. 5.17 THE EFFECT OF DEPOSITION RATE AND SUBSTRATE TEMPERATURE ON INTERFACE DEPTH

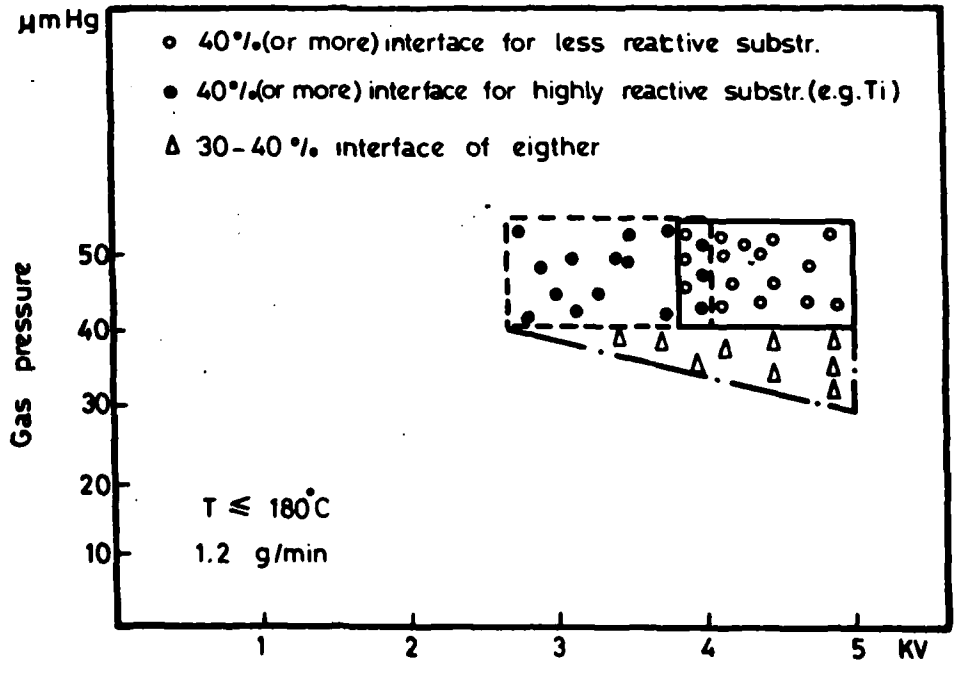

Fig. 5.18 OPTIMUM PROCESSING CONDITICNS FOR EXTENSIVE GRADED INTERFACES.

CHAPTER 6

ADHESION TESTING

6.1 Introduction

Adhesion can be defined as the ability of two materials to remain in contact under a tensile force. Two difficulties are often exercised in measuring adhesion between thin metallic films and substrates. These include the difficulty in obtaining perfect contact or even a known area of perfect contact and the inability to apply pure tensile stresses normal to the interface without attaching a connection to the thin film(54). Lack of susceptibility of adhesion to measurement, encouraged many investigators to neglect the above men - tioned defintion and to look out for new definitions and measures.

6.1.1 Scratch test

The scratch test(55) has long been used in quantitative measurements of thin film adhesion . In this test, a finely pointed stylus is drawn across the film under incr-easing normal loads. The critical load required to strip the film from the substrate and leave a clear track behined it is taken as a measure for adhesion. Analysis of the failure mechanism(56) was used to correlate measured creitical forces to interfacial bonding. In a more recent work (57) the process was shown to be more complex than was previosly visualized,

and that the failure mechanism varies from one system to another making a single theoretical model untenable. It was also found that the transparency of the track is not a suitable measure.

6.1.2 Pull test

The pull test (58) was used to measure the tensile force required to pull the film from the substrate surface. Pins were soldered to various metal films either directly or through an overcoat. The pins were then subjected to either a tensile force (59) or bending force (57). In either case the method of applying the load remained questionable as regards the effect of soldering process on interface stability, structure, and strength.

6.1.3 Tensile test

Tension tests conducted on coated tensile test specimens(4) and on coated fibers(60) proved to be reasonable qualitative methods. Tensile tests made by centrifugal forces of a rotating disc in vacuum(61) were also used but no direct correlation between adhesion and the critical angular speed at which film failure was observed can be deduced. A similar technique utilizing forces generated by longitudnal vibrations of a coated beam was adopted, but the generated forces were found to be usually limited and insufficient to detach the film.

6.1.4 Peel tests

Tape peel tests (62) are still in qualitive use, inspite of the fact that this test failed to produce any reasonable measure. This test was further developed (63) to test the shear strength of a lap joint with interfacial film. Shear-test results showed scatter over an order of magnitude of the measured value

6.2 Adhesion test results

6.2.1 Preliminary results

a- Ultrasonic test.

In the present work ultrasonic cleaning was made to each and every produced film prior to any subsequent processing and or testing. Ultrasonic vibratory motion is a well known simple adhesion test(43). This test has never resulted in adhesion failure of ion plated films. On the contrary all, vacuum deposited films which were made by straight evaporation in vacuum showed considerable film detachment after 1-2 minutes ultrasonic testing, see table (6.1) for metal combinations and results.

Deposition	Metal pair Film/Substrate	Result	Metal pair Film/Substrate	Result
IP	Pb/Steel Ag/St Cu/St Al/St In/St Ag/Cu Ag/Al In/Cu Pb/Cu	NF	Pb O/Cu Pb O/St $Al_2 O_3$/Cu $Al_2 O_3$/St	NF
VD	Pb/St Ag/St Cu/St Al/St In/St	F	Pb/Cu Ag/Cu Al/Cu In/Cu	F
SP	Pb/St Ag/St Cu/St Al/St In/St	F NF NF F F	Pb/Cu Ag/Cu Al/Cu In/Cu	NF NF F NF
EP	Ag/St Cu/St Pb/St	NF F F	Pb/Cu Ag/Cu	F NF

Table 6.1 Ultrasonic results

IP: Ion plated VD: Vacuum deposited SP: Sputtered
EP: Electroplated F: Failed NF: No failure

b- Tape test

In this test strong adhesive tape is pressed onto the surface film. The tape is then pulled off, and adhesion is classified according to whether the film is wholly, partially, or not stripped by the tape. This test again never resulted in film stripping when used on ion-plated films. Vacuum deposited coatings consistantly were wholly stripped, while

electroplated and sputtered coatings were often partially removed by the tape, see table(6.2)for metal combinations and results.

Coating	Film/Substrate	Result	Film/Substrate	Result
IP	Pb/Steel Ag/St Cu/St Al/St In/St Ag/Cu Ag/Al Al/Cu In/Cu Pb/Cu	NF	Pb O/Cu Pb O/St Al_2O_3/Cu Al_2O_3/ST	NF
VD	Pb/St Ag/St Cu/St Al/St In/St	F	Pb/Cu Ag/Cu Al/Cu In/Cu	F
SP	Pb/St Ag/St Cu/St Al/St In/St	F PF PF F PF	Pb/Cu Ag/Cu Al/Cu In/Cu	F NF F NF
EP	Ag/St Cu/St Pb/St	F PF F	Pb/Cu Ag/Cu	PF NF

Table 6.2 Tape test results

IP: Ion plated VD: Vacuum deposited

SP: Sputtered EP: Electroplated

F : Failed NF: No failure

PF: Partial failure

6.2.2 Tensile test

In the present work, Hounsfield tensile test specimens of 0.04 m length, 6 mm diameter and 12.6 mm gauge length are used. To extend comparisons to non-compatible metal pairs as well as compatible combinations, three base metals were selected. These are 70/30 Brass, 0.1% carbon mild steel, and 99.95% pure Aluminium. The specimens of all three base metals were coated by both ion plating and vacuum coatings. The average film thickness was estimated to be 3 μm for ion plated films and 5 μm for vacuum deposited coatings.

Ion plated silver films on brass test specimens (compatible) remained intact, and the film plastically flowed with the bulk substrate as shown in figure(6.1a) . The vacuum deposited silver film, however, broken down showing wide surface cracks as early as the necking has just started, see for example figure (b) . A small effect of 1.5% increase in ultimate fracture load was recorded for the ion plates test specimens, while trifling effects up to 0.1% were recorded for vacuum test specimens.

On the other hand, ion plated aluminium films on steel test specimens(non-compatible) remained also intact and plastically flowing with the bulk substrate, while the vacuum deposited Al film peeled off at 1.0% strain. Figure 6.2 shows the ion plated test specimen in necking conditions, in

(a) I.P
SILVER/BRASS

(b) V.D.
SILVER/BRASS

FIG. 6.1 SCANNING ELECTRON MICROGRAPHS SHOWING THE SURFACE OF THE TENSILE TEST SPECIMENS WITHIN THE NECKING ZONE

(a) I.P.
ALUMINIUM/STEEL

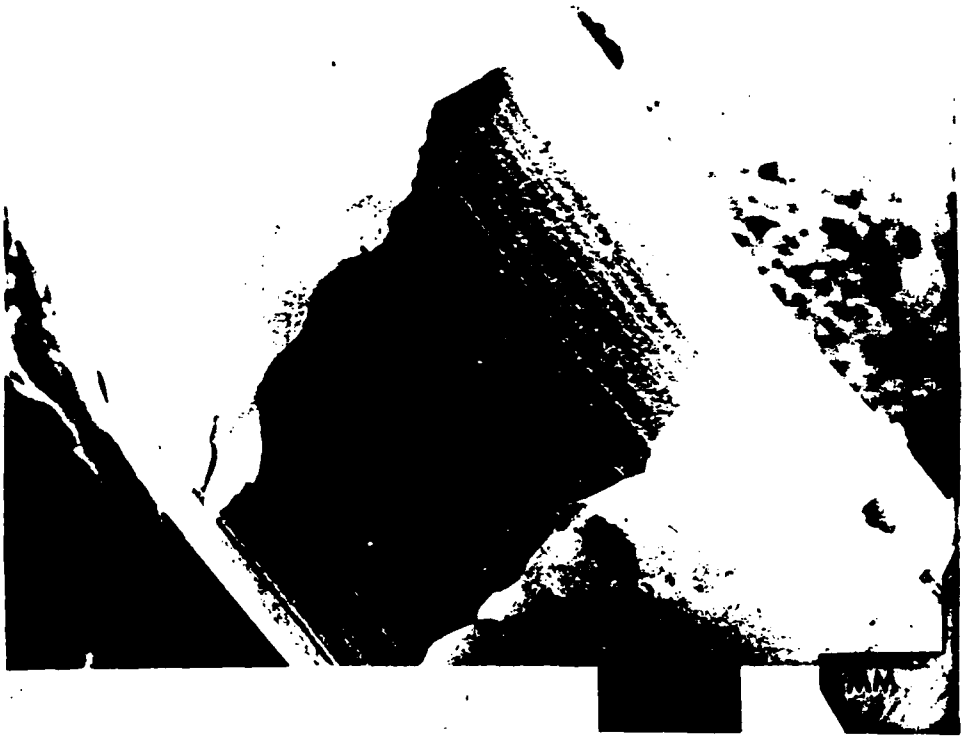

(b) V.D.
ALUMINIUM/STEEL

FIG. 6.2 SCANNING ELECTRON MICROGRAPHS OF ALUMINIUM COATED STEEL TEST SPECIMENS
(a) PULLED UP TO NECKING, I.P.
(b) PULLED UP TO 0.1% STRAIN, V.D.

comparison with the vacuum deposited specimen, unloaded after 1% strain as the film peeled off.

All tensile test results indicate outstanding adhesion for the ion plated films where the interfacial strength was capable to take tensile stresses up to the ultimate strength of the specimen without any predictable failure.

6.2.3 Pull test

A cylinderical rod 1 cm. diameter and 8 cm long made of mild steel was stuck onto the film surface with epoxy resin. After curing of the resin the plated specimen was mounted as shown in figure 6.3 and a gradually increasing load is applied to the free end of the rod. The adhesion strength is estimated to be the maximum resultant stress, when the rod falls down stripping the film. Therefore the adherence strength (A) is given by :

$$A = 7.995\ (w + 0.11)\ N/mm^2$$

where w is the applied load in kgs.

A limiting value for this test is determined by the strength of the cement used, which is 58.86 N/mm^2.
With ion plated films silver films on copper substrstes failure has never took place at the film substrate interface. It was either between the binding resin and the film or between the binding agent and the rod. In few cases, however, failure

AD-A160 165 ADHERENCE AND BONDING OF THE ION PLATED FILMS(U) CAIRO UNIV (EGYPT) DEPT OF MECHANICAL DESIGN AND PRODUCTION M EL-SHERBINY ET AL. JUL 83 R/D-2723-MS-01 2/2

UNCLASSIFIED DAJA37-80-C-0034 F/G 7/4 NL

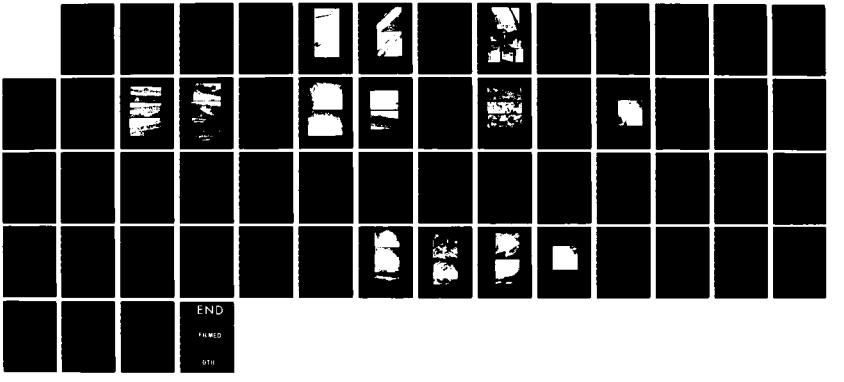

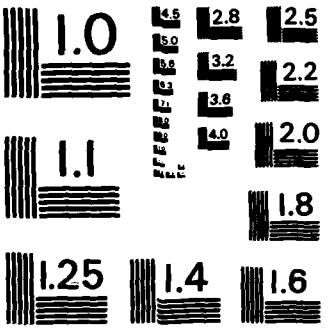

occurred within the resin itself. This implies that the adherence strength of the film is exceeding the test limiting value.

Vacuum deposited films consistantly showed interfacial failures at stress level of 16.7 N/mm^2. These films were produced by straight evaporation in vacuum without substrate precleaning. Admission of inert gases into the chamber during the depostition resulted in poorly adherent coatings reaching a stress level of 1.96 N/mm^2 at 30 μm Argon pressure. Precleaning of the substrate by Sputter etching up to 30 minutes prior to film deposition resulted in better adherence strength of up 39.2 N/mm^2 .

Electroplated films, however, showed a consistant interfacial failure within the range 20-28.4 N/mm^2. On the other hand Sputtered films frequently showed interfacial failures within the range 42.18-51 N/mm^2. In two odd cases, however, Sputtered film showed interfacial strength exceeding the test limit $\sigma > 59$ N/mm^2, and therefore failure took place within the resin.

6.2.4 Scratch test

In this test both scratch diamond and Knoop indenters were used to test film adherence on a Leitz miniload microhardness tester. Films of up to 5 μm thickness were deposited on copper substrates for this purpose. The scratches

were produced with the indenter moving at a constant speed of 0.5 mm/ minute. This was achieved by coupling a 1 rev/ minute D.C. motor to the front micrometer of the tester table. Scanning electron microscopic examination of the scratches confirmed the outstanding adhesion of the ion plated films. At small loads (up to 50 grams) vacuum deposited films showed high surface deformation and film distortion around both sides of the scratch, while the ion plated films showed very smooth scratch edge, indicating strong adhesion every where up to the scratch edge.

When the load was increased to 200 grams, the vacuum deposited films showed complete detachment from substrate, while the electroplated films showed localized rupture and localized detachment particularly at the scratch edge. Figure 6.4 shows such remarkable features. On the other hand Sputtered films showed nonuniform track width with film grains being knocked out of the loosely packed grain structure of the film, while the ion plated film remained intact right up to the scratch edge as shown in figure 6.5 . These remarkable differences adds up to the qualitative assessment of ion plated film adhesion as compared with conventional coatings.

6.2.5 Shear test

The shear test was also used to determine interfacial shear stresses of ion plated films at which interfacial adherence failure may occur.

Thin copper strip was cemented to film surface by means of a special epoxy cement. A gradually increasing load was applied to the strip and shear stresses are worked out at the load causing interfacial failure.

For thin films up to 1 μm the shear failure never occurred, either within the film or the interface. It was generally observed within the binding epoxy resin. When thick films (5-10 μm) were tested the shear failure generally took place within the film itself. Therefore, it was almost impossible to achieve any quantitative value for adhesion by these conventional tests.

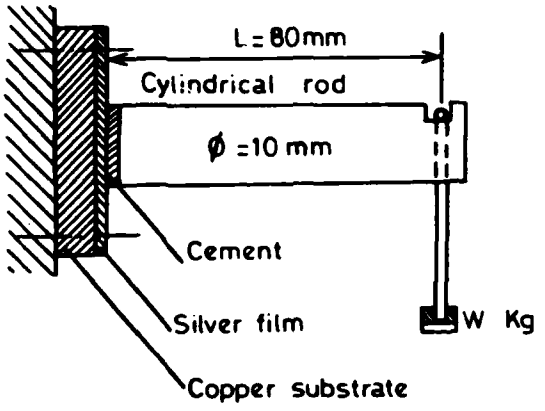

Fig. 6.3
PULL TEST ARRANGEMENT

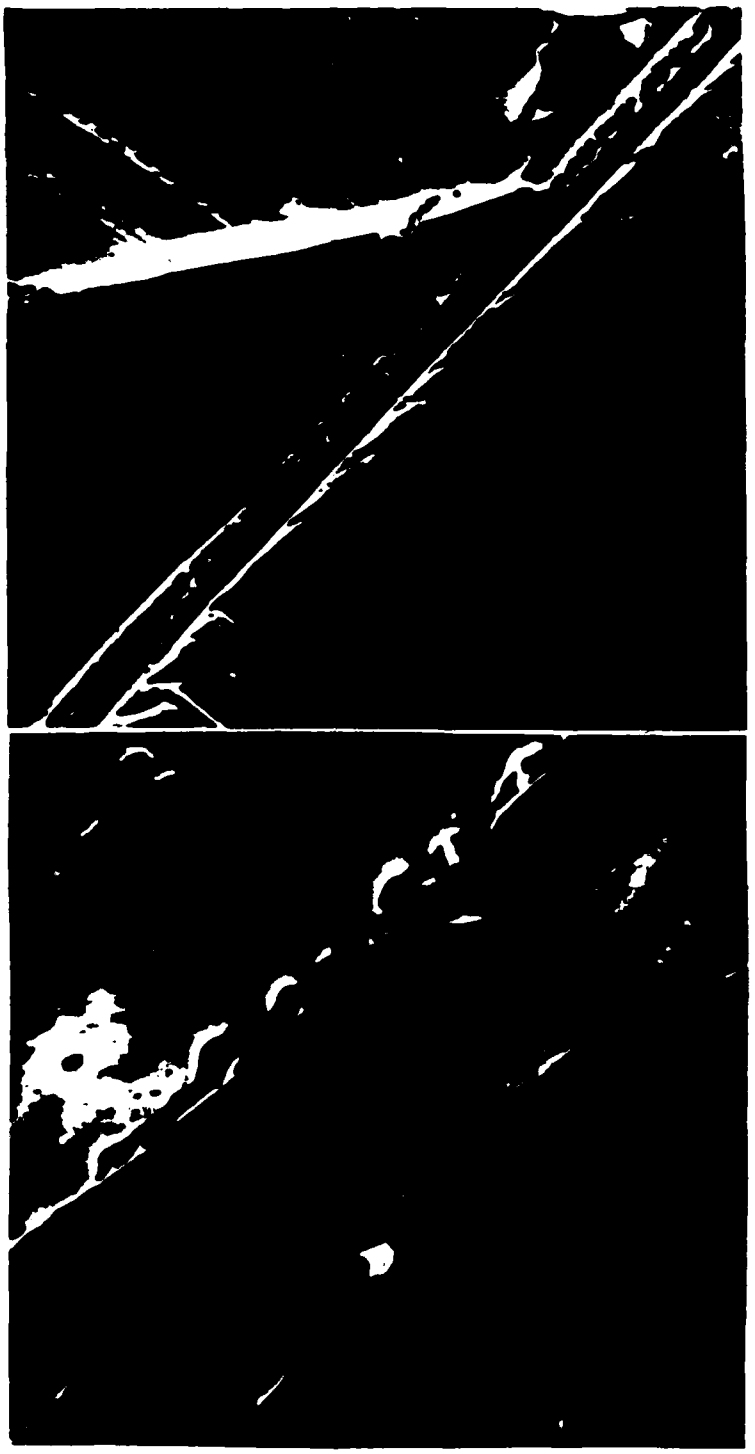

(a) V.D.

(b)E.P.

FIG. 6.4 SEM MICROGRAPHS SHOWING THE COATING FAILURES BY SCRATCH TESTS.
(a) V.D. , 50 GRAM LOAD
(b) ELECTROPLATED , 200 GRAM LOAD

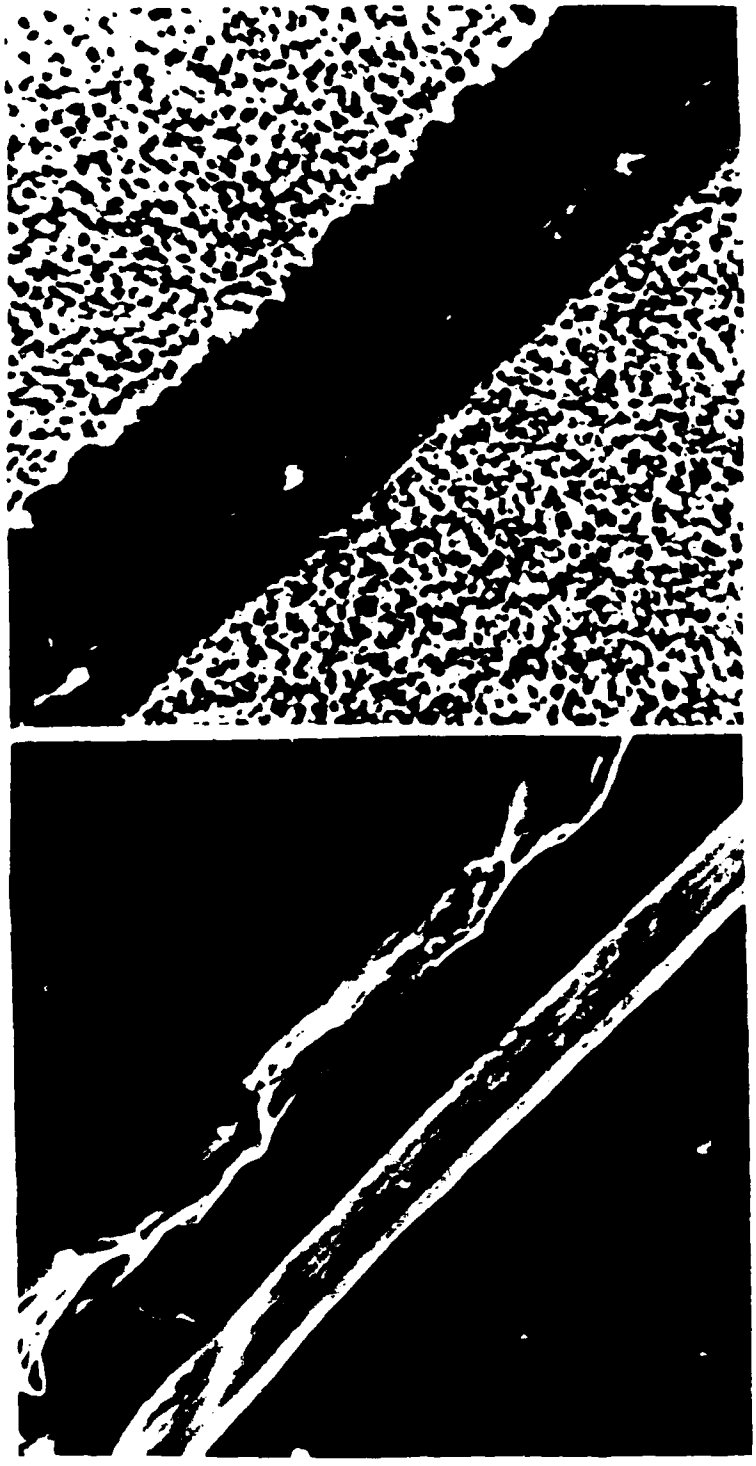

(a)
SPUTTERED

(b)
ICN PLATED

FIG. 6.5 SEM MICROGRAPHS SHOWING SCRATCHED SPECIMENS UNDER A LOAD OF 200 GRAMS.

6.2.6 X-ray diffraction: A quantitative measure

X-ray diffraction has been successfully employed for measurements of mechanical properties of ion-plated films (5). The authors, however, extended the idea of employing x-ray diffraction in measurement of mechanical properties into a new area of adhesion measurements. In this test silver coatings were deposited on the gauge length of flat copper test specimens. Coated specimens were produced two at a time, allowing a spare specimen for annealing and measurement of lattice parameter of stress free film. The specimen under consideration was mounted on a special straining device. The device was so designed in compact size to suite mounting on specimen holders of x-ray apparatus. Figure 6.6 shows the mounted straining device in the test set up. A calibrated strain gauge load cell was also built in the device to read the applied tensile load, and hence the mode of deformation of the specimen. Since the specimen is coated within the gauge length only, film strain is provided only by interfacial bonding at the film substrate interface.

Stress free specimens were checked for flatness by optical microscope prior to mounting into the device. Leveling of mounted specimens was achieved by leveling screws, which are inserted into the device. After each incremental loading releveling was made for the loaded specimen. Preselected incremental loads were applied in steps with the total load displayed from the device load cell. Cobalt radiation was then used and the counter

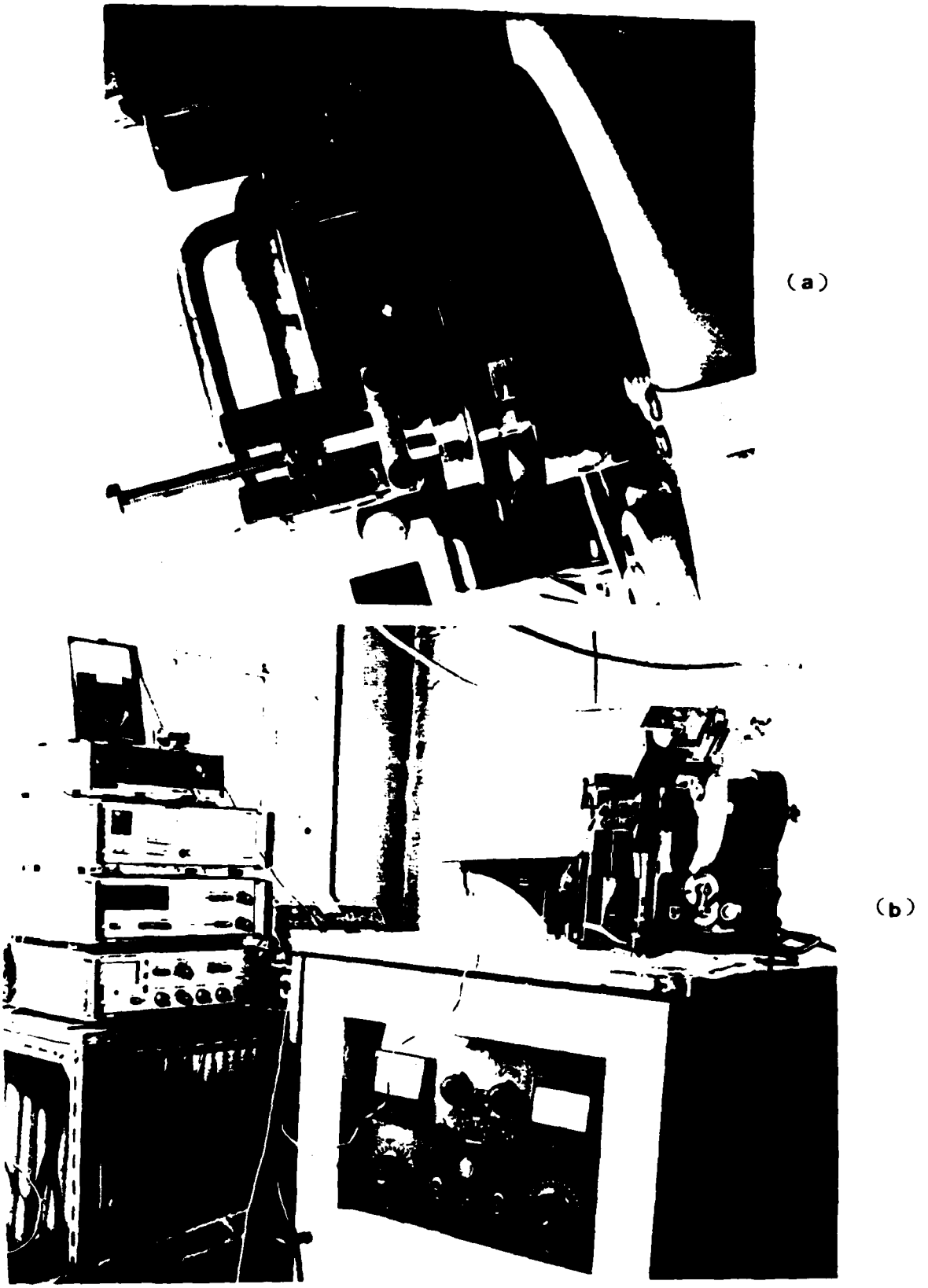

FIG. 6.6 X-RAY TEST SET UP
(a) STRAINING DEVICE
(b) SET UP

diffractometer was set to count the reflected intensity by step scanning over the silver peaks.

Analysis

Employment of x-ray diffraction in stress and strain measurements necessarily requires accurate measurements of lattice strain(68). Every substance, however, has a unique set of planer specings d_{hkl}, associated with some reflection angles θ_{hkl}. They are related to each other by the well known Bragg equation

$$n\lambda = 2\, d_{hkl} \sin(\theta_{hkl})$$

where λ is the radiation wave length.

The d values define the lattice parameters of any atomic structure through a structure geometry relationship. For face centered cubic metals (e.g. Silver)

the relationship is given by :

$$a = d\sqrt{h^2 + k^2 + l^2}$$

Because of the high resoultion at high Bragg angles, the a values must be determined at the different (hkl) peaks up to the highest possible Bragg angle (θ). Further minimzation of errors necessarily requires extrapolation of the a values up to $\theta = 90^{o}$.

Once the lattice parameter is determined for the plane parallel surfaces at any stress level, the engineering definition of strain is used to calculte lattice strain (ε)

$$\varepsilon = \frac{a - a_o}{a_o}$$

where a_o is the lattice parameter of stress free lattice.

Since the bulk yield of the film is associated with plan slip rather than lattice deformation, the initial yield strain of the film can be defined interms of the maximum lattice strain. Therefore, the yield strength of the film (σ) is given by

$$\sigma = E \dot{e}_m/\nu$$

where E is the Young's modulus of elasticity,

ν is the poisson's ratio., and

ε_m maximum lattice strain

The coating atoms covering the necking zone of the specimen are generally expected to suffer the highest stress level within the film. This is due to the biaxial state of stress within such zone. Interfacial bonding, however, would generally allow film atoms to share in the increasing load, and hence lattice strain is due to occur . Once interfacial failures dose occur , these atoms are expected to show some recovery as a result of relaxation from axial stresses. This can be easily predicted by the sudden recovery in lattice strain or lattice parameter (a).

Results

Since the above mentioned analysis essentially requires a considerable amount of data handling,Results were obtained through a computer program which resolves the radiation reflection into two monochromatic $k\alpha_1$ and $k\alpha_2$ radiations, by doublet separation at each peak, having done this the lattice parameter is computed for each peak data, and extrapolation is made by a chebyshev polynomial of the fourth order . The process is then repeated at each loading level. An increasing value of (a)

indicates elastic mode of deformation for the film, while a constant value of (a) indicated either localized yielding or bulk film plastic flow . Any subsequent reduction in (a), however insicates either film failure or interfacial failures . Examination of film surface by scanning electron microscopy at some later stage, defines whether film or inter interfacial failure are responsible for the recovery of the lattice strain . Accurate determination of interface strength was achieved for various silver coatings deposited by different technques under different processing conditions. These are summarized in table 5.3. Further experimental results correlating adhesion with processinf conditions are now in progress, and the will be reported in the final report .

Process	Interface Strength Ag/Cu Range N/mm^2 From N/mm^2	To N/mm^2	Weighted average N/mm^2	Remarks
VD	12.4	28.8	16.3	Low values for poorly precleaned substrates and high values for Sputter etched substrates
EP	16.5	47.4	34.7	Low values for low current densities and high values for high current densities.
SP	36.8	69.3	65.4	High values obtained for low Sputtering yield.
IP	73.1	78.6	76.1	High values for high energy deposition

Table 6.3 Measured interfacial strength by x-ray diffraction for Ag/Cu system.

IV. CHARACTERISTICS

CHAPTER 7
STRUCTURAL DETAILS

7.1 Introduction

A diverse range of film characteristics, physieal and mechanical properties can be obtained by controlling the film structure. Film columnar growth, nodular grains, and film aggregates have been reported for ion plated films produced under specific processing conditions (40,52) . The aggregates and nodule boundaries are very vulnerable to chemical attack, and corrosion initiation. Cracks may also initiate at these boundaries causing stress concentration and shortening the fatigue life of the component. Furthermore, the wear rate of surface coating and film life are very much dependent on both the failure mechanism which may produce a loose wear particle and the microstructure of the surface film itself.

The microstructure of vacuum deposited coatings is investigated in several reports (64-66). The field effects on the microstructure of the substrate may be extracted from the reported effects of ion bombardment on the cathode in bias sputtering (67) . The structural morphology of the ion plated coatings is also demonstrated in a recent work (4). The results indicate that the structure of the ion plated films is significantly affected by the bias voltage, whilst the structure of vacuum deposited coatings is primarily determined by the deposition rate and the substrate temperature. They concluded that the presence of gas scattering reduces the dependency of structure on the deposition rate .

The objectives of the present work are to present now studies on the characteristics of ion plated coatings, and the effect of the most important processing parameters on these characteristics.

7.2 EXPERIMENTAL

In the present study, copper films are deposited on copper substrates by ion plating . A particular advantage of using this system (Cu-Cu) is that the same chemical solution is used for etching both the substrate and the film . Titanium substrates are also used for its high ability to be contaminated with oxygen, nitrogen,hydrogen, carbon monoxides and carbon dioxiodes. These contaminations are more serious for titanium than for any other metal. Since these gases do not only form surface compounds, but also penetrate into the titanium lattice causing high hardness or severe embrittlement, they are expected to seriously affect the microstructure of the deposited film.

For the latter substrates, aluminium films are deposited on titanium substrates by ion plating. The main prblem of this system (AI-Ti) is the extreme difficulty to prepare satisfactory etched sections through the aluminium, Al-Ti interface, and the titanium substrate. Several etching techniques were tried, without success. The mechanical method suggested by the IMI new metal division for polishing by silicon carbide paper up tp 600 grits as usual. This was followed by a final polishing on a diamond wheel with alumina suspension in water as a polishing paste.

Finally the specimen was etched by the developed etching solution of 3% hydroflouric acid and 2% nitric acid in water.

Optical, replica, and scanning microscopy are used in examining the microstructure of the sectioned test specimens.

7.3 RESULTS

Aitogether 100 test specimens were prepared under ion plating conditions within the ranges shown in table(7.1). Inthese deposition experiments,argon was used as the discharge gas, the substrates were square sheet. 04x.04 m, and the cathode to anode distance was 0.16 m .

metal pair	Gas pressure µm Hg Ar	Substrate temp. ^{o}C	Conating thickness µm	Deposition rate µm/min.	Bias Voltage Kv	Power watts
Cu/Cu	10 - 50	below	1 - 50	2 - 5	0-5	15-40
Al/Ti	5 - 55	100 ^{o}C	1 - 50	1 - 8	0-5.5	12-52

Table (7.1): Processing conditions of the ion plated films

7.3.1 Microstructure

The effect of substrate bias voltage on film structure is shown in figure (7.1) for Cu-Cu and in figure (7.2) for Al-Ti systems. It is seen that the effect of increasing the substrate voltage is to produce clean surface during film deposition, thus reducing the chances of growing domed nodular grains at contaminated surface points. Apart from particle implantation and interface formation, increasing the bias voltage introduces higher energy into the system, which in turn increase the average kinetic energy of the impinging particle, thereby results in fine dense grain structure.

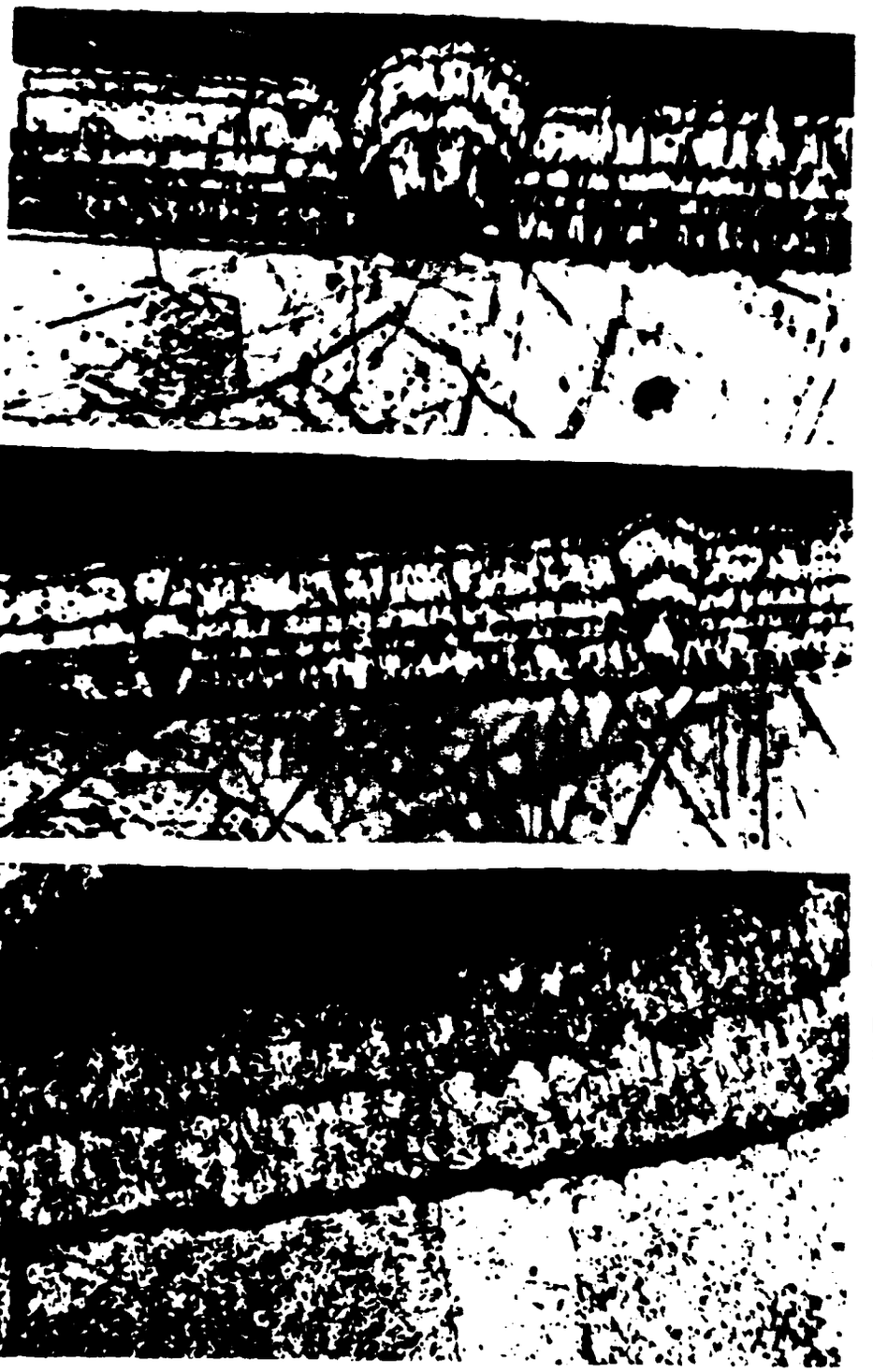

FIG. 7.1 THE EFFECT OF SUBSTRATE BIAS VOLTAGE ON THE MICROSTRUCTURE OF COPPER FILMS DEPOSITED ON COPPER SUBSTRATES (X 1 200)

1 Kv
35 µm Hg
Figure of merit 57

2 Kv
25 µm Hg
Figure of merit 72

3 Kv
35 µm Hg
Figure of merit 80

Figure (7.2): Effect of substrate bias voltage on microstructure of Al film on Ti substrate, (x 1200).

A note worthy, however, is that if the substrate is not efficiently cooled in such away that the heat generated by surface bombardment is taken away by the water cooling, bulk substrate temperature may go up,giving rise to problems of grain growth and coarse grain structure. Such effects are illustrated in figure (7.3) by electron microscope micrographs taken for a shadowed carbon replica.

The effect of gas pressure is more conveniently illustrated by the microstructure of Al-Ti system as shown in figure (7.4). It is shown that the effect of high gas pressure (45 um Hg) is to produce more film aggregates. These are much smaller in size as compared with the domed grains found in vacuum deposted films. On the other hand, lower gas pressures (15 um Hg) showed a very limited number of film aggregates which are considerably smaller in size. Such effects are less pronounced in Cu-Cu system.

7.3.2 Surface Structure

The surface structure of the film is investigated by both scanning electron microscopy and by the foil technique on a transmission electron microscope. The main objrctives of this study was to establish the density of voids, porosity and grain boundaries within the surface of the film. These are the basic parameters in the assessment of anticorrosive coatings, where the corrosive media finds its way to the substrate through such surface defects. Apart from the porosity, the nodular grain density is also very important. This is simply because these nodules are usually very poorly adherent and can be lost when the component is subjected to mechanical stresses.

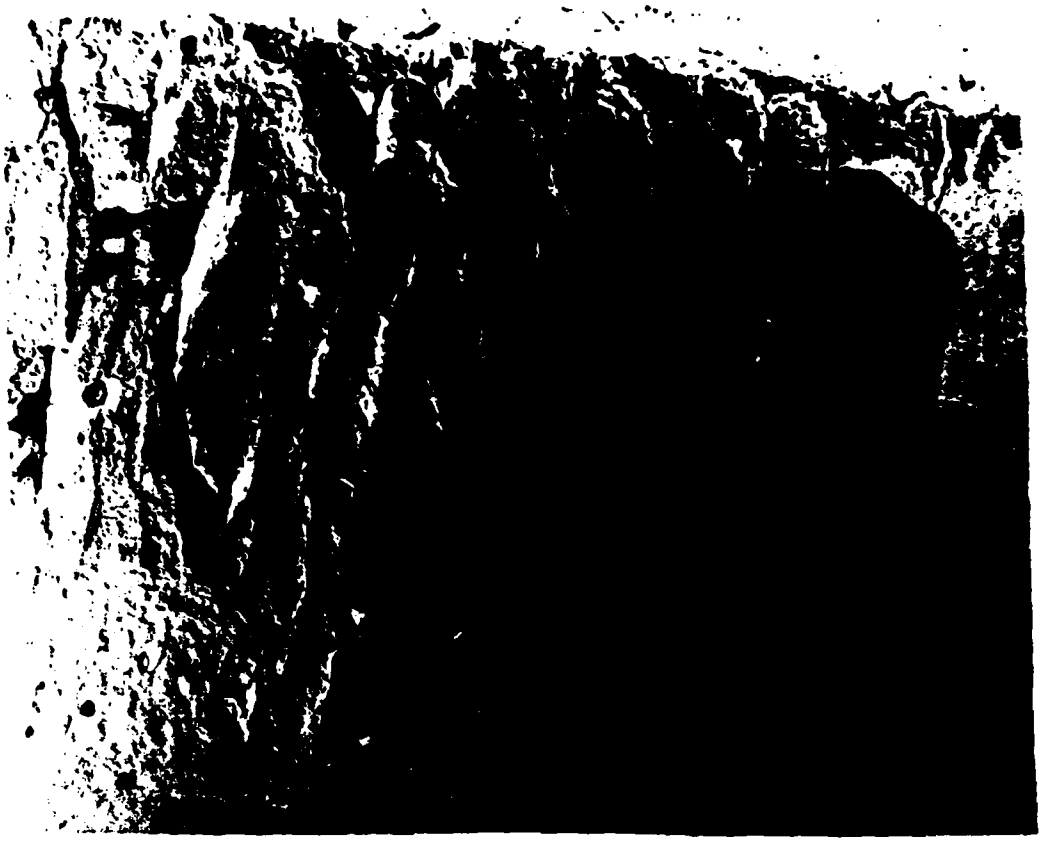

5 Kv
12 μm Hg
Substrate
temp. 200
Figure of
merit 69

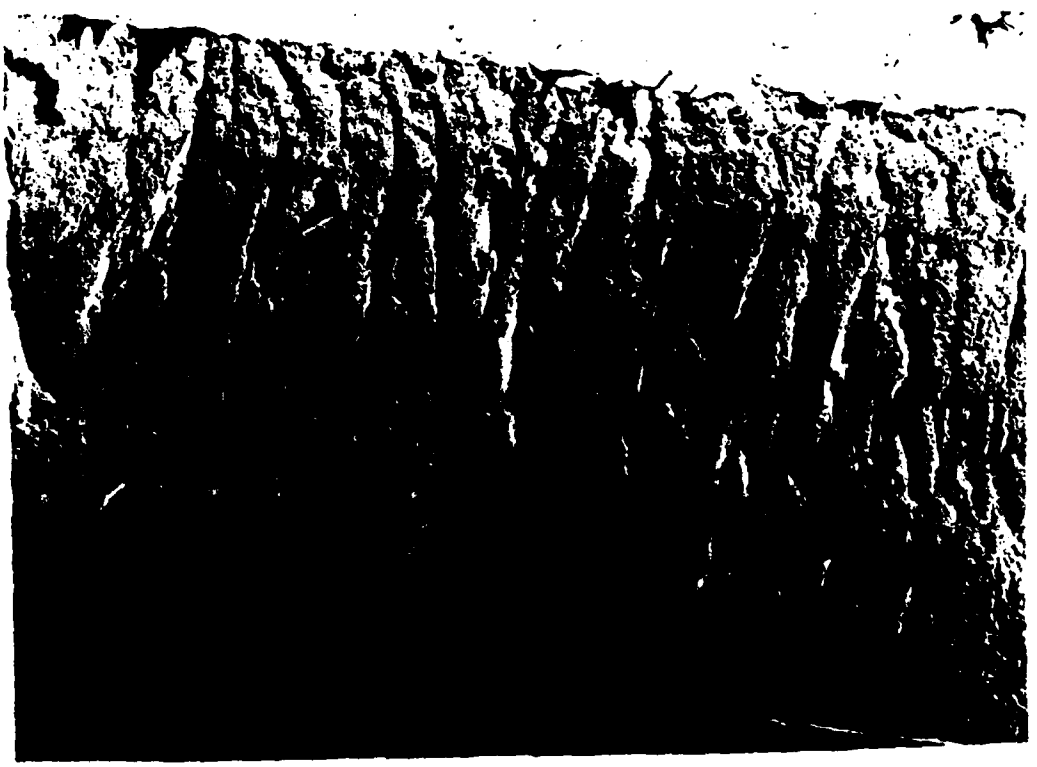

5 Kv
12 μm Hg
Substrate
temp. 80
Figure of
merit 91

Figure (7.3) : Electron micrographs of a shadowed carbon replica showing the effect of substrate temperature on microstructure of Cu film on Cu Substrate (x 5000)

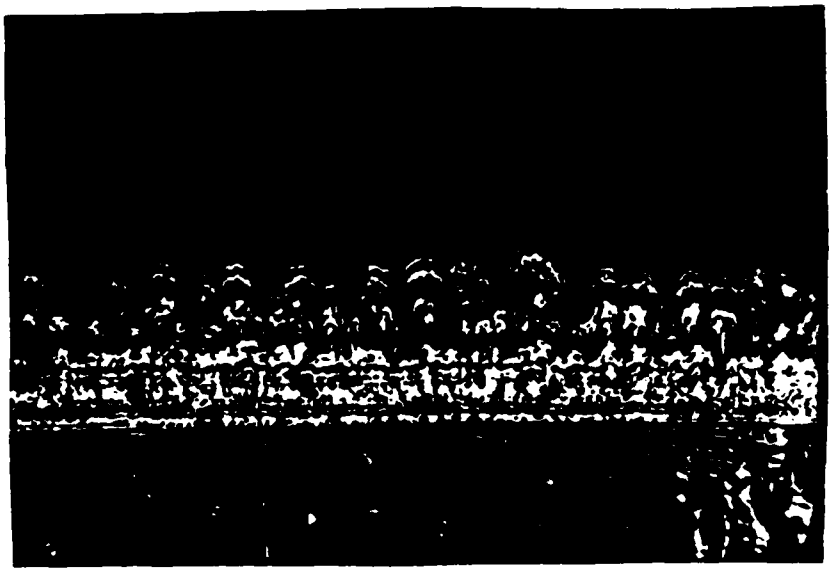

5 Kv
45 µm Hg
Figure of merit 74

5 Kv
15 µm Hg
Figure of merit 89

Figure (7.4): The effect of gas pressure on microstructure of Al-Ti system

Figure (7.5) shows a high magnification transmission micrographs obtained for foils which are produced by chemical etching of the substrate. These are made for film thicknesses of 8,10 and 20 um respectively. Generally, it is found that the grain size increases with increasing film thickness. The films having finer grain sizes (thinner films) showed more of the film pitting caused by chemical attack of the etching solution. This is probably due to the high surface to volume ratio in some areas of the thin films. A pitting pattern of the thin film (8 um) is shown in full in figure (7.6).

7.4 Nodule Density

Nodule density (number per unit area) is measured directly in radom areas on the screen of a scanning electron microscope.

The result are summarized in table (7.2). These results show that the vacuum deposited films are inferior to the ion plated films, furthermore, the high energy ion plated films contain more film nodules when compared with the low energy films.

Film thickness (μm)	Nodule Density per cm²		
	Ion plated 3 Kv, 35 μm Hg	Ion plated 5 Kv, 35 μm	Vacuum Deposited
1	0	0	100
2	0	0	393
4	500	632	1811
6	720	1004	-
8	1107	1313	2324
10	1564	2130	3640

Table (7.2) : Nodule density as measured on random areas of test specimens.

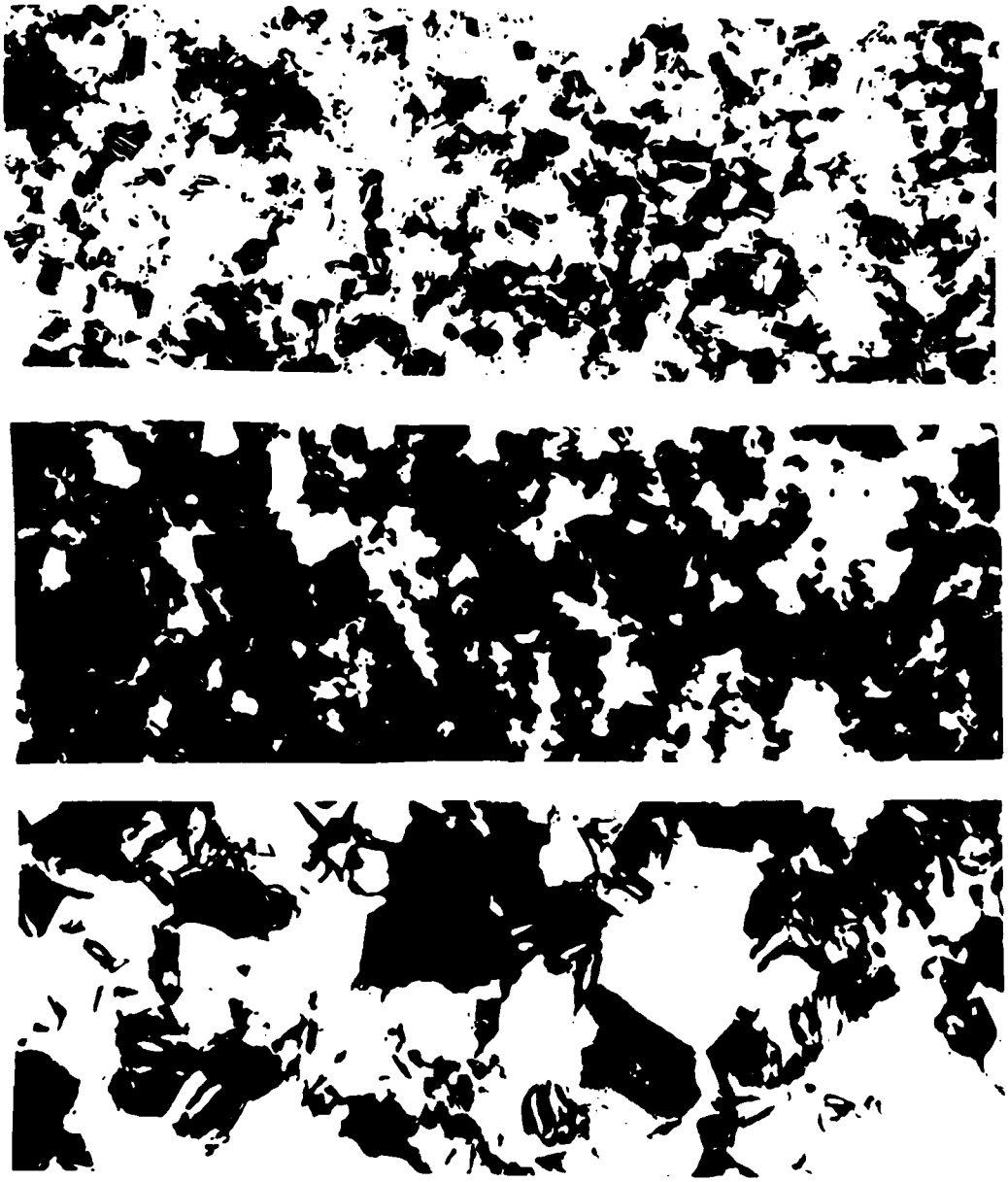

Figure (7.5) : Electron micrographs of thin foils obtained for ion plated copper films 3 Kv, 15 µm Hg (x 100 000)

7.5 Porosity Density

Accelerated tests were made by using a direct contact galvanic cell. Aluminium coated on titanium test specimen is made the anode and a low carbon steel specimen of the same surface area is made the cathode of 4 volt Dc circuit. The two electrodes are made as a sandwich in which a filter paper wetted by the electrolyte is inserted. Five percent chromotropic acid (C_{10} h_8 0_8 S_2) with a few drops of 5% stannous chloride are used to make the filter paper uniformly damp.

The presence of stannous chloride had the sdvantage of preventing the chemical reaction between the steel cathode and the chromotropic acid, hence preventing the ferritic salts to interfere and forming a greenish colour. The reaction between the uncovered area of the anode (Ti) and the electrolyte is accelerated by the activation of the Dc potential. The reaction contain TiO_2 of redish colour which contaminates the filter paper and is detected by the red spots appearing on the damp filter paper.

Thick film (>10 μm) did not show any significant porosity density, whilst thin films showed high density of surface voids, pinholes and pores. Table (7.3) shows the porosity density as measured over an area of 16 cm^2.

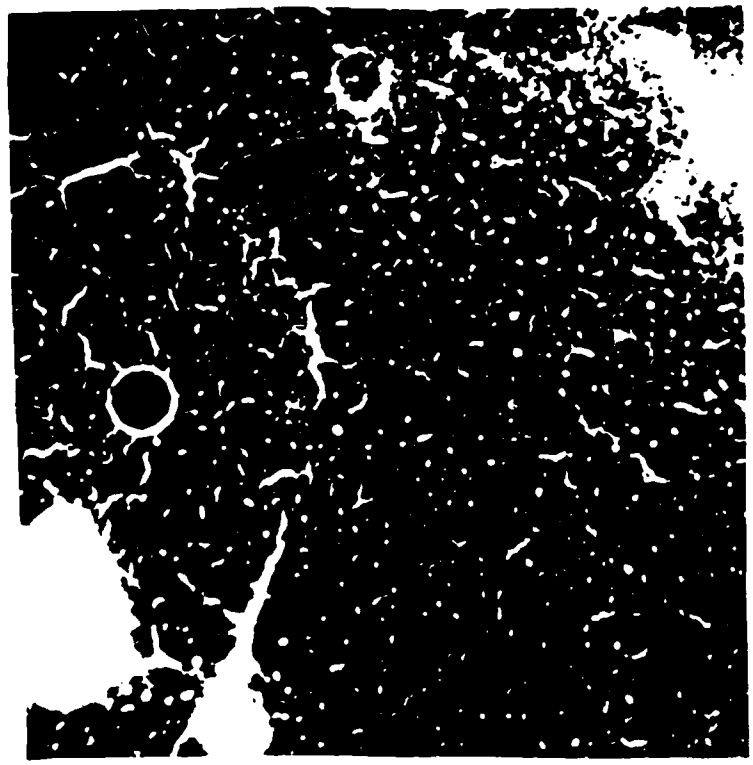

FIG. 7.6 ELECTRON MICROGRAPH SHOWING THE PITTING PATTERN AS CAUSED BY THE ETCHING SOLUTION IN A THIN FOIL (X 12 000)

Film thickness (μm)	Number of pores/16 cm^2 Ion plated 3 Kv, μm Hg	Remarks
0.5	293	Medium spots
0.8	244	Medium "
1.0	176	" "
2.0	109	Faint "
4.0	10	" "
10.0	1	very faint spot
12.0	0	-
15.0	0	-

Table (7.3): Surface porosity of ion plated films

7.6 OPTLMUM PROCESSING CONDITONS

A relative scale of figure of merit based on the morphology of the deposited film was defined as shown in table (7.4) Based on the presented exerimental results, it was found that the fifure of merit can be correlated to the most important deposition parameters throough consisten relationship .

Property	Points	Full points are given for	Zero points are given for
Adhesion	20	No interfacial failure	Interfacial failure
Grain size	10	4000 A° or less	10,000 A° or higher
Grain shape	10	Equiaxed/ Rounded	Elongated
Porosity density	10	Zero/ cm^2	15/ cm^2 and higher
Nodules & aggregates density	10	Zero/ cm^2	1000/cm^2 and higher
Mech. Properties	10	Comparable to bulk of film metal or higher	50% reduction in values of bulk film metal
Grain boundary cracks	10	Zero cracks	loosely packed grains
Orientation	5	No prefered orientation	Columnar
Surface roughness	5	Comparable to substrate roughness	Double substrate roughness
Uniformity	10	10% variation and less	40& variation or higher

Table (7.4) : Relative scale of figure of merit

Figure (7.7) and (7.8) shows the effect of gas pressure and bias voltage on figure of merit for low and high deposition rates respectively. It is shown that the figure of merit decreases as the deposition rate is increased. If the deposition rate is held constant, however, the figure of merit decreases as the pressure increases, and it increases as the bias voltage increases. Such relationships may be used in selecting optimum processing conditions for producing near ideal film characteristics.

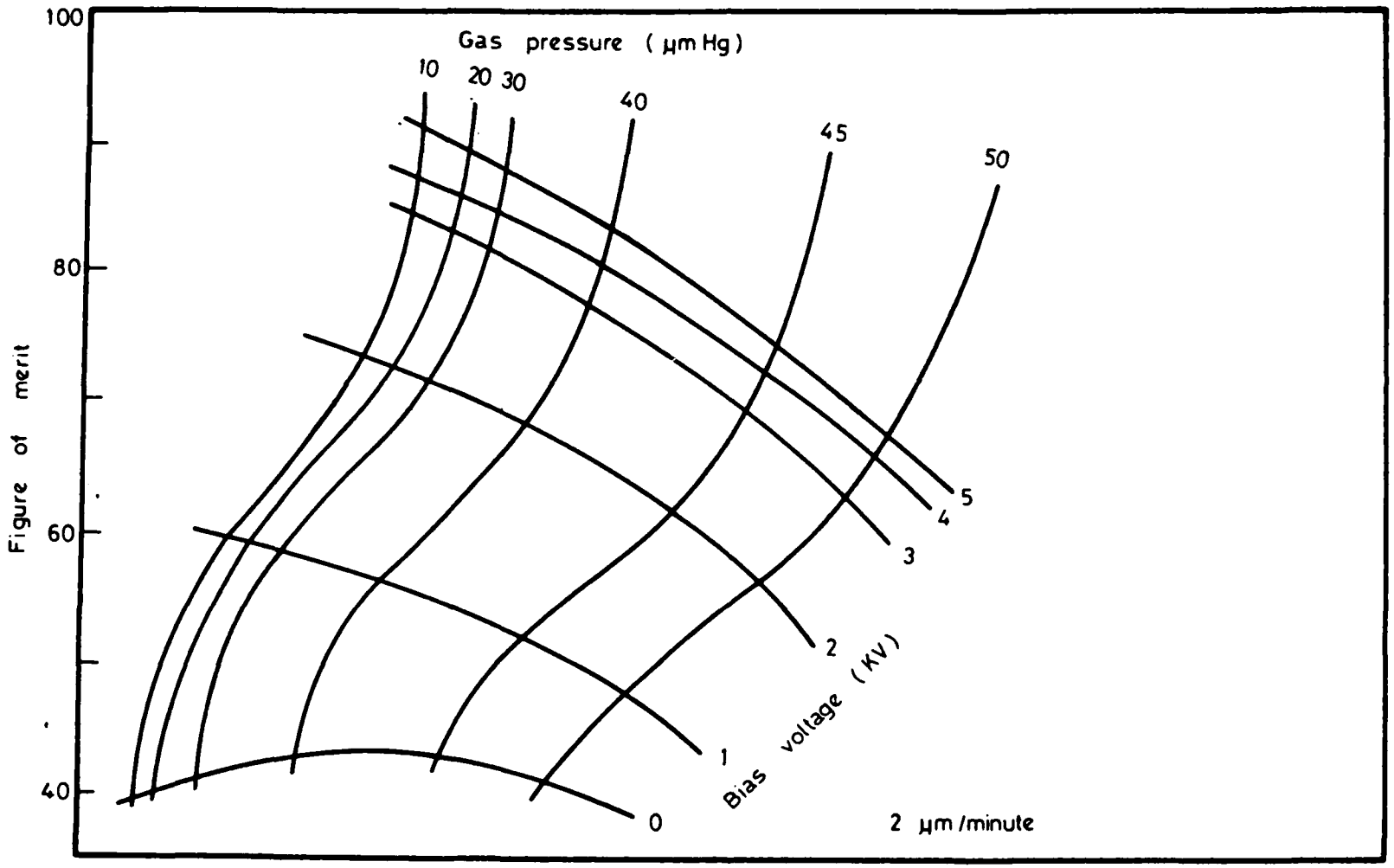

Fig. 7.7 VARIATIONS OF THE FIGURE OF MERIT WITH THE PRCCESSING CONDITIONS AT LOW RATES OF DEPOSITION.

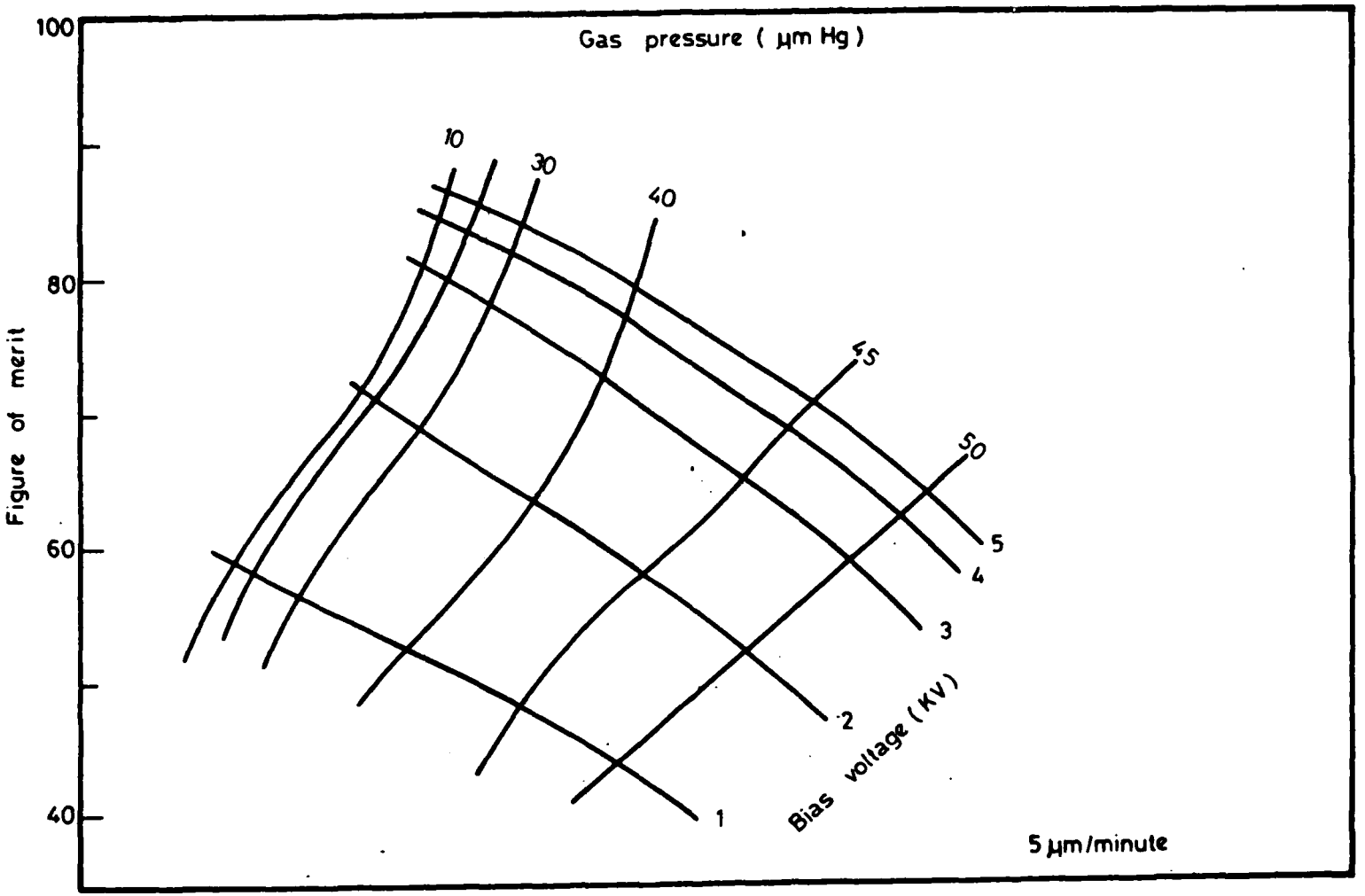

Fig. 7.8 VARIATIONS OF THE FIGURE OF MERIT WITH THE PROCESSING CONDITIONS AT HIGH RATES OF DEPOSITION.

CHAPTER 8
MECHANICAL PROPERTIES

8.1 Microhardness tests

A leitz miniload microhardness tester is used in measuring the microhardness distribution within a film-substrate cross sections and also for measuring the surface hardness of various films. Fig. 8.1 shows the microhardness measurements across a 25 μm thick silver film on copper substratc. Fig.8.2 shows the variations in hardness with film thichness for Al film on titanium substrate. The surface hardness measurments made for both the film and the interface for Al coated titanium sheets are also shown in fig. 8.3.

8.2 X-Ray measurements

The x-ray set described earlier in section 6.2.6 was used again for simultanious measurments of film thickness, grain size and yield stress of silver films on copper substrates. Fig. 8.4 shows the variations in yield stress and grain size with film thickness.

8.3 Fatigne Strength

Rotating bending fatigue tests were made on steel test specimens, sputter etched specimens, and aluminium coated specimens. The S- N curves of these tests are shown in fig. 8.5. It is shown that the sputter etching psocess results in accelerated fatigue damage due to stress concentration at grain boundaries. The ion plated films however showed improved fatigue strength due to localized sealing at grain boundaries. On the contrary,

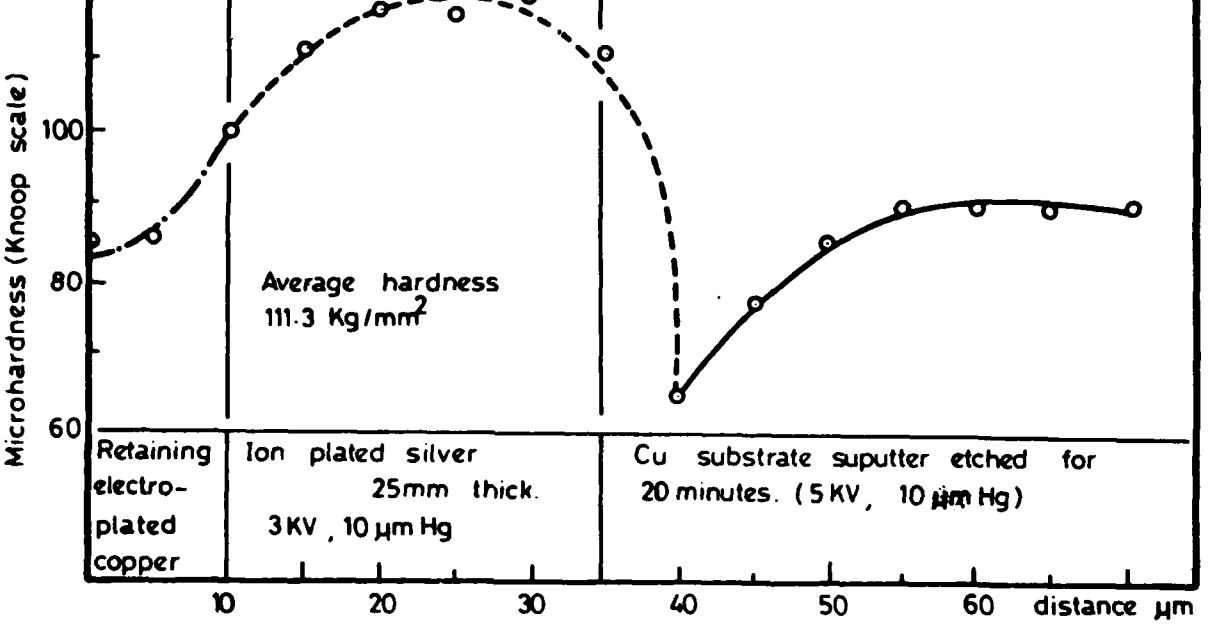

Fig. 8.1 MICROHARDNESS RESULTS ACROSS AN ION PLATED SILVER FILM ON COPPER SUBSTRATE.

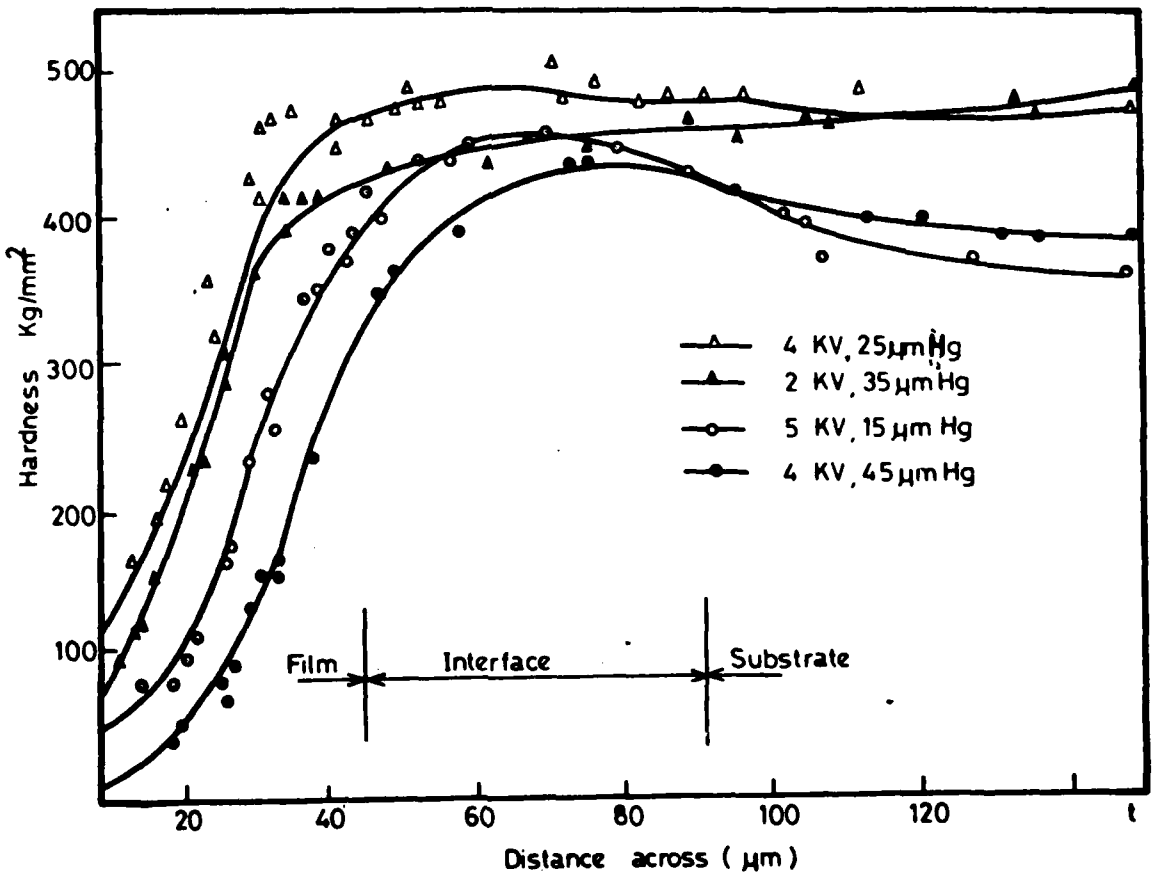

Fig. 8.2 MICROHARDNESS RESULTS FOR ALUMINIUM FILMS DEPOSITED ON TITANIUM SUBSTRATES

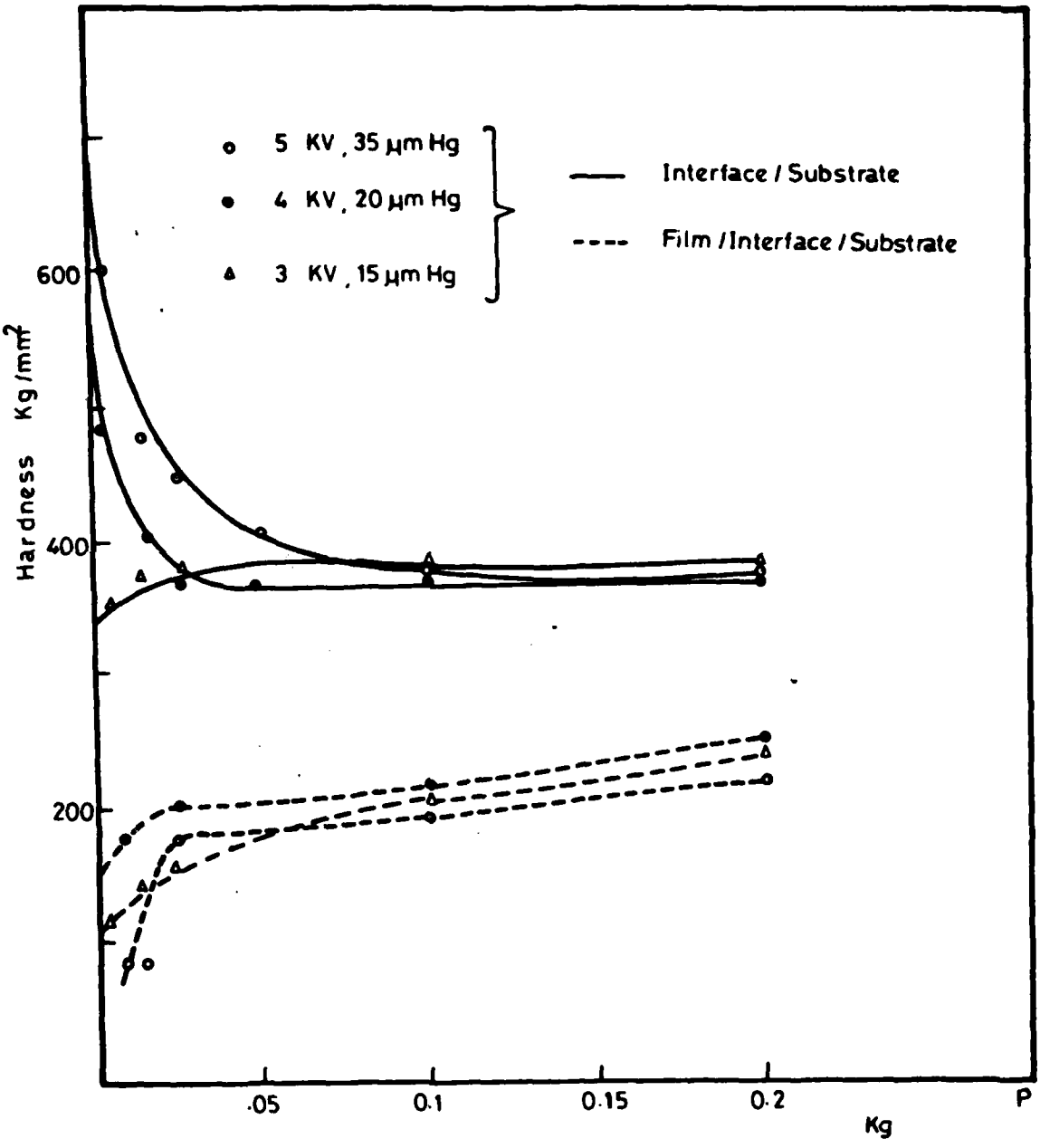

Fig. 8.3 SURFACE HARDNESS OF ALUMINIUM COATINGS DEPOSITED ON TITANIUM SUBSTRATES.

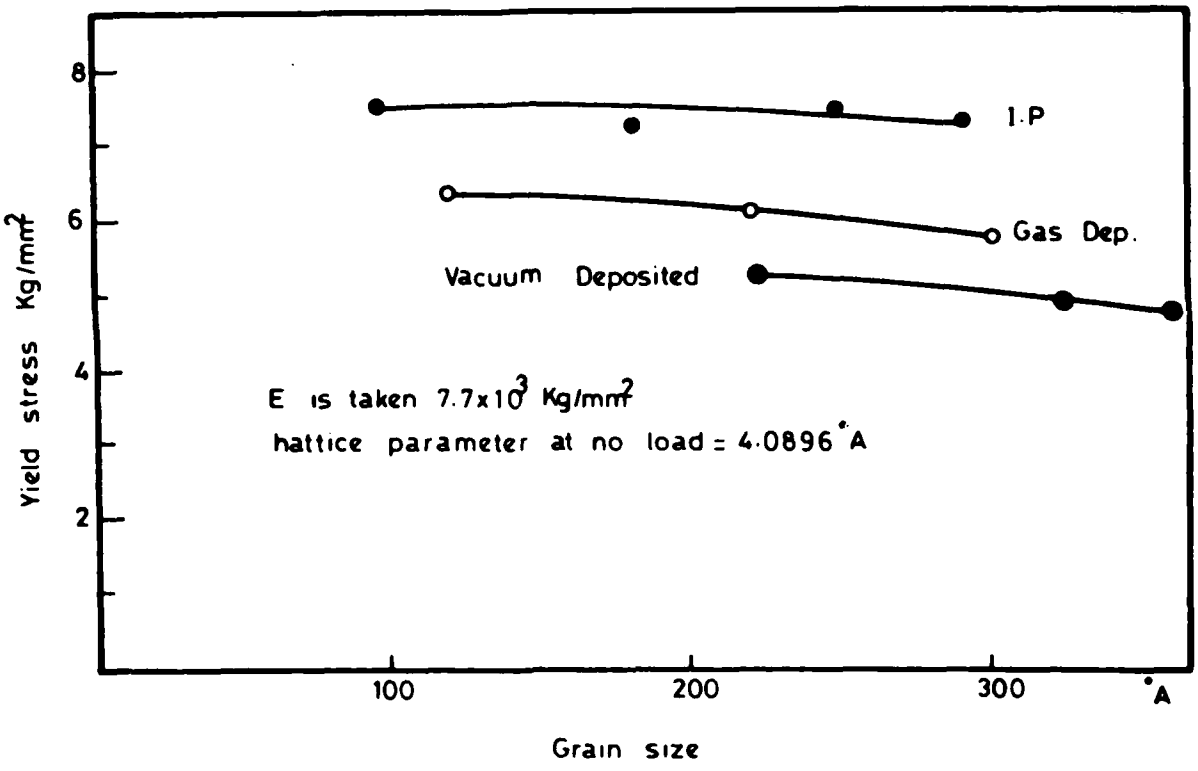

Fig. 8.4 VARIATIONS OF YIELD STRESS OF SILVER FILMS WITH GRAIN SIZE

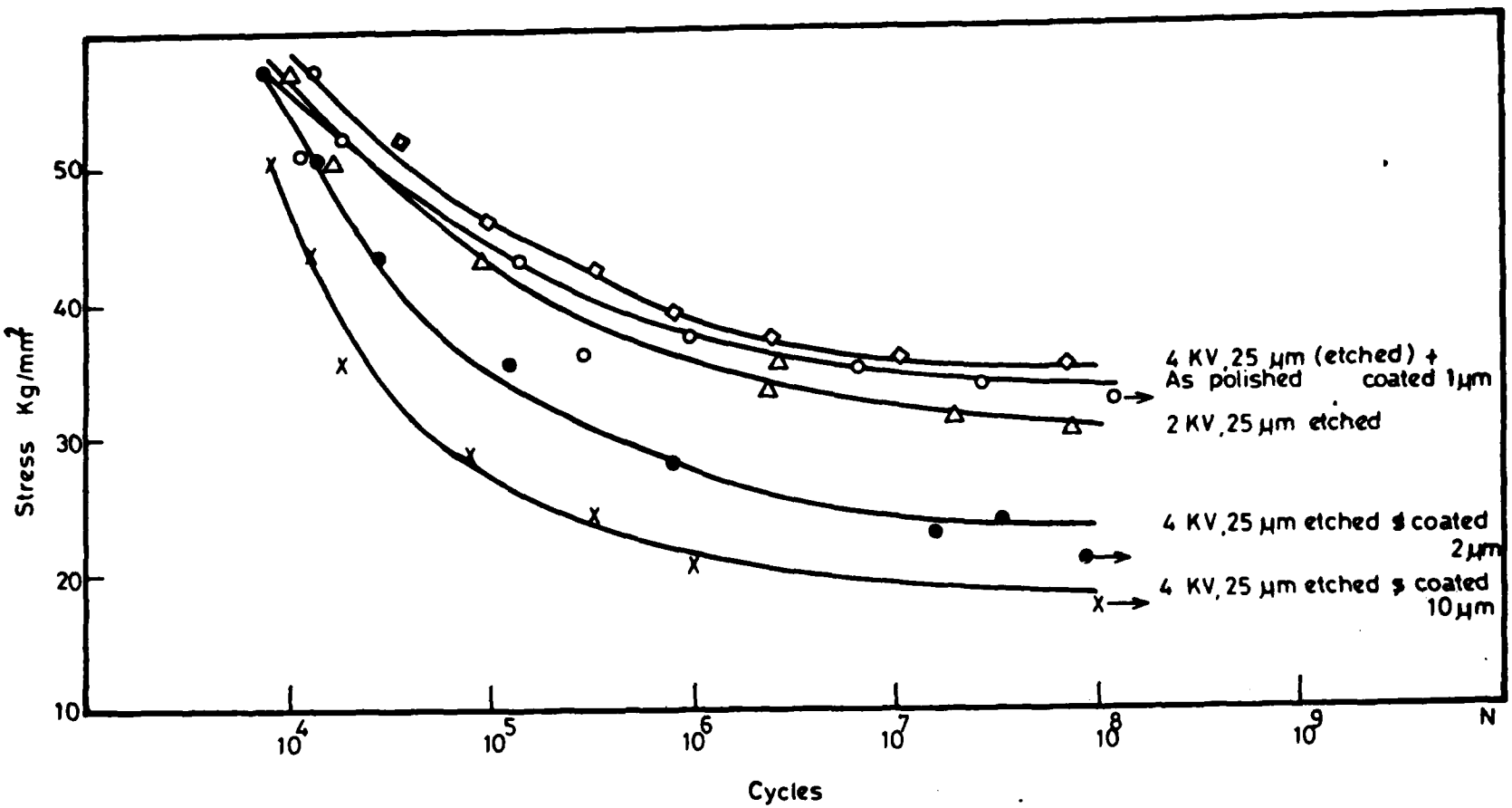

Fig. 8.5 THE EFFECT OF SURFACE COATINGS ON THE FATIGUE LIFE (ALUMINIUM/STEEL)

thick films of Rongh domed structures showed lower fatigue strength. It is therefore beleived that thin uniform coatings of chromium which can result in residual compressive stresses at the surface are beneficial in this respect, but unfortunately the present ion plating facilities does not include an electron beam gun for evaporation of chromium .

V. TRIBOLOGICAL PROPERTIES

CHAPTER 9

FRICTION AND WEAR

9.1 Introduction

This chapter is devoted to the experimental work made on ion plated soft metallic films of lead, Indium, tin and silver . A convrntional pin disc machine was used for normal atmosphere tribotesting of the soft coatings on steel EN-31 substrates. The steel substrates were finely ground to a surface roughness better than 0.18 μm C.L.A.

9.2 Fciction-time relationships

Fig. 9.1 shows a comporison between the coefficients of friction of silver coatings deposited by different techniques. The longer life and effectiveness of the ion ptated films are attributed to the strong adhesion at the film substrate interface. The effectiveness of various ion plated coatings are also compared in figure 9.2. Among these the lead film showed the best results. This was attributed to the good lubrication preperties of lead oxides pbO. (69).

9.3 Effect of sliding speed

The coefficient of fsiction was measured after the tenth revolution of the disc for a range of sliding velocities. These resesults are shown in fig. 9.3 where a maximum reduction of about 20% occured for changes in velocity of more than one order of magnitude .

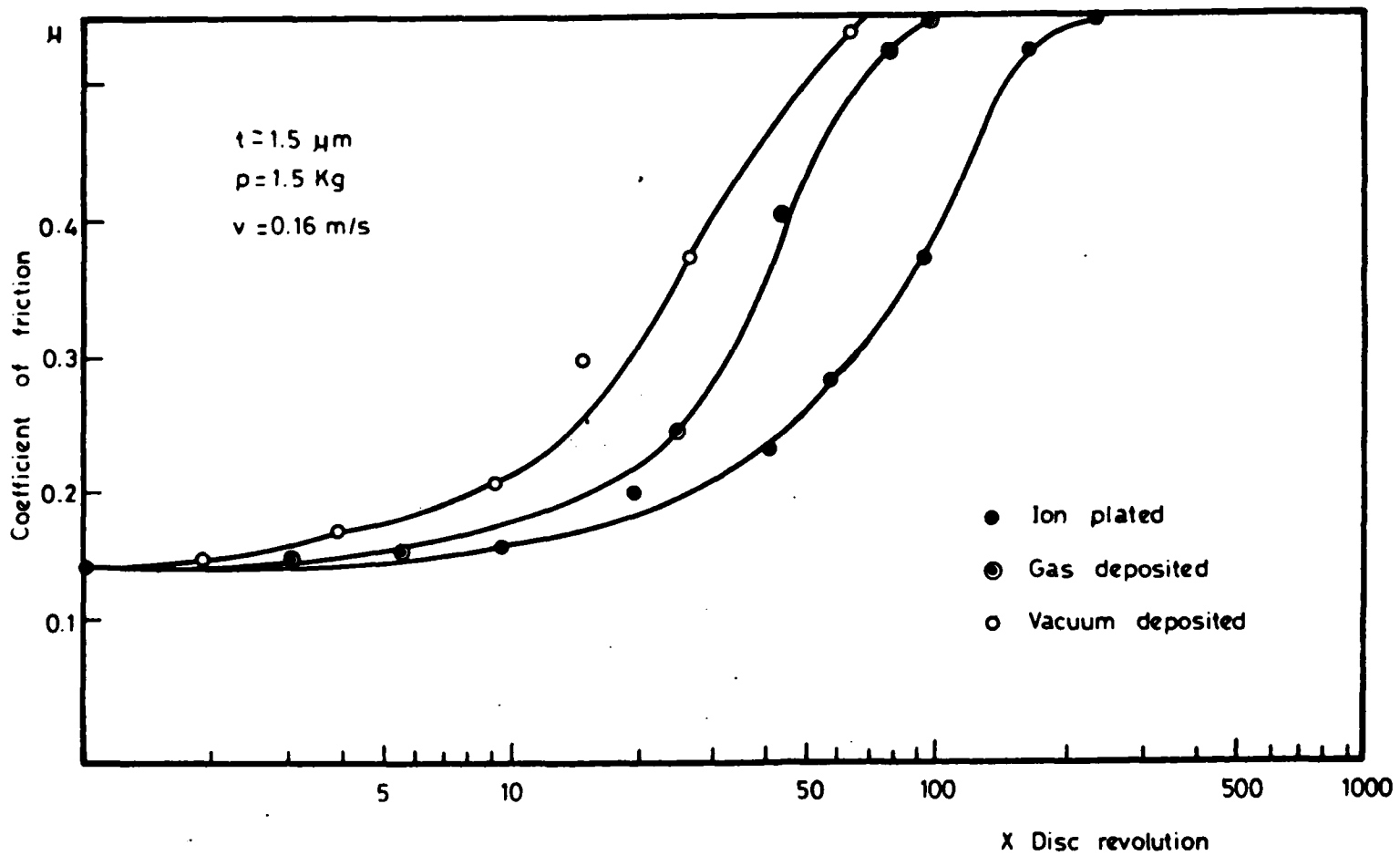

Fig. 9.1 FRICTION HISTORY OF SILVER FILMS

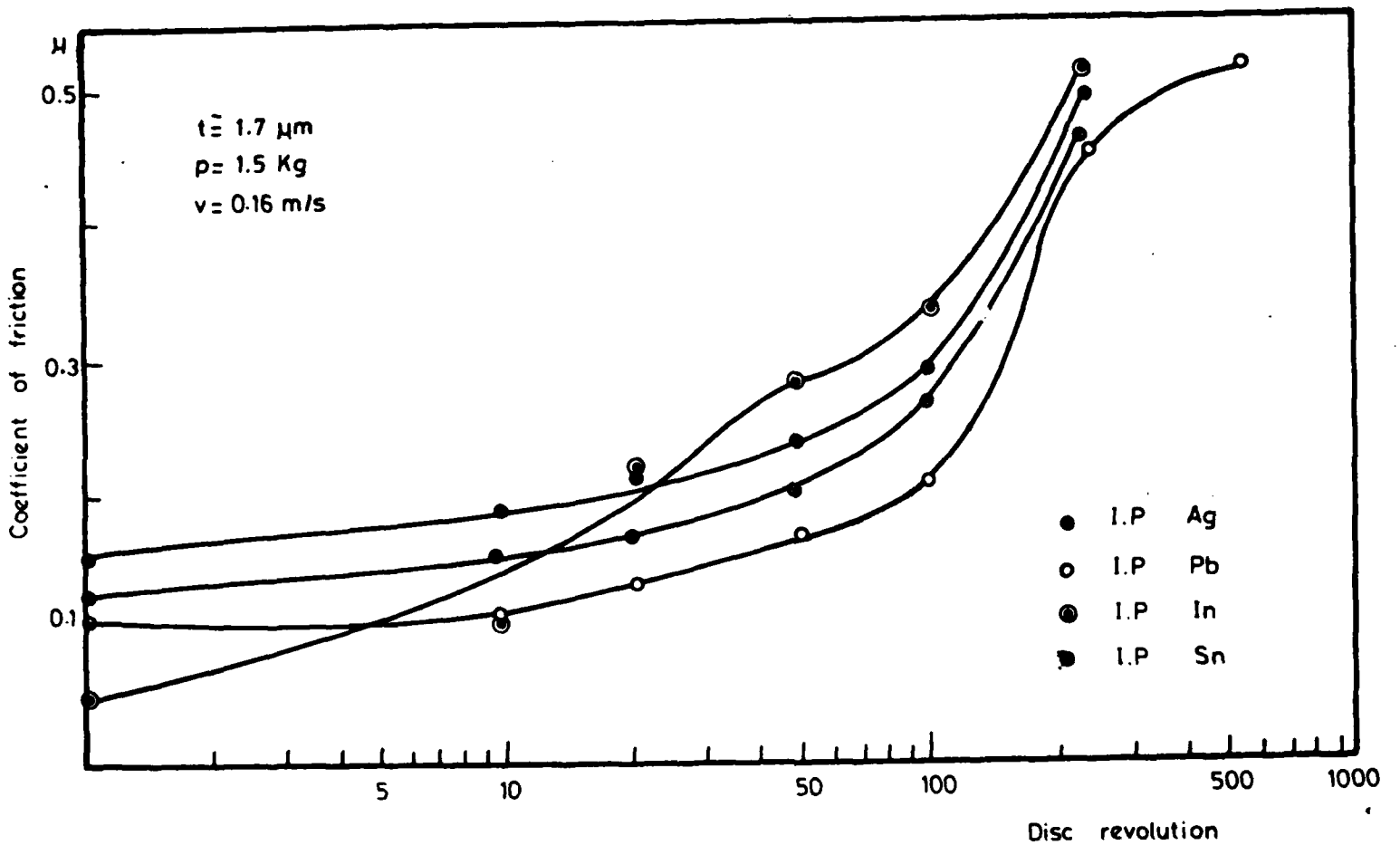

Fig. 9.2 FRICTION HISTORY OF FOUR ION PLATED FILMS
(SILVER, LEAD, INDIUM & TIN)

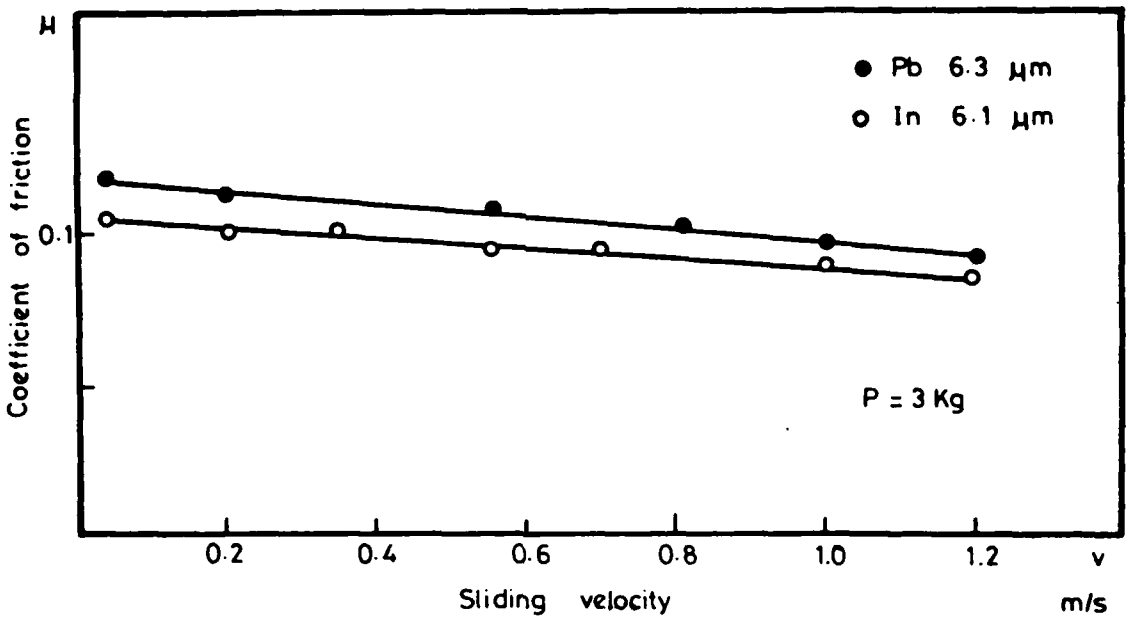

Fig. 9.3 THE EFFECT OF SLIDING VELOCITY ON THE COEFFICIENT OF FRICTION

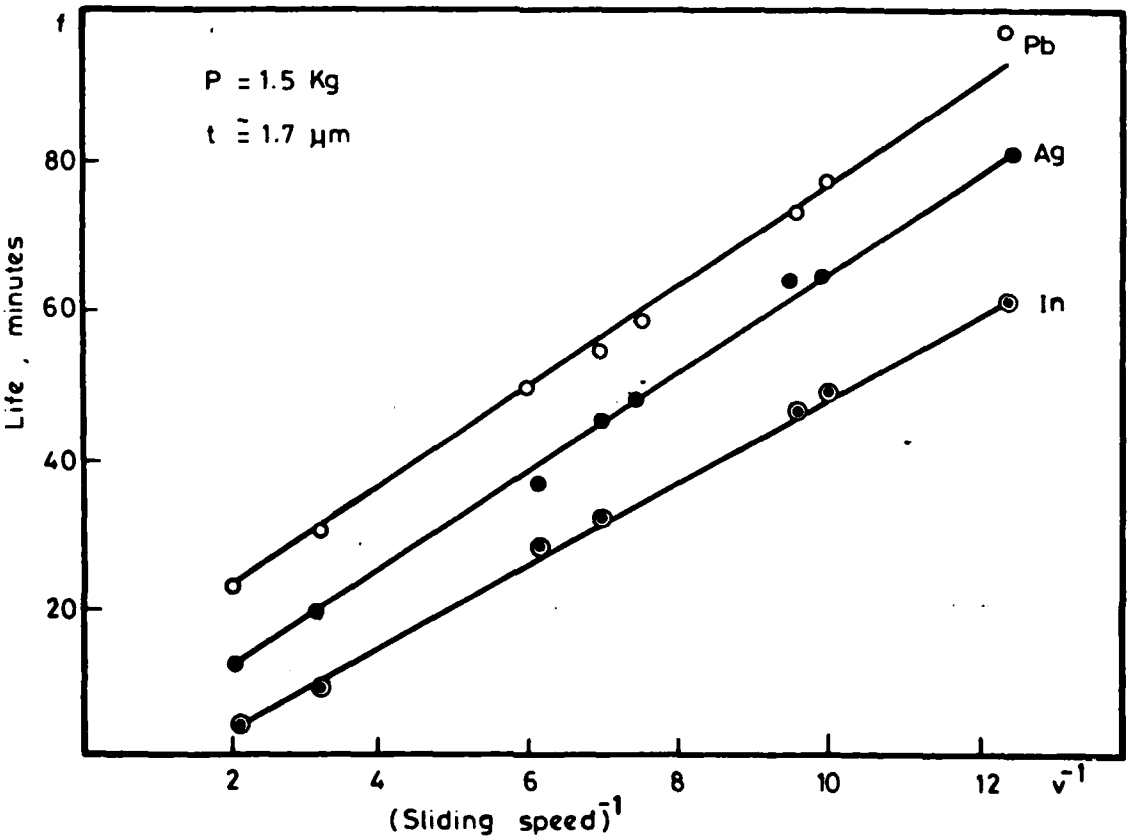

Fig. 9.4 THE EFFECT OF SLIDING VELOCITY ON FILM LIFE

This change in the coefficient of friction is attributable to thermal softening, particularly for the film material in the regions of contact. This thermal softening results in a reduction in shear strength at the contacts without significant reduction in the load carrying capacity, thereby producing a lower value of the coefficient of friction .

The life was shown to be much more dependent on velocity than on the coefficient of friction. (Fig. 9.4). For a given film thickness the life of the film may be interpreted approximately as the length of sliding to achieve a given wear volume of films of the same initial thickness. These results are shown in fig. 9.5. The generally accepted law that the wear volume is a linear function of the sliding distance in not universally true at different velocities. Indeed one obtains the surprising result with lead that the same amount of wear requires a greater sliding distance at the higher velocities, whilst the contrary is true with indium. With silver the law appears to be validated . The effect of increasing sliding speed is to produce higher contact temperatures which result in some degree of thermal softening . This mechanism would explain the behaviour of the very soft indium films and, at the velocities considered, the relatively much harder silver films. On this basis the lead film would be expected to lie between these two results rather than demonstrate the actual behaviour shown in Fig. 9.5. This apparent discrepancy, which has already been noted in the film life results of Fig. 9.2. is thought to be due to the presence of pbO which is a very effective lubricant (70). At the higher velocities

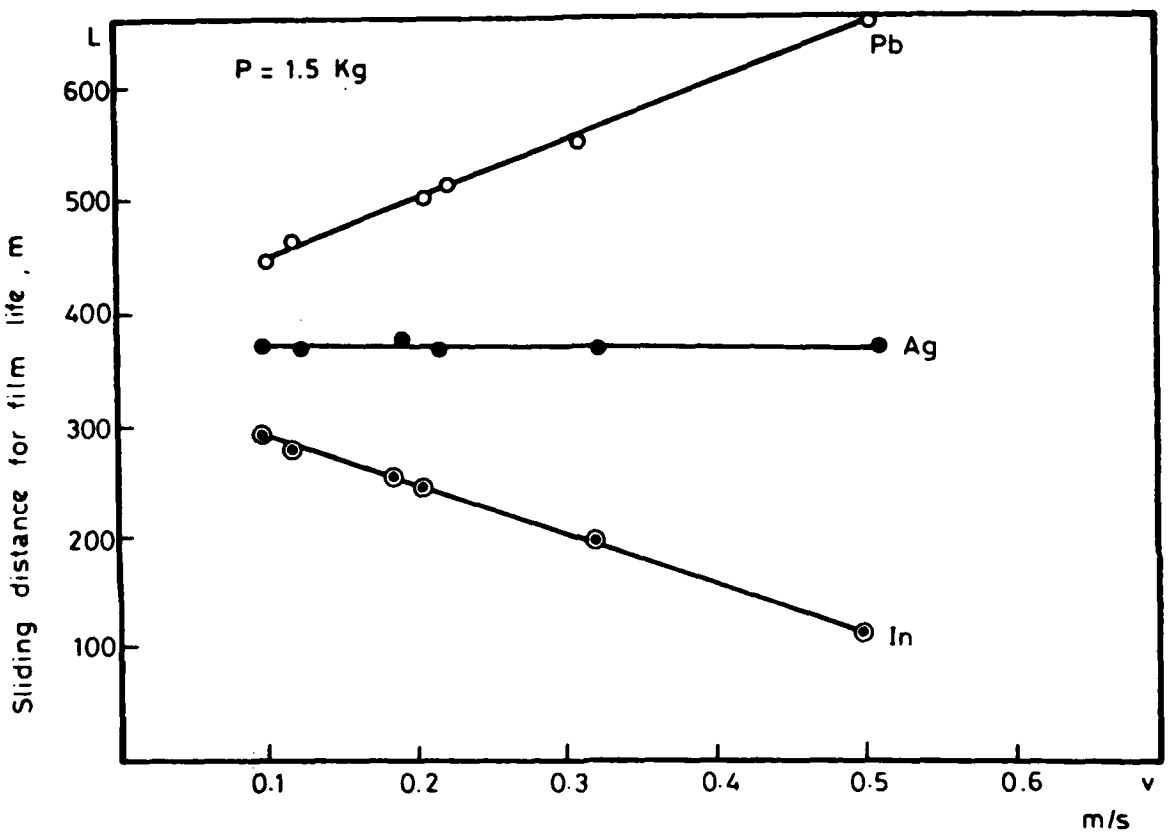

Fig. 9.5 ESTIMATED SLIDING DISTANCE FOR FILM LIFE

the increased temperature leads to a larger concentration of PbO, which is consistent with the results shown in Fig. 9.5.

9.4 The effect of film thickness

The values of the initial coefficeint of friction at various values of film thickness for both lead and indium are shown by the experimental points in Fig. 9.6 .With very thin films the high value of the coefficient of friction is associated with breakthrough of the film by mating asperities .This effect is lessened as the film thickness increases. However, as the film thickness increases the load-carrying capacity of the surface will decrease, which leads to an increasing friction coefficient. Using these concepts the authors have developed a theoretical model for this situation, the predictions of which are also shown in Fig.9.6 [7] .The matching of the experimental and theoretical results in Fig. 9.6 requires that certain unknown system constants are appropriately chosen. These constants define the relationship between the contact area and the compliance of a film-covered asperity, and the variation of surface hardness with film thickness and with such constants as f and αin the well known theory of friction. The shear stress$\tau\tau$is

$$\tau = f\tau_{max}$$

where $0 < f < 1$, and the equilibrium equation relating $\tau$and the contact pressure p is

$$p^2 + \alpha^2\tau^2 = \text{constant}$$

It should be noted that the film life characteristics shown in

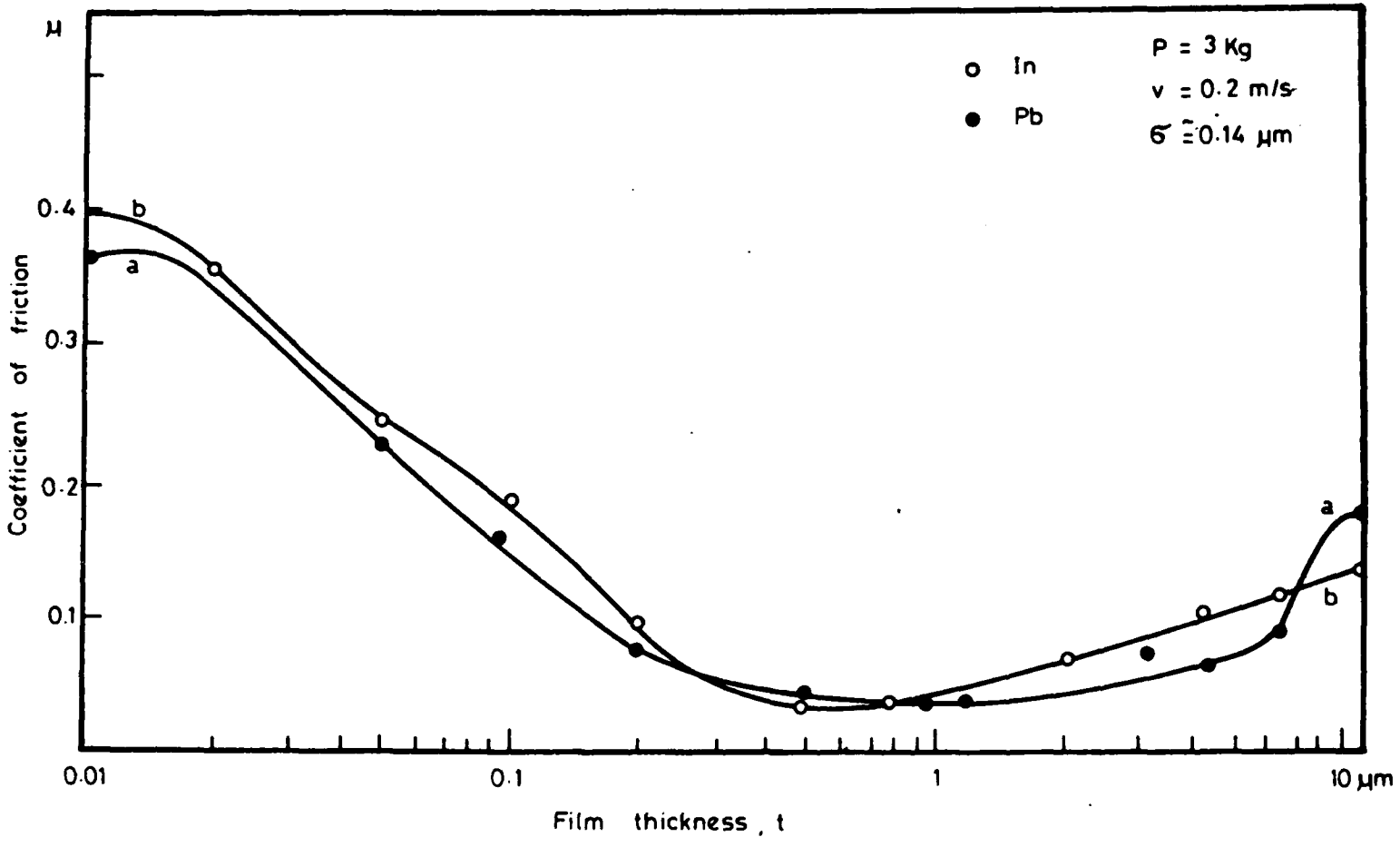

Fig. 9.6 THE EFFECT OF FILM THICKNESS ON FRICTION

Fig. 9.2 are entirely consistent with the results of Fig.9.6. With a reasonable initial film thickness the coefficient of friction is small, and as wear reduces the effective film thickness its value increases in the manner shown by the left-hand limb of the curve in Fig.9.6 which is confirmed by the results shown in Fig 9.2 .

Since the shape of the curves in Fig.9.6 has been associated with asperity breakthrough in the thin film regime, surface roughness must be an important parameter. Some experimental and associated theoretical predictions indicating the effect of surface roughness σ in this regime are shown in Fig. 9.7. Theory and experiment are in agreement and indicate the extreme importance of surface roughness for very thin films of soft metals.

The effect of film thickness on film life is best demonstrated by the parameter of film life per unit thickness of initial film thickness, (Fig. 9.8). For the reasons which have been discussed previously lead is superior to both silver and indium. None the less all these films clearly demonstrate that the wear rate of the film is much less for thinner films than for the thicker films, and this tendency accelerates as the initial film thickness decreases. With thick films it is considered that the wear mechanism is essentially a process of microcutting of the soft material. As the film thickness decreases many more contacts between the asperities and the hard substrate occur, so that the microcutting failures are reduced and a more moderate

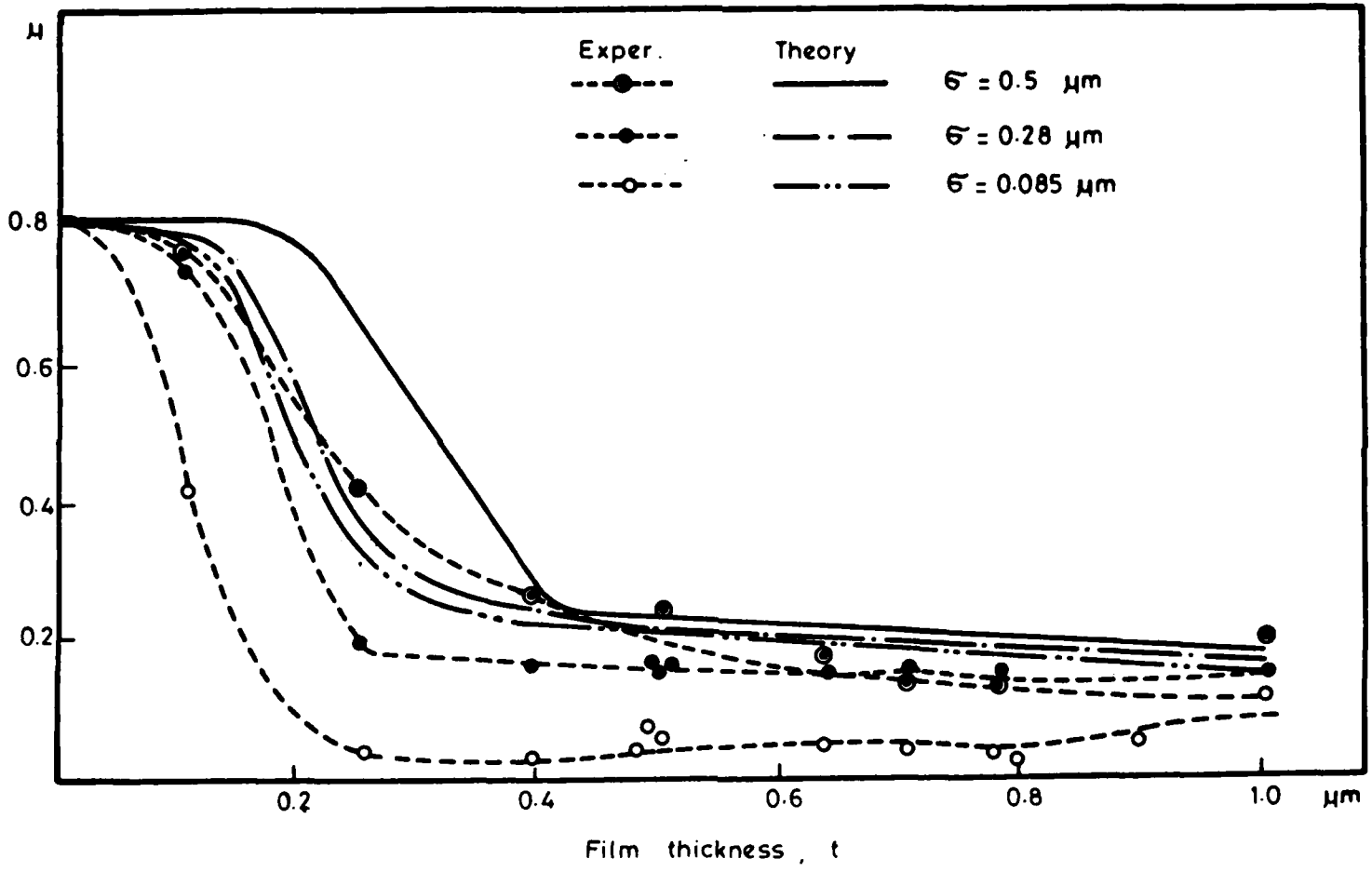

Fig. 9.7 THE EFFECT OF SURFACE FINISH ON THE COEFFICIENT OF FRICTION

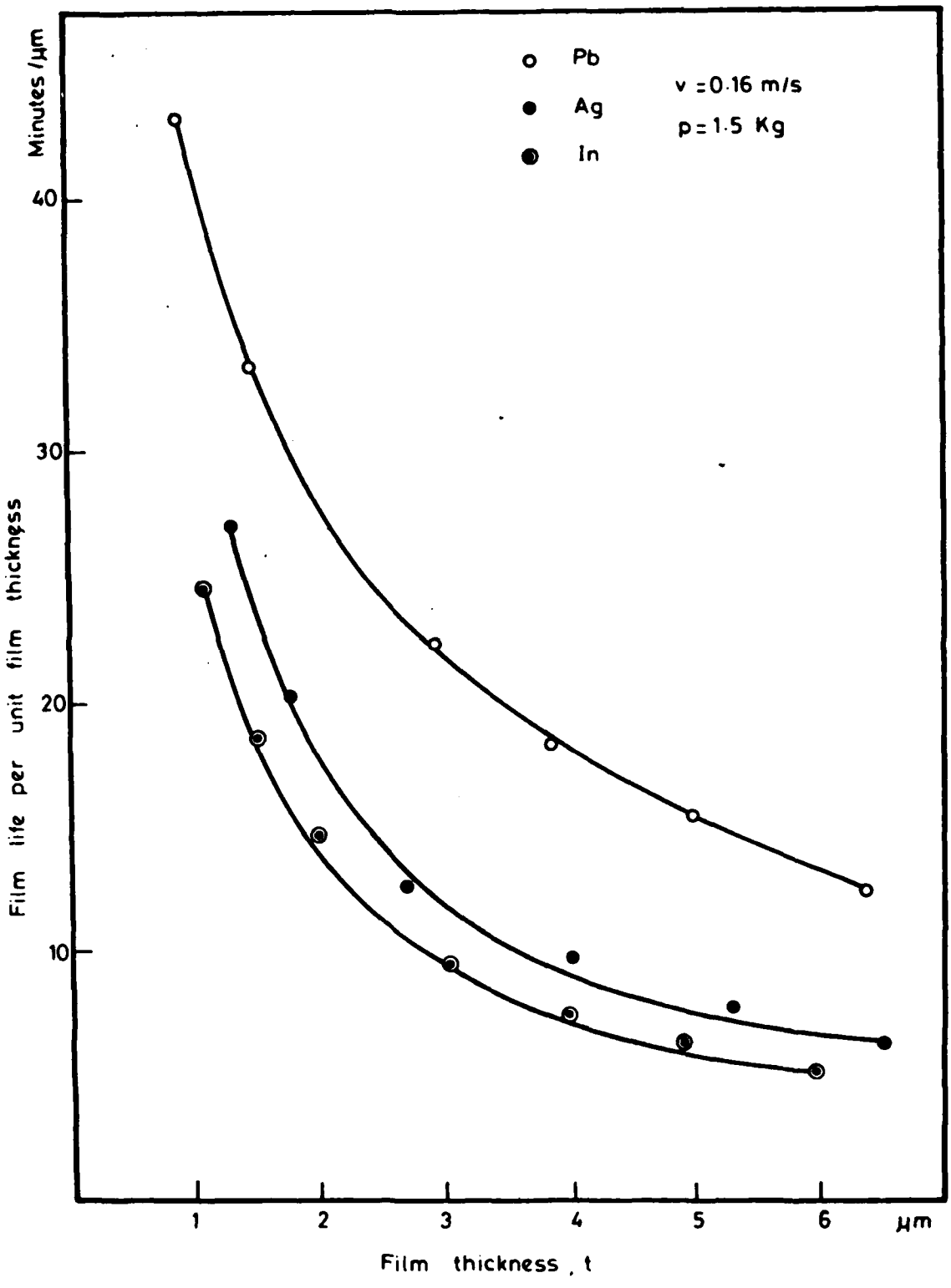

Fig. 9.8 THE MEASURED LIFE PER UNIT FILM THICKNESS FOR FILMS OF DIFFERENT INITIAL THICKNESS

fatigue and possibly an abrasive wear mechanism occurs at the substrate contacts [72] .

9.5 Wear Mechanisms

The nature of the wear mechanisms is illustrated in the scanning electron micrographs shown in Fig. 9.9 and 9.10 . At the start of the test the surface asperities produce a microcutting form of wear in the film on the stationary rider. The wear rates vary in different parts of the contact patch and produce a build-up of wear debris. The wear rate during this period is high and is responsible for most of the loss of film material. In due course much of the film is removed leaving a very thin non- uniform smear of solft metal on parts of the track. The wear debris at this time is in flakes rather than particles and a more steady form of wear rate exists.

When the bulk of the film material has been removed the asperities of the disc are in contact with the substrate of the rider. The rate is considerably reduced producing much finer wear particles. This debris abrades the substrate to produce a polished appearance of the film-substrate interface. The very much reduced wear rate during this process suggests that fatigue mechanisms could be the principal mode of wear. It is also belived that the low wear rate in this regime arises from the special characteristics of the graded interface which is a feature of the ion-plating process.

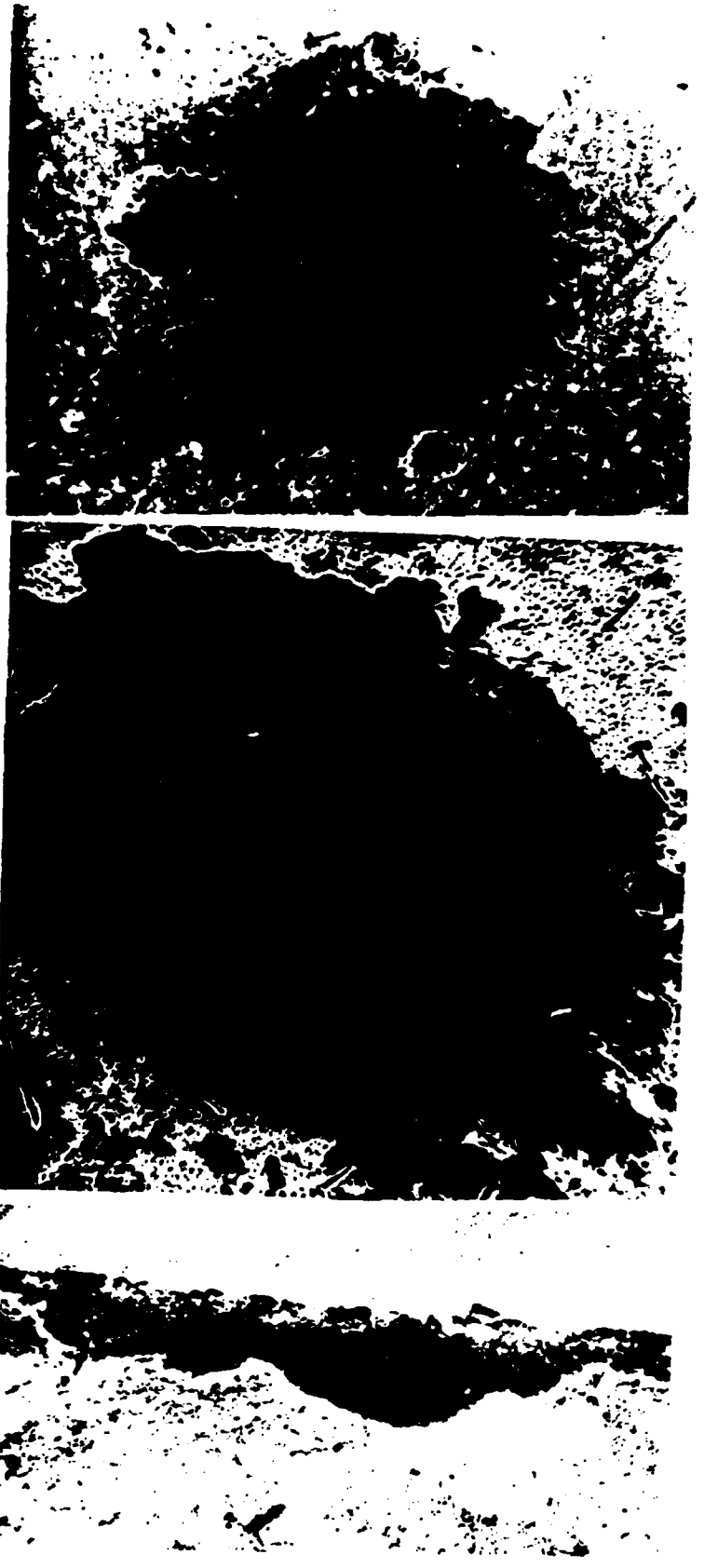

FIG. 9.9 COMPARISON BETWEEN THE WEAR SCAR OF
(a) VACUUM DEPOSITED (DETACHMENT AT LEADING EDGE)
(b) SPUTTERED (PEELING ARCUND THE SCAR)
(c) THICK ION PLATED (PLUCKING & SMEARING)

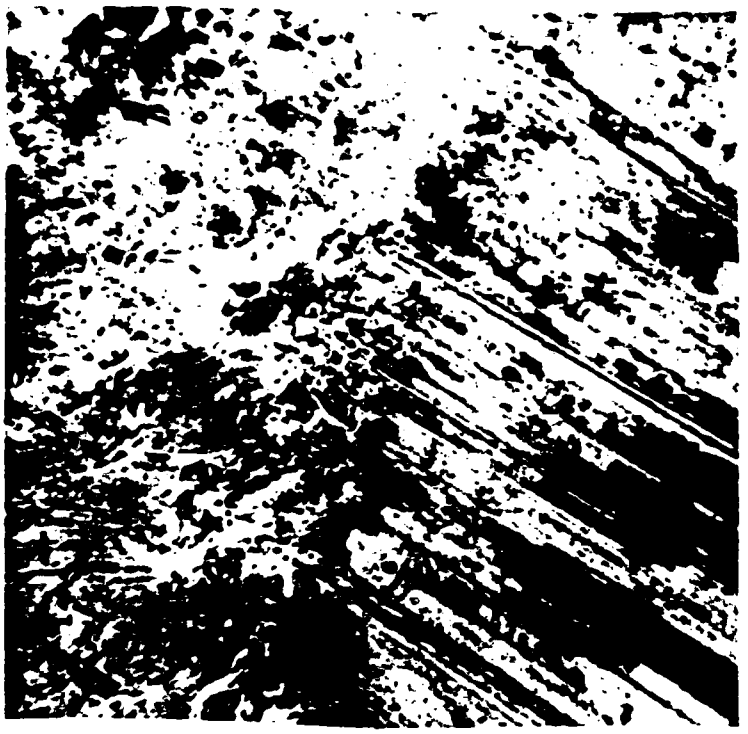

X 350

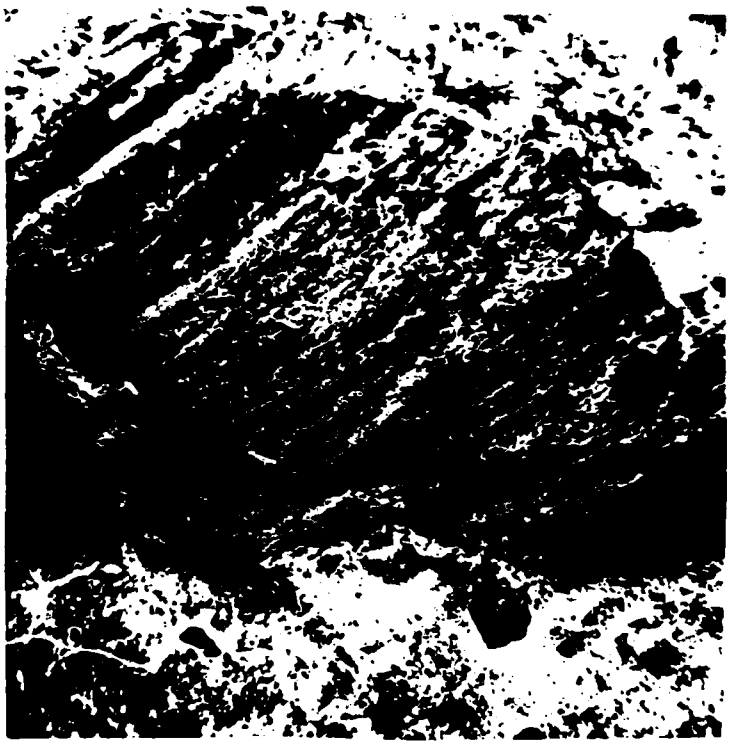

X 300

FIG. 9.10 WEAR PROCESS IN ION PLATED FILMS
(a) INITIAL MICROCUTTING (BEDING-IN)
(b) SUBSEQUENT FILM WEAR (BUILD UP OF WEAR DEBRIS)

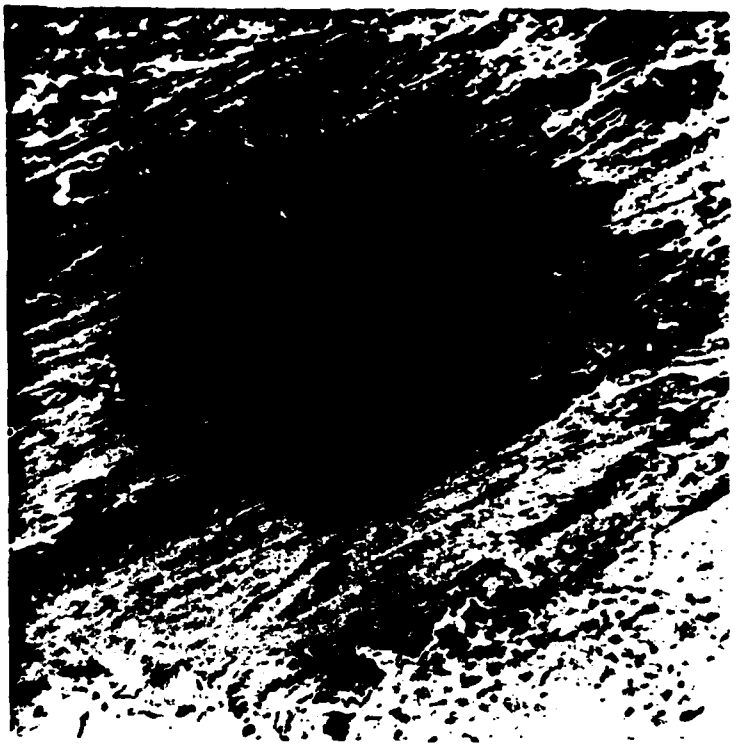

X 200

X 100

FIG. 9.10 WEAR PROCESS IN ION PLATED FILMS
(c) SCAR POLISHING BY DISC WEAR DEBRIS
(d) FLAK WEAR DEBRIS AND STEADY WEAR

X 230

FIG. 9.10 WEAR PROCESS IN ION PLATED FILMS
(e) BACK-TRANSFER FILM

VI CONCLUSIONS

An extensive study on adherence and bonding of the ion plated coatings is presented. Details of physical mechanisms taking place during the deposition process are discussed. Dominant factors such as the collision factors, ionization efficiency, average energy and ion energy distribution are reported in details. The mechanisms of ion-solid interactions, nucleation and atomistic mixing are experimentally investigated before adhesion testing and evaluation is considered. Some other characterristics of the ion plated coatings such as structural details, mechanical and tribological properties are also included.

In conclusion ,

The outstanding adhesion of the ion plated films was attributed to the:

1. Atomically clean surfaces produced by sputter etching perior to and during film formation
2. Surface defects and mobile vacancies produced by ion-solid interactions
3. High energy ion entrapment as a result of the sputtering back of the low energy particles
4. Atomistic mixing of both the film and the substrate atoms
5. Gas scattering resulting in finer deposites
6. Thermally assisted diffusion
7. Intermetallic compounds formed at the film substrate interface for the compatible metal pairs
8. Extensive graded interfaces for incompatible metal pairs.

REFERENCES

(1) Mattox,D. Sandia Corporation Report SC-DR-281,U.S.A.,1963

(2) Mattox,D. Sandia Corporation Monograph SC-R-65,852 ,1965

(3) Mattox,D. NASA Special Publication Sp 5111,U.S.A. ,1972

(4) Wan,C. ,Chambers,D. and Carmichael,D. Proceedings. Int. Conf. On Vacuum Technology , Tokyo, Japan , 1973

(5) El-Sherbiny,M. Ph.D. Thesis, University of Salford , U.K. ,1975

(6) Salem,F Ph.D. Thesis, University of Salford , U.K. ,1977

(7) Johnson, R. NASA Special publication Sp 5111, U.S.A. ,1972,p.1

(8) Teer,D. Intemational conf. on advances in surface coating Technology, Institule of welding, London ,Feb.1978, Paper 33

(9) Mattox,D. J. Vac. Sci. and Technol. , Vol. 10 no.1,1973,p.47

(10) Leder,L. Metal Finishing, March 1974 , p.41

(11) Buckley,D. , Johnson,R. and Bisson, E. NASA Special Publication Sp 5111, March 1972, P.149

(12) Aisenberg,S. and chabot,R. J.Vac. Sci. Technol. Vol. 10, 1973, p.104

(13) Mattox,D. Proc. of the 12th National vac. Symposium of Amer. Vac. Soc. , New York, 1965

(14) Lundin, B. (Editor) NASA Special publication sp 5111, 1972

(15) Davies,W. and Vanderslice, T. Phys. Rev. Vol. 131,1963,p.219

(16) Teer, D. AGARD lecture series No. 106,North Atlantic treaty organization, 1981, paper 3

(17) Teer,D. J. Adhesion, vol.8 ,1977, P.289

(18) Francis in the book" Handbuk der physik" edited by S. Flugge, Springer verlag, Berlin, vol.22,1956,P.53

(32) Libbrecht,K. , Griffith,J. , Weller,R. and Tombrello, T. Radiat. Eff., Vol. 49 , 1980,P.196

(33) Weller M. and Tombrello ,T. Radat. Eff. Vol.49,1980,P.239

(34) Hurkmans,A. , Overbosch,E . and los, J. Surf.Sci Vol.62, 1977, P.621

(35) Modak,A. and Pagni, P J. chem. Phys. Vol.59, 1973, P.2019

(36) Trilling,L. and Hurkmans,A. Surf. Sci. Vol.59,1976,P.361

(37) Littmark,U. and Hofer,W. Nucl. Instrum. Methods Vol.170 1980, P.177

(38) Mattox,D. Trans. ASE , 1969, P.2175

(39) Chambers ,D. and Carmichael,D. Research and development Vol. 22, 1971, P. 32

(40) Wan,C. , Chambers,D. and Carmichael,D. J. Vac. Sci. and Technol. Vol.8, 1971 , P.99

(41) Spalvins,T. , Przybysz ewski, J. and Buckley, D. NASA TN D- 3707 , 1966

(42) Weaver,C. J. Vac. Sci. Technol. Vol.12 no.1, 1975, P.18

(43) Shawki,G. , El-Sherbiny,M. and Salem,F. 1st Cairo univ. conf. on mechanical design and production. MDP. 79, Dec. 1979,Cairo, 1979, Paper MAT-19, Also in the book "recent advances in mech. Engg. Sci." edited by G. Shawki, Pergamon press, N.Y, 1980, P.

(44) Martinson,C. Vacuum , Vol. 27, no.3, 1976, P.119

(45) Erlich, G. Conf. on Clean Surfaces, Ann. N.Y., A cad. Sci., Vol.101, 1963, P.583

(46) Wheeler, A. Structure and Properties of Solid surfaces, univ. of chicago press, U.S.A, 1953,P.455

(19) Ahmed, N. M.SC. Thesis, University of salford,U.K.,1974

(20) Houston,J and Uhl,J. Sandia corporation Report SC-RR-710122, 1971

(21) Sigmund,P Phys. Review Vol. 184, 1969,P.383

(22) Weissman,M.and Sigmund,P. Radiat. Eff. Vol. 19,1973,P.7

(23) Bohdansky,J. Roth,J. and Bay, H. J. Appl. Phys.,Vol.51,1981, P.2861

(24) Matsunami,N., Yamamura,Y. Itikawa,Y., Itoh,N., Kazumata, Y., Miyagawa,S. , Morita ,K. and Shimizu, R. Radiat. Eff., Vol. 50, 1980,P.39

(25) Haggmack,L. and wilson, W. J. Nucl. Mater. Vol. 76 and, 77, 1978, P. 149

(26) Yamamura,Y. Int. Ion Engg. congress ISIAT-IPAT-83 To be held in kyoto, Japon. sept. 1983,Vol. 3, 1983, P. 1875

(27) Lindhard, L., Nielsen, V. and schaff, M. Mat. phys. Medd. Dan. vid. selsk., Vol. 36, no. 10, 1968

(28) Carter, G. and Armour, D. Thin solid films, Vol.80, 1981.P.13

(29) Taglauer, E., Beitat, V., Martin, G. and Heiland, W. J. Nucl. Mater. Vol. 63, 1976,P. 193

(30) Van den Berg,J., Aromour,D. and verheij.L. Proc. Int. conf. on low energy ion beams, salford, 1978,edited by wilson, I.and Moruzzi,J. ,Inst. Phys. conf. Series 38, 1978,P.298

(31) Winters,H. and Sigmund,P. J.Appl. Phys., Vol.45,1974,P.4760

(47) Latimer, W. Oxidation Potentials, Prentice-Hall, London,1952

(48) Bassett,G. , Menter, J. and Pashley,D. International conference on the structure of thin films, Bolton New York, 1959

(49) Yambia,Y. and Moria,T. J. Vac. Sci. Technol, Vol.13 no.3 , 1976, P 693

(50) Showki,G. , El- Sherbiny,M. and Salem,F. Thin Solid films Vol. 75, 1981, P. 29

(51) Davies, J. , Mc Intrye, J. and Cushing , R. Can. J. Chem., Vol. 38, 1960

(52) El-Sherbiny, M. and Salem,F. a Paper postered at the 3rd ion and plasma assisted techniques IPAT-81 , Amsterdam, June 1981

(53) Bland, R. Sandia Laboratory report Sc-R-68-1781,1968

(54) Chapman,B. J. Vac. Sci. Technol. Vol.11, 1974, P.106

(55) Heavens, O. J. Phys. Res. VOL.11, 1950, P.355

(56) Benjamin,P. and Weavel,C. Proc. Roy. Soc. A254, 1960,P.163

(57) Butler,D. , Stoddart, C. and Stuart, P. J.Phys. D3,1970,P.877

(58) Belser,R. and Hicklin , W Rev. Sci. Instrum. 27, 1956,P.293

(59) Jacobson,L. Vacuum deposition of thin films, chapman and Hall London, 1960

(60) Ohame,N. J. Vac. Sci. & Technol. ,13, 1976, P.82

(61) Beams,J Structure and properties of thin films, J. Wiley , N.Y. , 1959

(62) Strong, J. Rev. Sci. Instrum., 6, 1935, P.97

(63) Lin,D. J. of Phys., D4 , 1971, P. 1977

(64) Neugebauer,C. , Newkirk, J. and Vermilyea,D. (Editors) Structure and properties of this films" J. Wiley , N.y. 1959

(65) Hass,G. (Editor) "Physics of thin films" Academic press N.y. , 1966

(66) Wilsdorf (Editor) "Thin Films" Amer. Sac. of Metals, 1964

(67) Mattox, D. and Kominiak, G.
J. Vac. Sci. Technol. Vol. 9 , no.1, (1972), P. 528

(68) Peiser, H. et. al x-Ray Diffraction, Inst. of Phys.,hondon,1959

(69) Peterson,M. and Johnson, R. Lub. Eng. Vol.13 1957

(70) Tsuya, Y. and Takagi, R. wear, Vol.7 1964 P.131

(71) Halling, J. and El- sherbing, M. , Tribology converntion, I. Mech.E., Swansea . April 3-4, 1978

(72) EL- SHERBINY,M. AND SALEM,F. Fatigue wear, wear, Vol. 66 , 1981, P.101-110

END

FILMED

11-85

DTIC